nature catalysis

SUPPLEMENTARY INFORMATION

https://doi.org/10.1038/s41929-019-0317-4

In the format provided by the authors and unedited.

Biocompatibility and therapeutic potential of glycosylated albumin artificial metalloenzymes

Shohei Eda[1,5,6], Igor Nasibullin[1,2,6], Kenward Vong[1,6], Norio Kudo[3], Minoru Yoshida[3,4], Almira Kurbangalieva[2] and Katsunori Tanaka[1,2,5*]

[1]Biofunctional Synthetic Chemistry Laboratory, RIKEN Cluster for Pioneering Research, Saitama, Japan. [2]Biofunctional Chemistry Laboratory, A. Butlerov Institute of Chemistry, Kazan Federal University, Kazan, Russia. [3]Drug Discovery Seed Compounds Exploratory Unit, RIKEN Center for Sustainable Resource Science, Saitama, Japan. [4]Department of Biotechnology, Graduate School of Agricultural and Life Sciences, The University of Tokyo, Tokyo, Japan. [5]GlycoTargeting Research Laboratory, RIKEN Baton Zone Program, Saitama, Japan. [6]These authors contributed equally: Shohei Eda, Igor Nasibullin, Kenward Vong *e-mail: kotzenori@riken.jp

Supplementary Information

Biocompatibility and Therapeutic Potential of Glycosylated Albumin Artificial Metalloenzymes

Shohei Eda,[1,5,#] Igor Nasibullin,[1,2,#] Kenward Vong,[1,#] Norio Kudo,[3] Minoru Yoshida,[3,4] Almira Kurbangalieva,[2] and Katsunori Tanaka*[,1,2,5]

[1] Biofunctional Synthetic Chemistry Laboratory, RIKEN Cluster for Pioneering Research, 2-1 Hirosawa, Wako-shi, Saitama, 351-0198, Japan

[2] Biofunctional Chemistry Laboratory, A. Butlerov Institute of Chemistry, Kazan Federal University, 18 Kremlyovskaya street, Kazan, 420008, Russia

[3] Drug Discovery Seed Compounds Exploratory Unit, RIKEN Center for Sustainable Resource Science, Hirosawa 2-1, Wako, Saitama 351-0198, Japan

[4] Department of Biotechnology, Graduate School of Agricultural and Life Sciences, The University of Tokyo, Yayoi, Tokyo 113-8657, Japan

[5] GlycoTargeting Research Laboratory, RIKEN Baton Zone Program, 2-1 Hirosawa, Wako-shi, Saitama, 351-0198, Japan

Corresponding Author E-mail: kotzenori@riken.jp

Table of Contents

Supplementary Figures

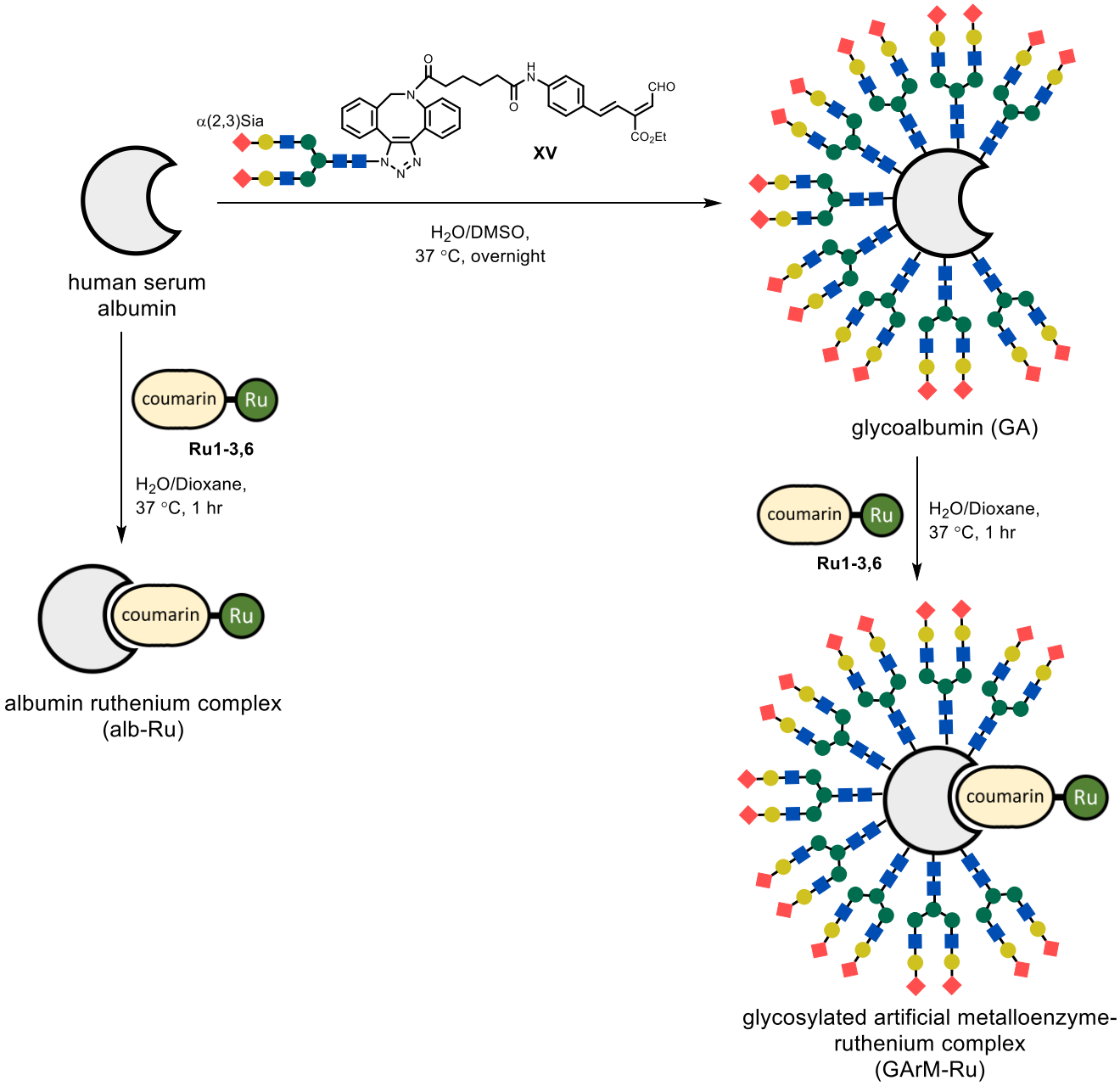

Supplementary Figure 1. Preparation of the protein complexes GA, alb-Ru, and GArM-Ru

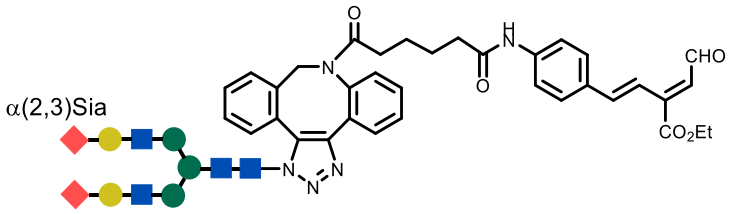

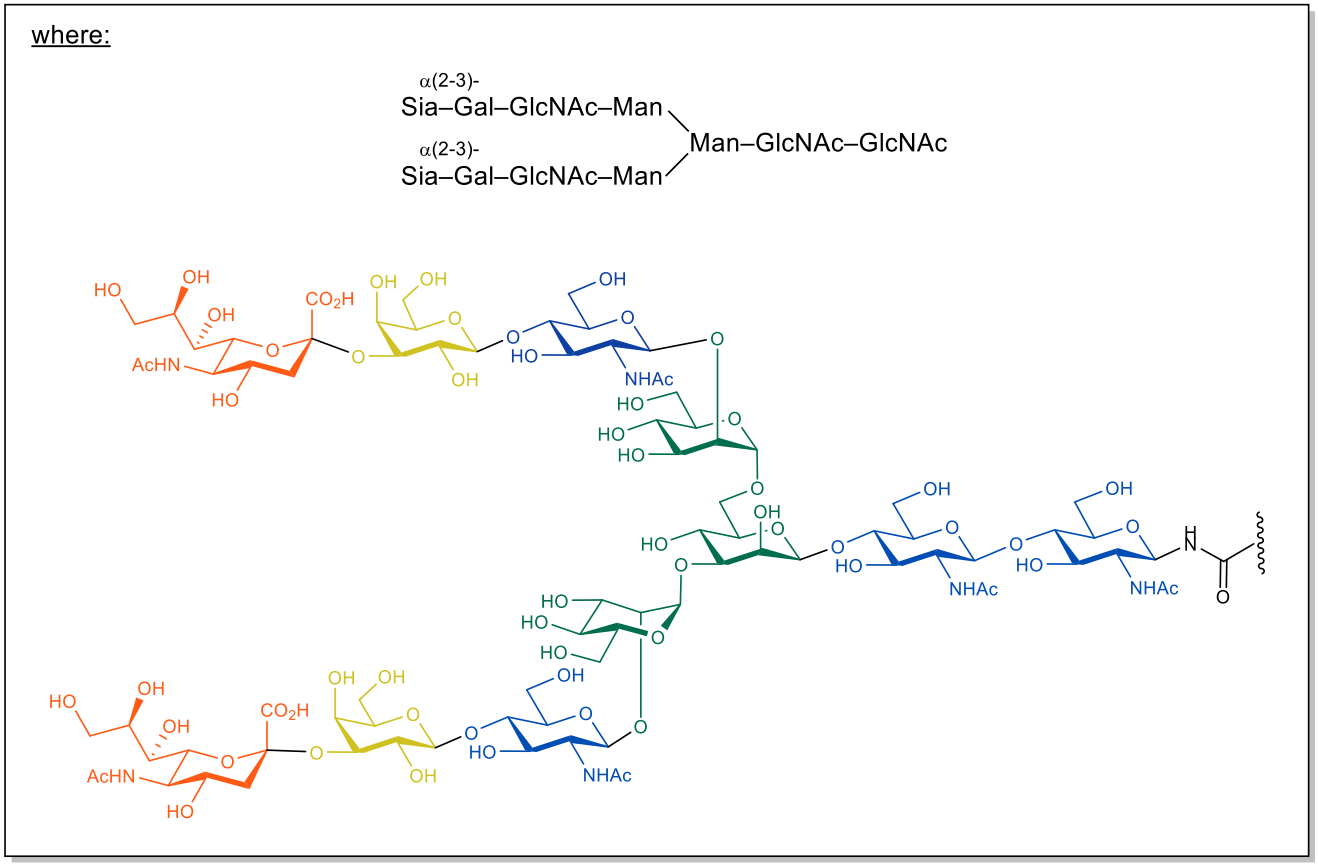

Supplementary Figure 2. Structure of the α(2,3)-Sia terminated glycan─aldehyde probe **XV**.

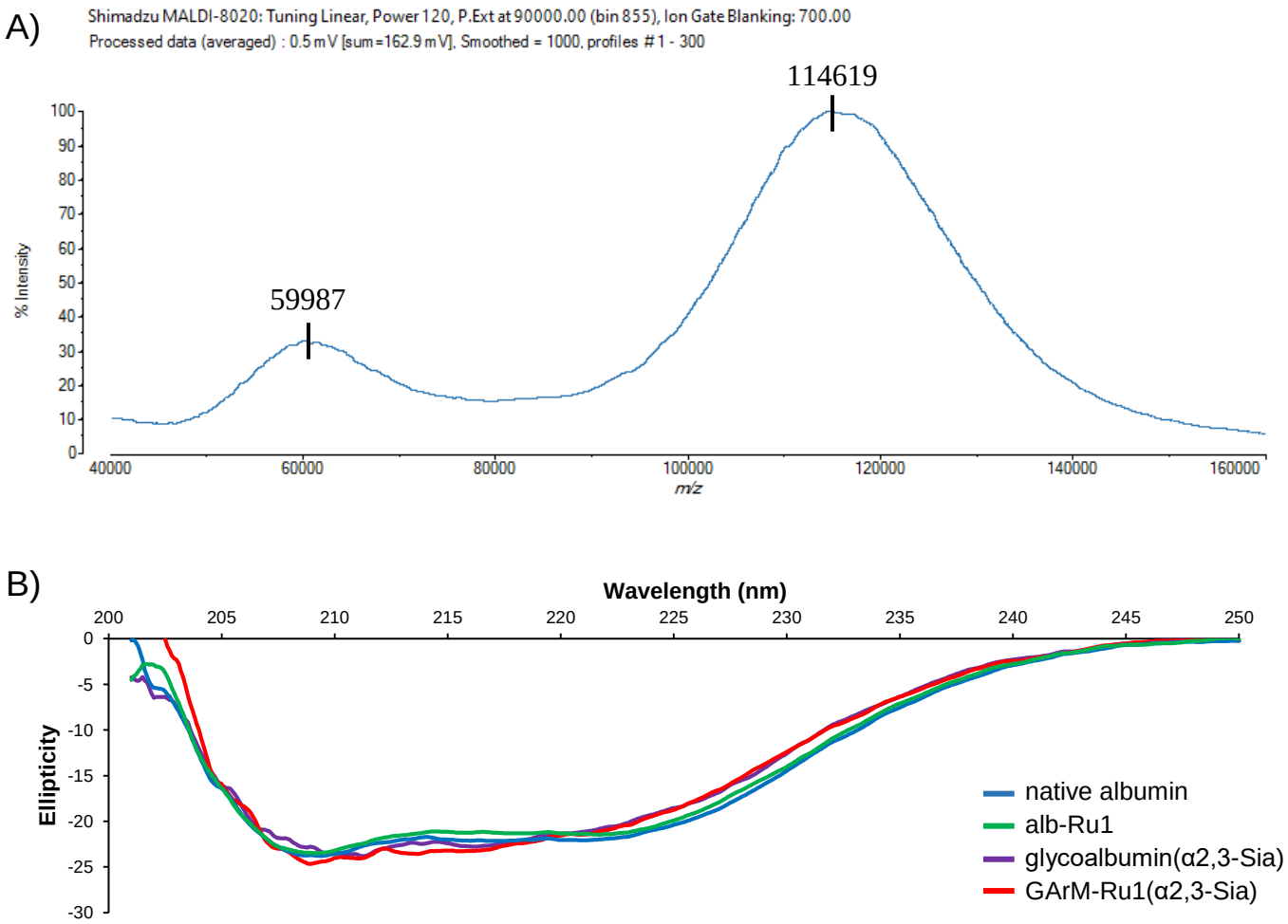

Supplementary Figure 3. Characterization of various protein structures in this study. A) MALDI-TOF-MS of GA showing a molecular weight of 114.6 kDa, which suggests that 15.4 molecules of glycan are conjugated per albumin. B) Overlaid CD spectra for 2.3 μM of either native albumin (blue), alb-Ru1 complex (green), GA (purple), and GArM-Ru complex (red).

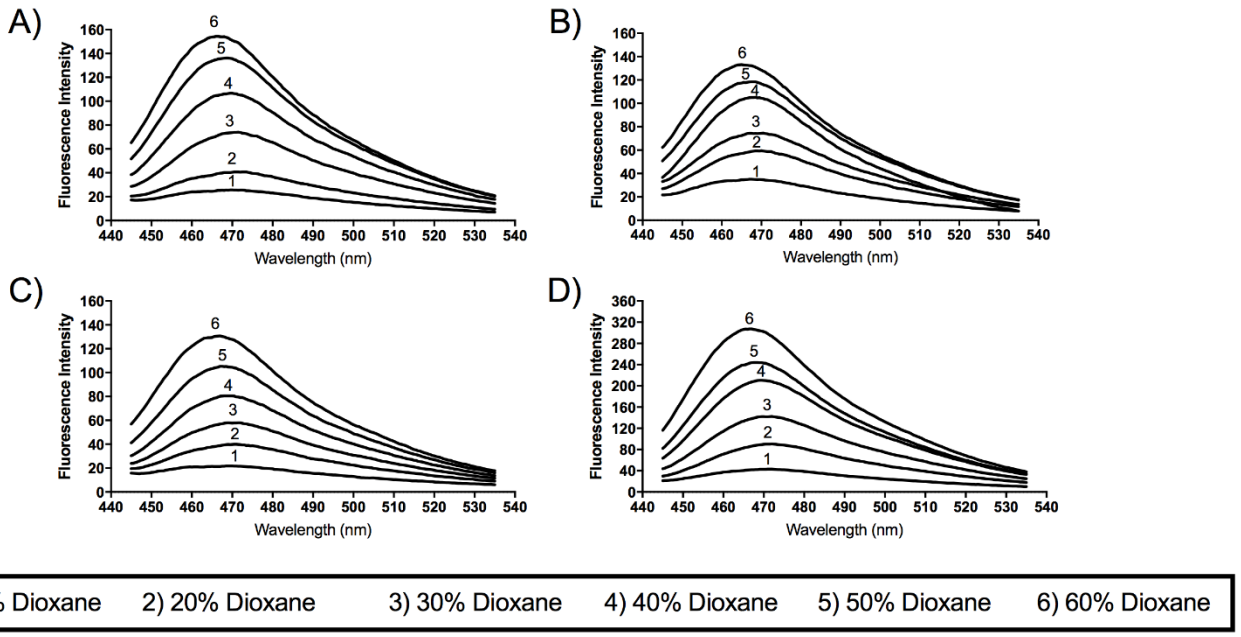

Supplementary Figure 4. Emission spectra under increasing concentrations of Dioxane in H_2O with A) **Ru1**, B) **Ru2**, C) **Ru3**, and D) **Ru6**. In this study, the fluorescence-emitting binding assay relies on the fact that coumarin-based molecules are highly sensitive to the polarity of the solvent. Coumarin-based molecules are typically non-fluorescent in aqueous solutions, but become highly fluorescent in nonpolar environments, such as the hydrophobic binding pockets of HSA. To investigate whether compounds **Ru1-3,6** can be used as a suitable probe, fluorescence measurements were taken for 7.5 μM of **Ru1-3,6** under increasing concentrations of Dioxane in H_2O at an excitation wavelength of 410 nm.

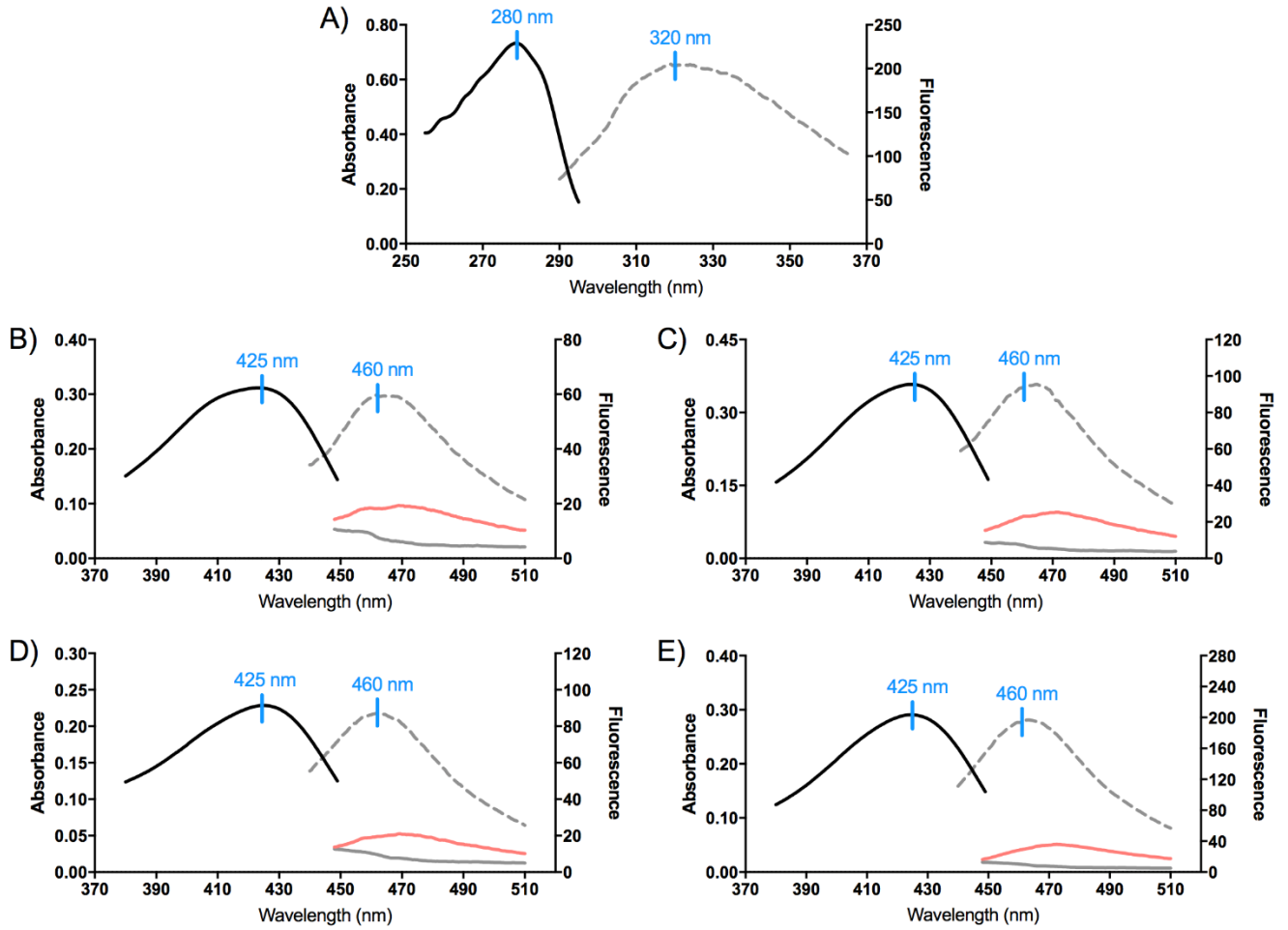

Supplementary Figure 5. Excitation (solid line) and emission (dotted line) spectra of molecules used for binding studies. Spectra of A) HSA, and 1:1 ligand-to-albumin complexes with B) **Ru1**, C) **Ru2**, D) **Ru3**, and E) **Ru6**. As a control, equivalent concentrations of compound-only (red line) and HSA-only (grey line) are shown. All compounds/albumin were used at a final concentration of 10 µM in 10% Dioxane/PBS buffer pH 7.4.

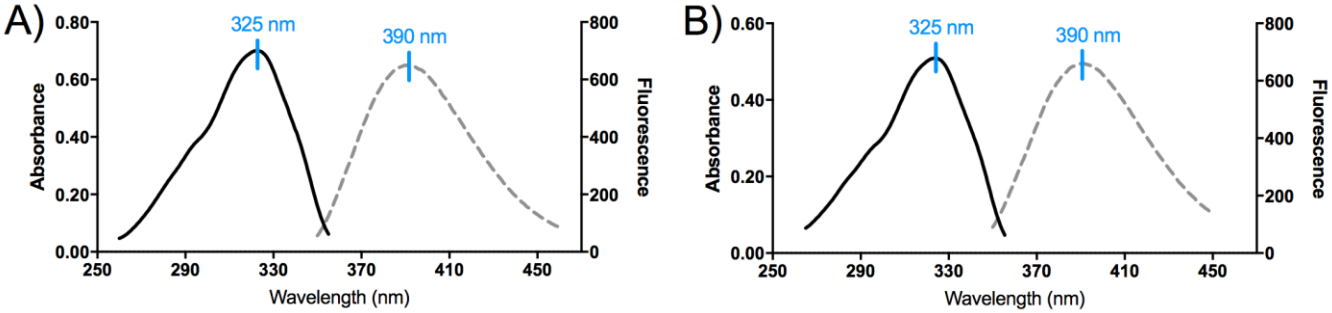

Supplementary Figure 6. Excitation (solid line) and emission (dotted line) spectra of coumarin-based substrates used in this study. Shown are spectra of A) **2g**, and B) **2h** (umbelliprenin) in 60% Dioxane/PBS buffer pH 7.4.

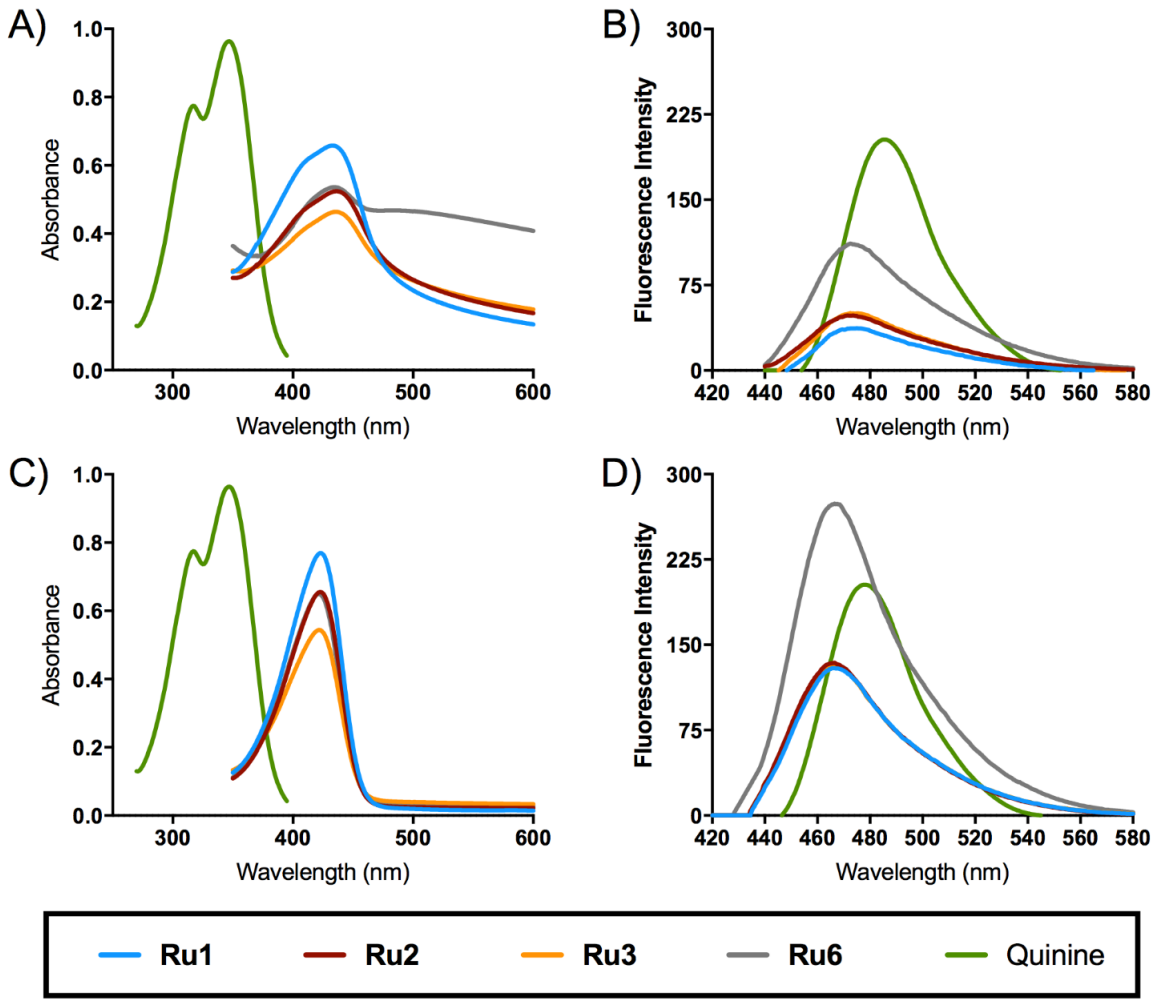

E)

	λ_{abs} [nm]	λ_{abs} [nm]	10% Dioxane in H_2O		60% Dioxane in H_2O	
			ε [M^{-1} cm^{-1}]	Φ_F ($\times10^{-3}$)	ε [M^{-1} cm^{-1}]	Φ_F ($\times10^{-3}$)
Ru1	425	460	18965 ± 1200	0.21 ± 0.02	42198 ± 359	4.2 ± 0.4
Ru2			14404 ± 751	0.40 ± 0.03	33333 ± 717	5.9 ± 1.3
Ru3			12619 ± 222	0.46 ± 0.03	27621 ± 709	7.3 ± 1.9
Ru6			15286 ± 938	0.88 ± 0.06	33559 ± 741	11.8 ± 2.6

Supplementary Figure 7. Photophysical characterization of **Ru1-3,6**. A) Overlay of absorbance spectra in 10% Dioxane in H_2O. B) Overlay of emission spectra in 10% Dioxane in H_2O with fixed excitation (425 nm). C) Overlay of absorbance spectra in 60% Dioxane in H_2O. D) Overlay of emission spectra in 60% Dioxane in H_2O with fixed excitation (425 nm). E) Calculated quantum yields of **Ru1-3,6** under solvent conditions of 10% and 60% Dioxane in H_2O. Literature values used were the refractive index of 10% Dioxane in H_2O (n_X = 1.3396) and 60% Dioxane in H_2O (n_X = 1.3868),[1] the refractive index of 1N H_2SO_4 (n_S = 1.346),[2] and the quantum yield of quinine sulfate ($\Phi_{F(S)}$ = 0.546 in 1N H_2SO_4).[2] The following nomenclature is used: quantum yield (Φ_F); extinction coefficient (ε); refractive index of solvent (n); while subscripts represent to the unknown (X) and standard (S). Error is represented as the standard deviation of three replicate measurements.

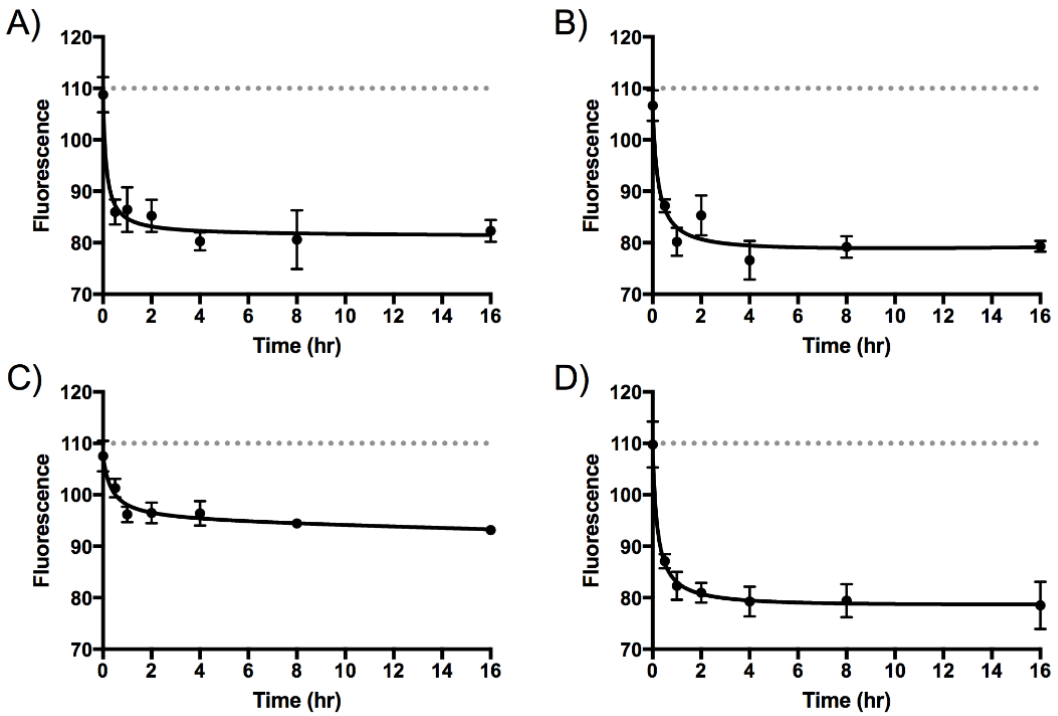

Supplementary Figure 8. Fluorescent quenching-based binding monitored over time between 10 µM of HSA and 10 µM of either A) **Ru1**, B) **Ru2**, C) **Ru3**, and D) **Ru6**. Incubations were done in 10% dioxane/PBS buffer pH 7.4 and monitored at λ_{EX} = 280 nm/λ_{EM} = 320 nm. As a result, an incubation time of 1 hr was deemed most appropriate for this study. Error bars represent the standard deviation of three replicate measurements.

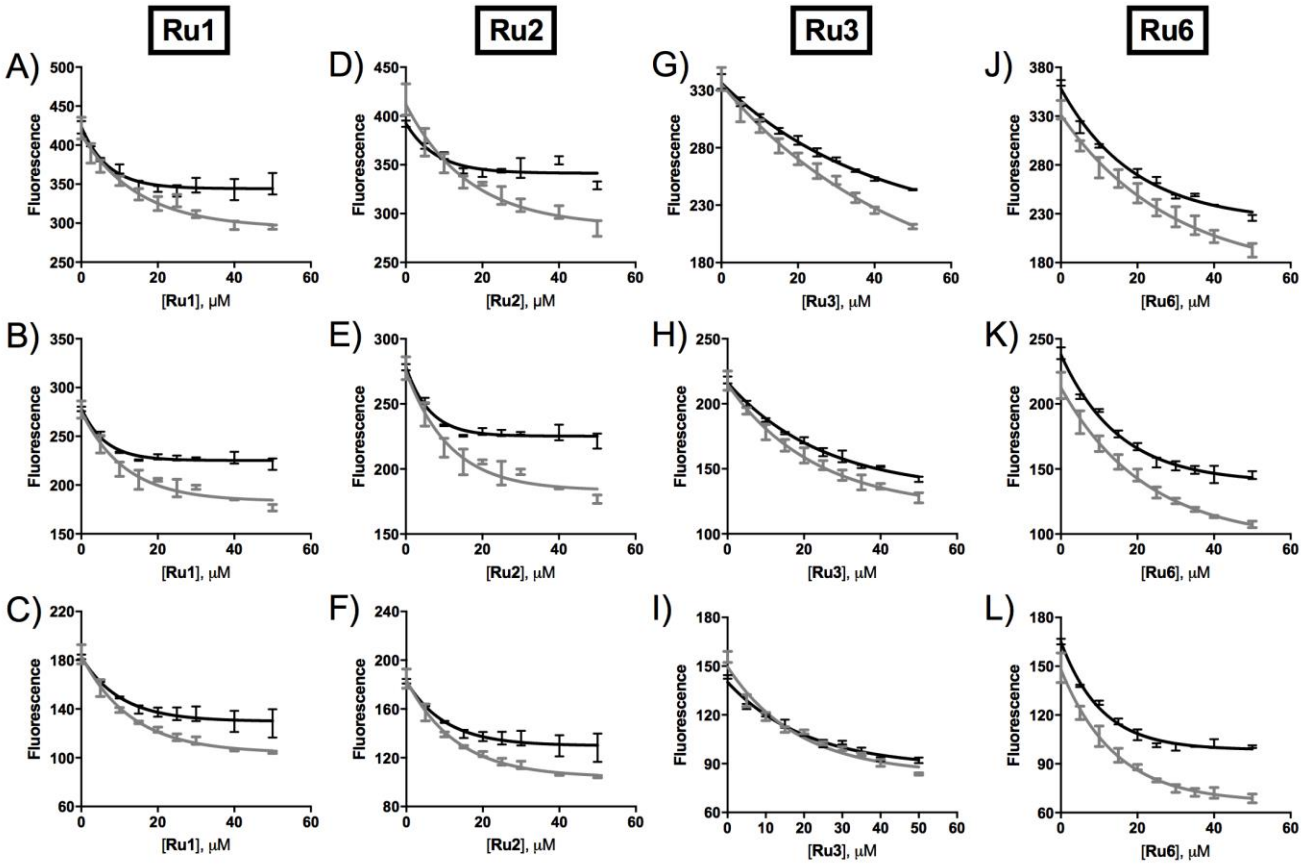

Supplementary Figure 9. Fluorescence quenching measurements from HSA binding to A) 30 μM of **Ru1**, B) 15 μM of **Ru1**, C) 7.5 μM of **Ru1**, D) 30 μM of **Ru2**, E) 15 μM of **Ru2**, F) 7.5 μM of **Ru2**, G) 20 μM of **Ru3**, H) 10 μM of **Ru3**, I) 5 μM of **Ru3**, J) 20 μM of **Ru6**, K) 10 μM of **Ru6**, and L) 5 μM of **Ru6**. Shown are the values obtained before (grey line) and after (black line) spin-column purification. Incubations were done in 10% Dioxane/PBS buffer pH 7.4 and monitored at λ_{EX} = 280 nm/λ_{EM} = 320 nm. Error bars represent the standard deviation of three replicate measurements.

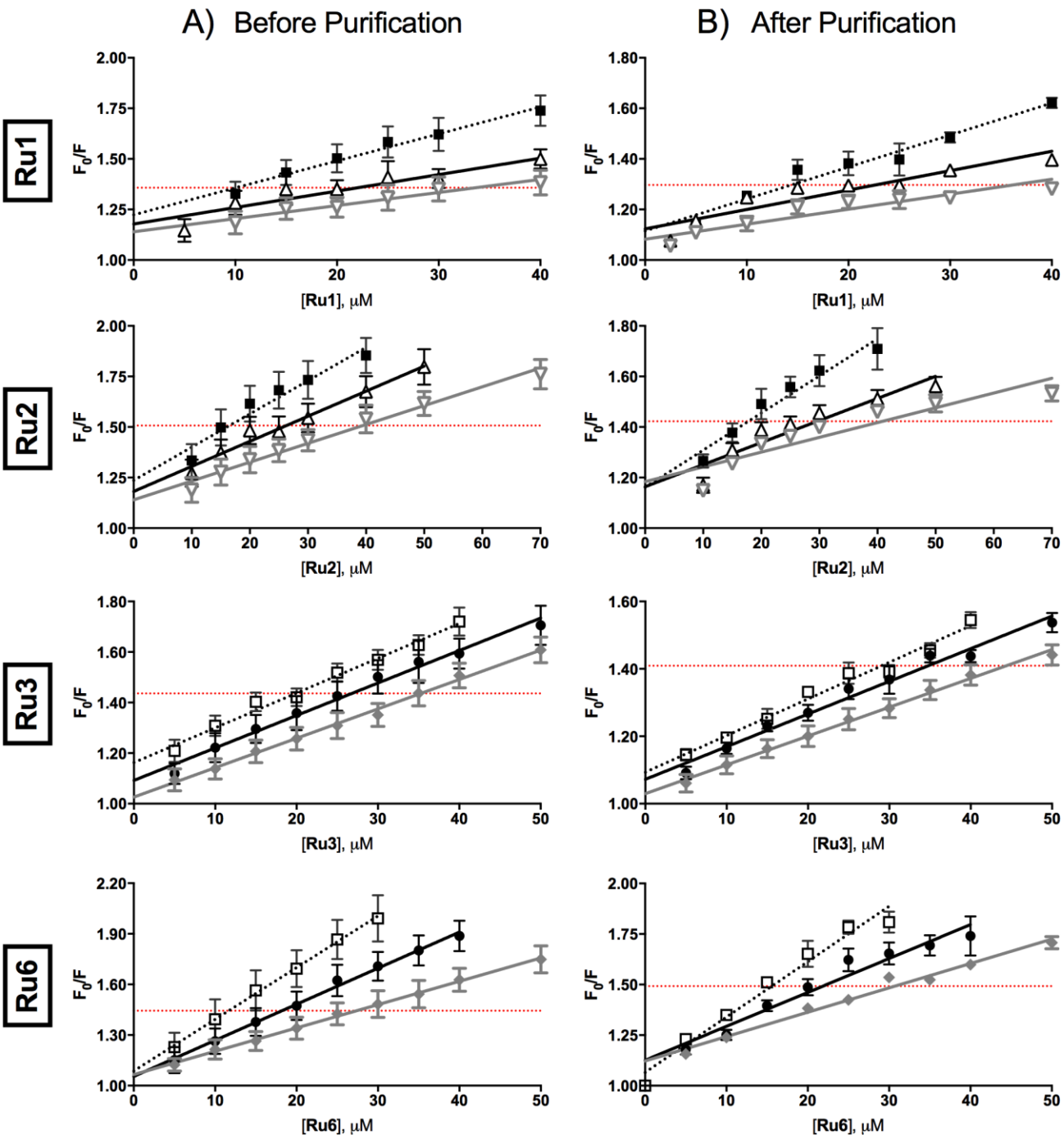

Supplementary Figure 10. Stern-Volmer plots for the quenching of albumin intrinsic fluorescence by compounds **Ru1-3,6** under varying concentrations of HSA, as depicted: 5 μM (□); 7.5 μM (■); 10 μM (●); 15 μM (△); 20 μM (♦); 30 μM (▽). Graphs are arranged to show values obtained before and after spin-column purification. The horizontal lines depict the F_0/F values used for compound **Ru1** (1.3573 and 1.2967), compound **Ru2** (1.5069 and 1.4225), compound **Ru3** (1.4360 and 1.4091), and compound **Ru6** (1.4438 and 1.4921) before and after purification, respectively. Error bars represent the standard deviation of three replicate measurements.

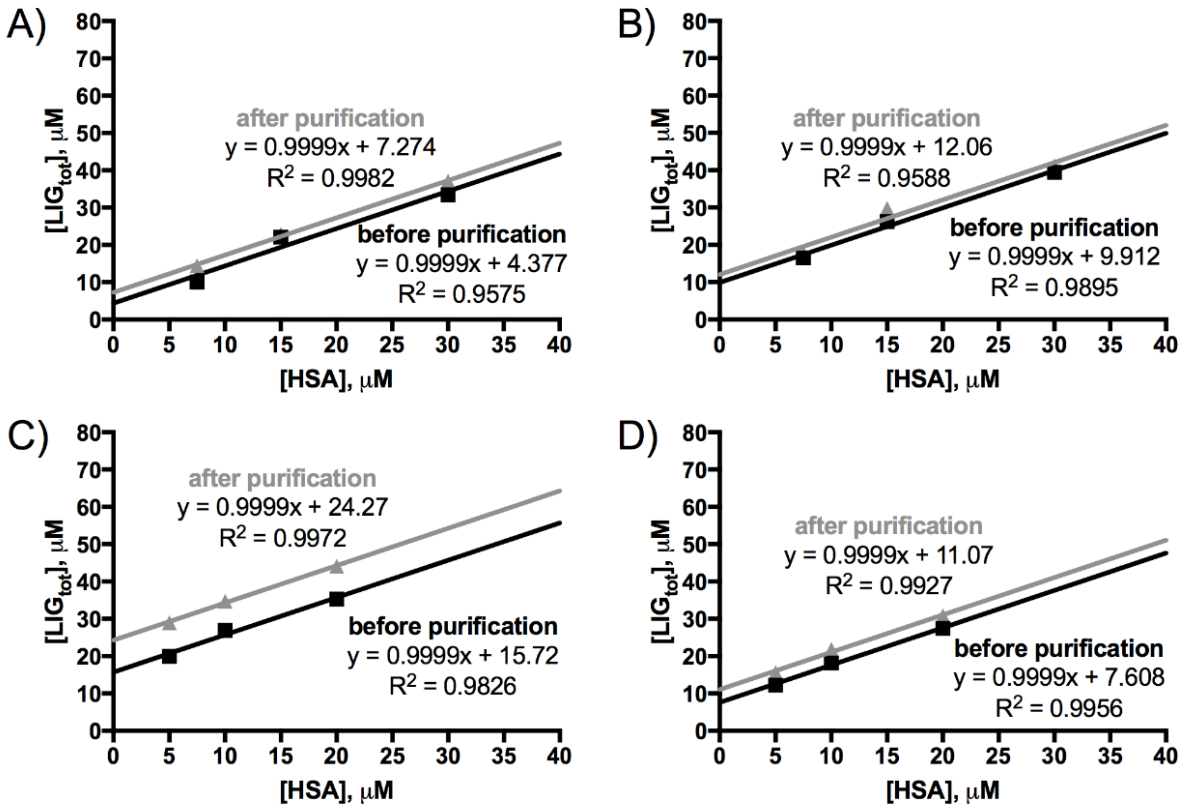

Supplementary Figure 11. Total ligand concentrations needed to produce a given F_0/F value as a function of HSA concentration. Shown are the plots obtained for the ligands under study; A) compound **Ru1**, B) compound **Ru2**, C) compound **Ru3**, and D) compound **Ru6**.

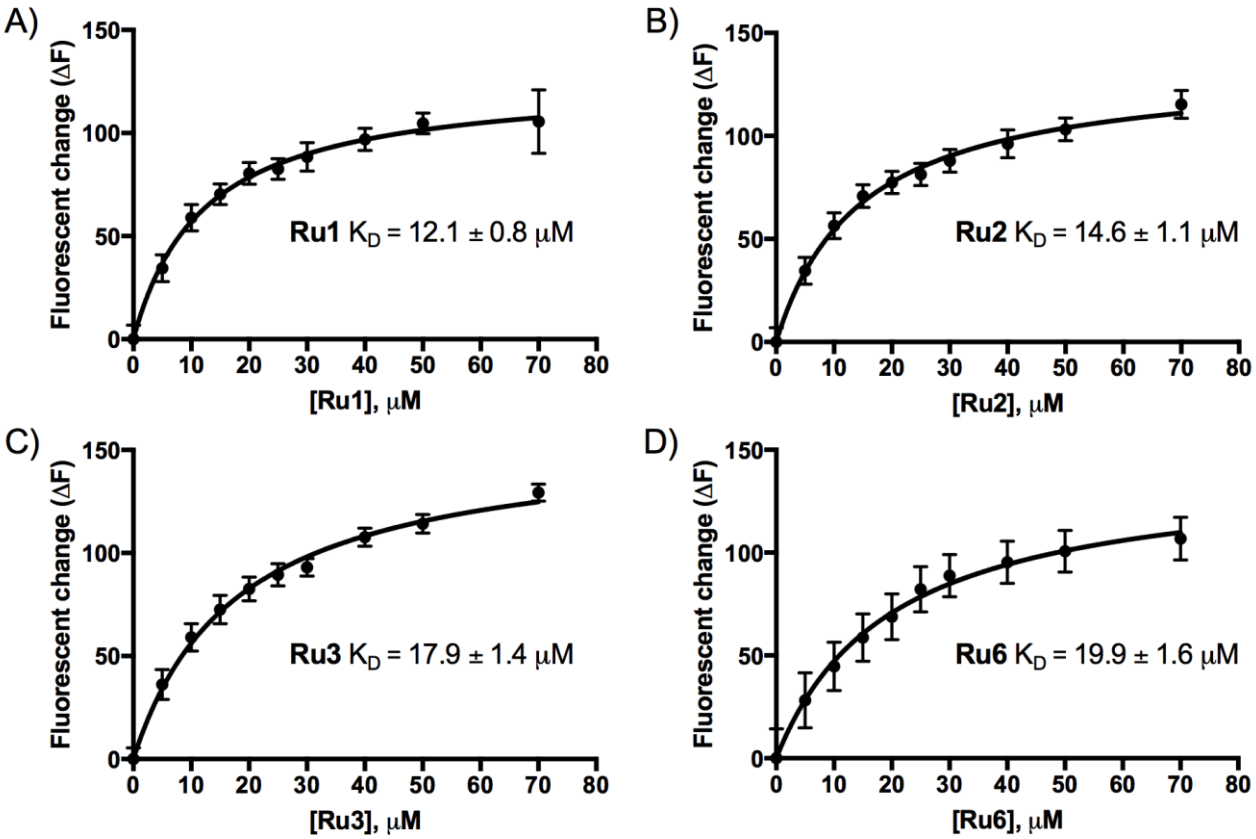

Supplementary Figure 12. Saturation binding curves based on the fluorescent quenching of HSA when bound to A) **Ru1**, B) **Ru2**, C) **Ru3**, and D) **Ru6**. Experiments were conducted at HSA concentrations of 10 μM (black line). The measured equilibrium dissociation constants (K_D) were determined by non-linear regression. Incubations were performed at 37 °C for 1 hr in 10% Dioxane/PBS buffer pH 7.4 and monitored at λ_{EX}=280 nm/λ_{EM}=320 nm. Error bars represent the standard deviation of three replicate measurements.

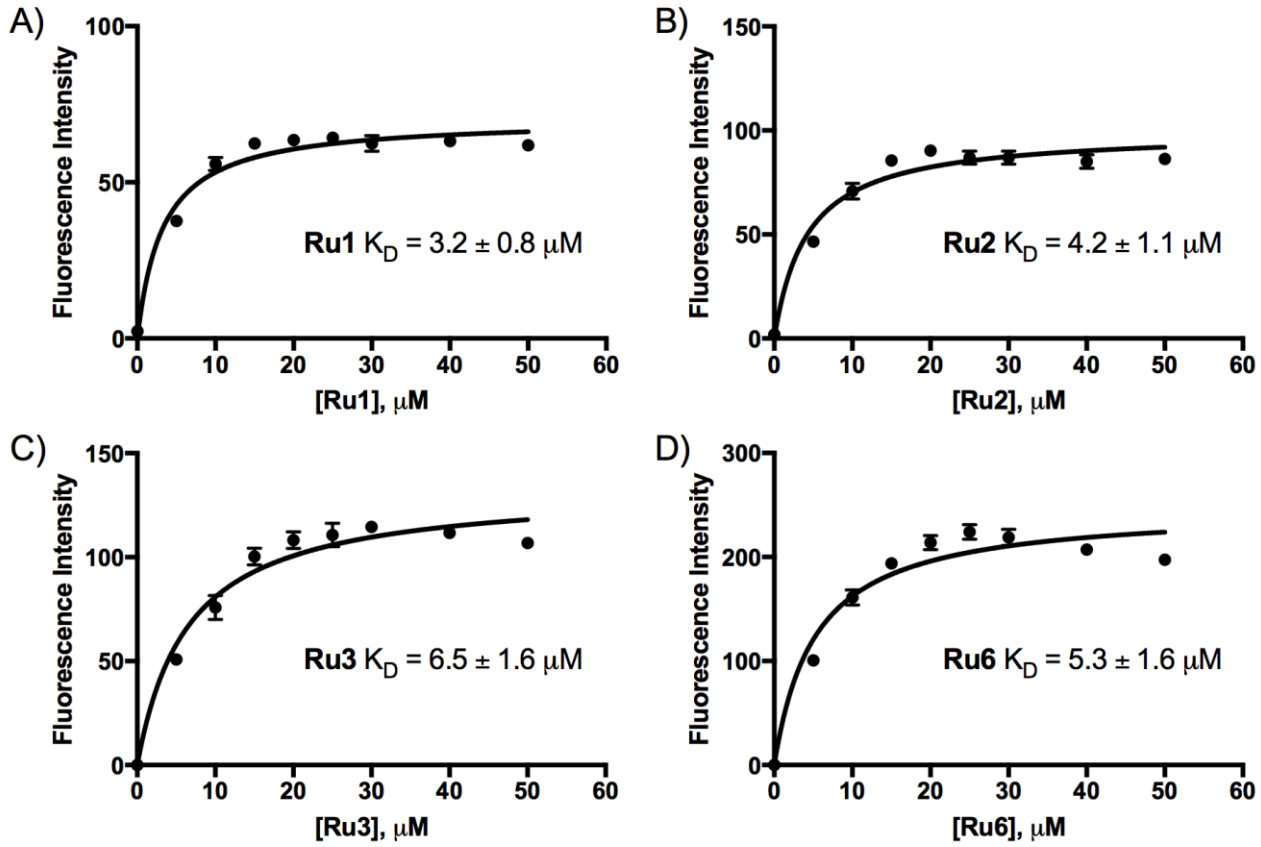

Supplementary Figure 13. Saturation binding curves based on the fluorescence emitted from A) **Ru1**, B) **Ru2**, C) **Ru3**, and D) **Ru6**, when bound to HSA. Experiments were conducted at HSA concentrations of 10 μM (black line). The measured equilibrium dissociation constants (K_D) were determined by non-linear regression. Incubations were performed at 37 °C for 1 hr in 10% Dioxane/PBS buffer pH 7.4 and monitored at λ_{EX}=425nm/λ_{EM}=460nm. Error bars represent the standard deviation of three replicate measurements.

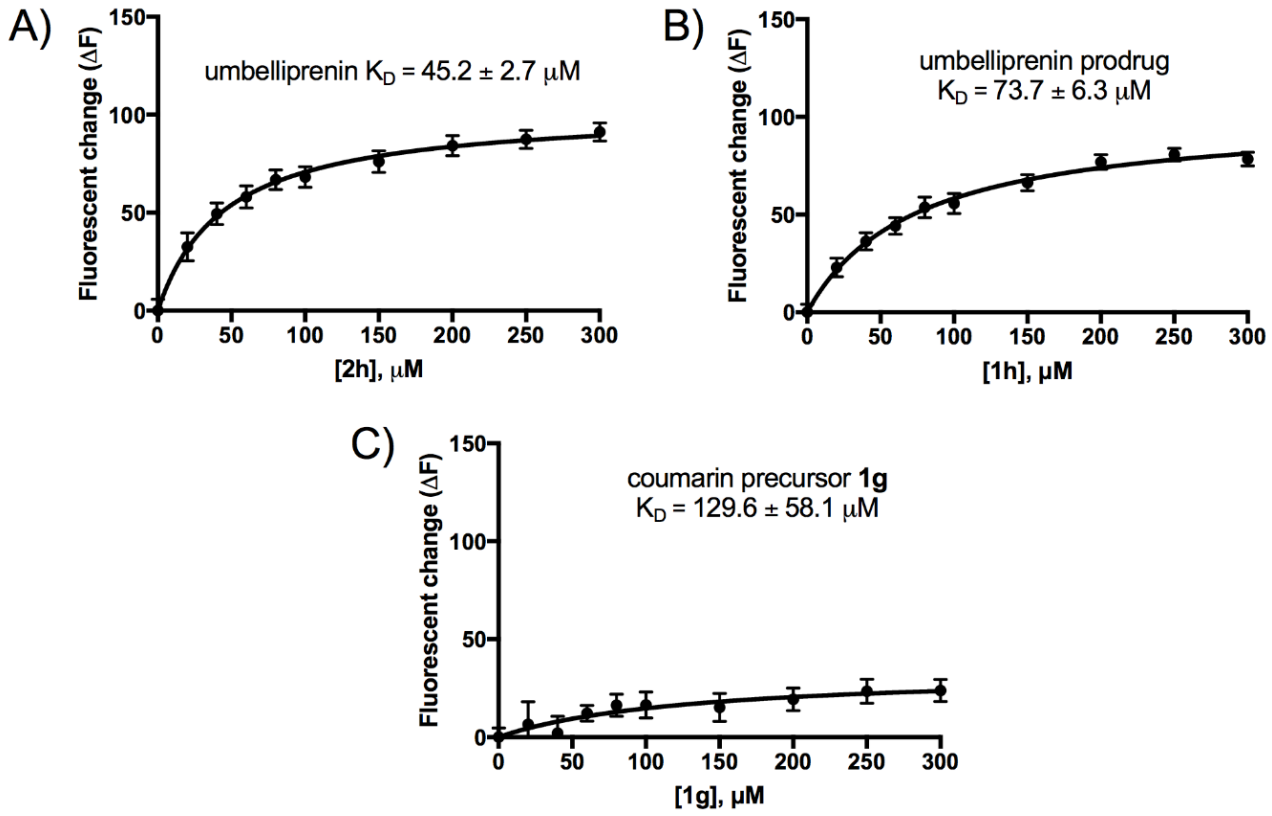

Supplementary Figure 14. Saturation binding curves based on the fluorescent quenching of HSA when bound to A) umbelliprenin **2h**, B) umbelliprenin prodrug **1h**, and C) coumarin precursor **1g**. Experiments were conducted at HSA concentrations of 10 μM (black line). The measured equilibrium dissociation constants (K_D) were determined by non-linear regression. Incubations were performed at 37 °C for 1 hr in 10% dioxane/PBS buffer pH 7.4 and monitored at λ_{EX}=280 nm/λ_{EM}=320 nm. Error bars represent the standard deviation of three replicate measurements.

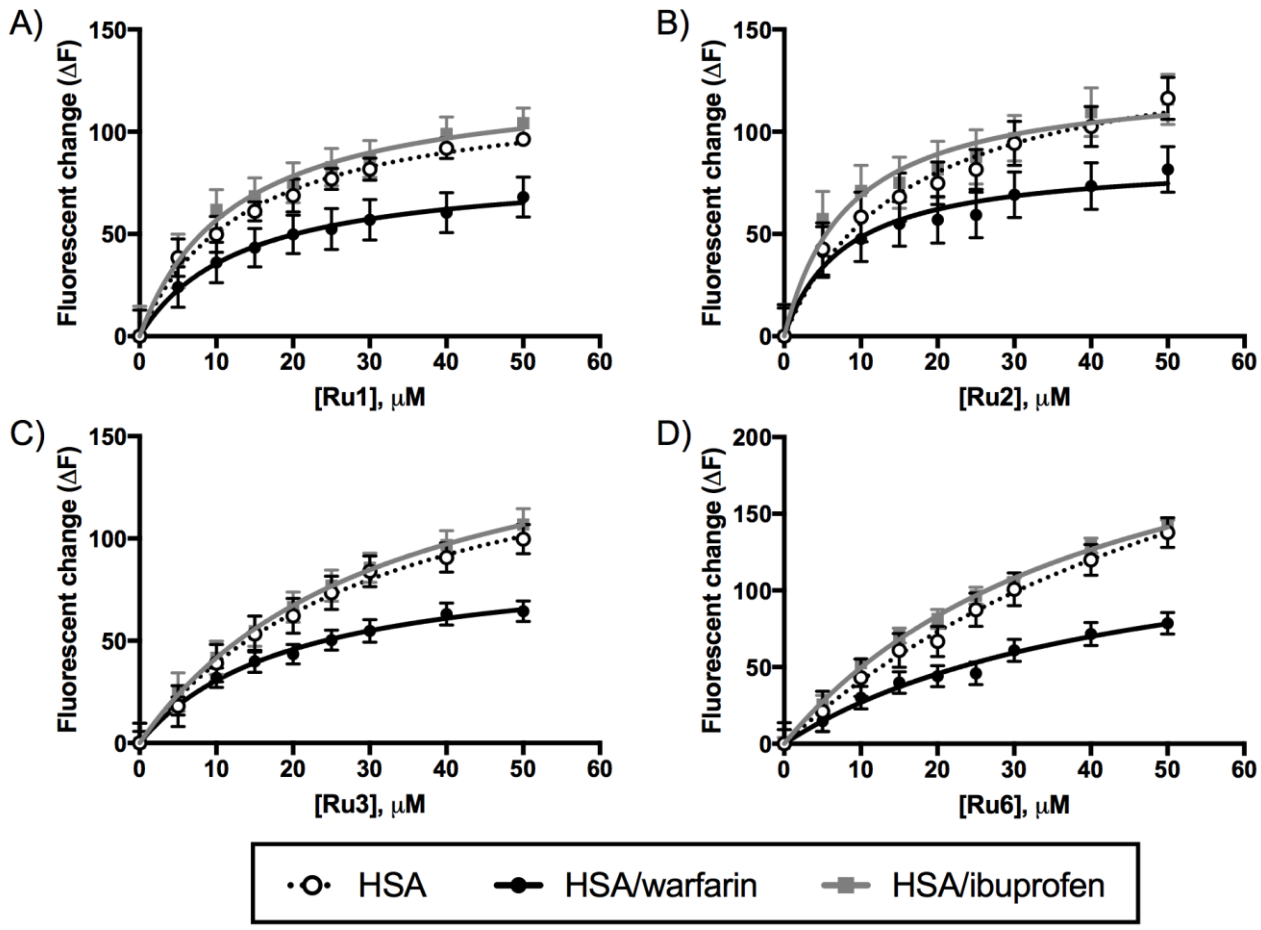

Supplementary Figure 15. Saturation binding curves based on the fluorescent quenching of HSA (dotted line), HSA preincubated with warfarin (black line), and HSA preincubated with ibuprofen (grey line). Preincubation was carried out with 20 μM of albumin and 40 μM of either buffer (control), warfarin, or ibuprofen for 1 hr at 37 °C. Binding to A) **Ru1**, B) **Ru2**, C) **Ru3**, and D) **Ru6**, was then tested at 37 °C for 1 hr in 10% Dioxane/PBS buffer pH 7.4 and monitored at λ_{EX}=280 nm/λ_{EM}=320 nm. Error bars represent the standard deviation of three replicate measurements.

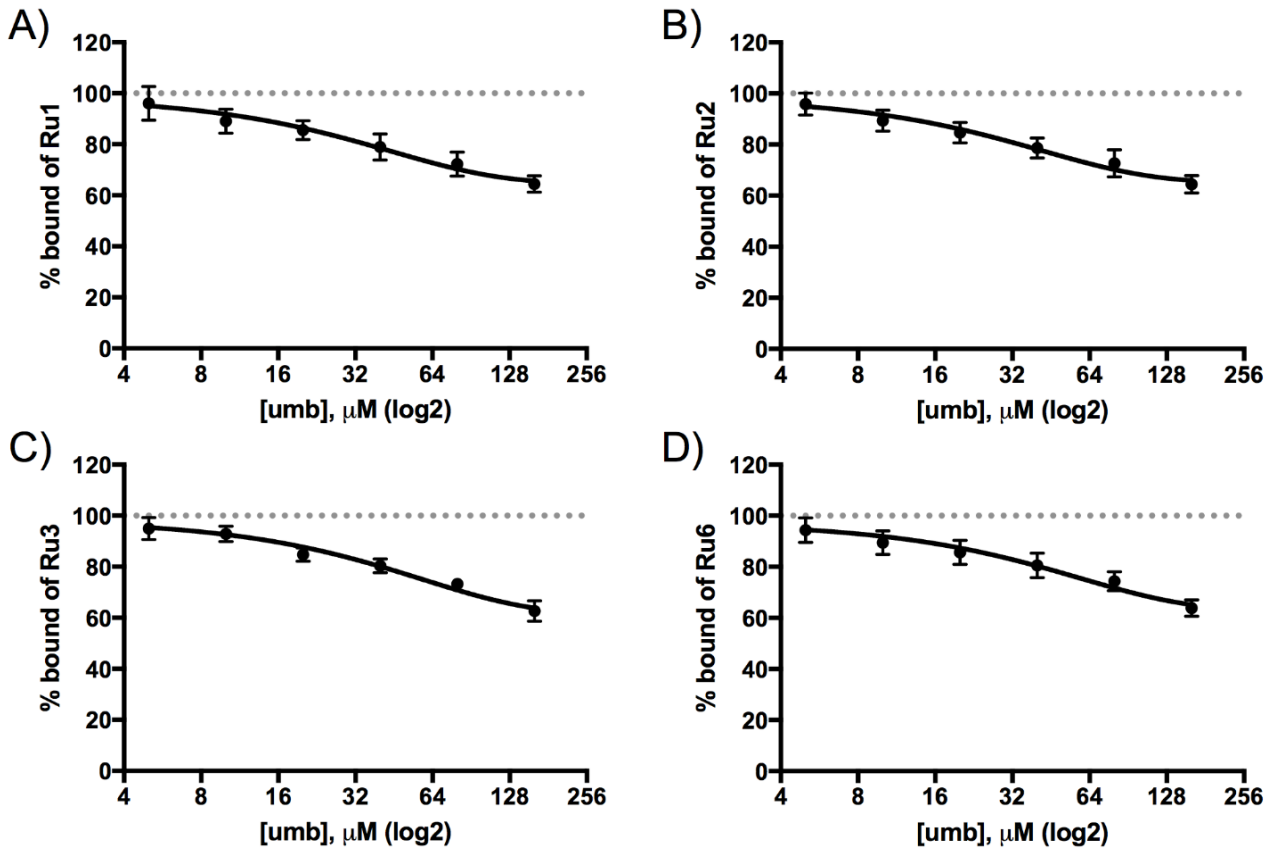

Supplementary Figure 16. Displacement assay to monitor the percentage of bound compounds **Ru1**-**3,6** to albumin in the presence of varying concentrations of **2h** (umb). Preincubations were done with 10 μM of either A) **Ru1**, B) **Ru2**, C) **Ru3**, or D) **Ru6** with HSA (10 μM) for 1 hr at 37 °C in 5% Dioxane/PBS buffer pH 7.4. Varying concentrations of umbelliprenin was then added and the mixture was further incubated for 1 hr at 37 °C in 10% Dioxane/PBS buffer pH 7.4. Fluorescence was monitored at λ_{EX}=425 nm/λ_{EM}=460 nm and the percentage bound was calculated based on the initial fluorescence in the absence of umbelliprenin. Error bars represent the standard deviation of three replicate measurements.

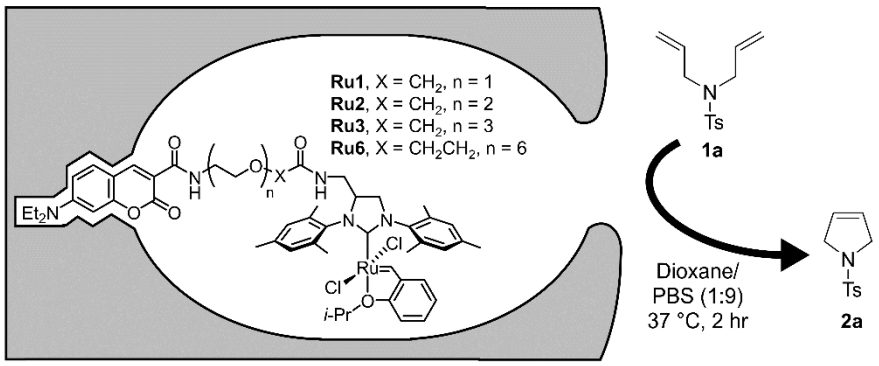

alb-Ru complex

Sub.	Catalyst loading	alb-Ru complex			
		Ru1 (n = 1)	**Ru2** (n = 2)	**Ru3** (n = 3)	**Ru6** (n = 6)
1a	5 mol%	*TON:* 1.5 ± 0.03 *Yield:* 7%	*TON:* 0.8 ± 0.01 *Yield:* 4%	*TON:* 0.5 ± 0.10 *Yield:* 3%	*TON:* 0.2 ± 0.01 *Yield:* 1%
	10 mol%	*TON:* 2.9 ± 0.02 *Yield:* 29%	*TON:* 1.6 ± 0.01 *Yield:* 16%	*TON:* 0.5 ± 0.01 *Yield:* 5%	*TON:* 0.2 ± 0.01 *Yield:* 2%
	25 mol%	*TON:* 2.4 ± 0.01 *Yield:* 59%	*TON:* 1.5 ± 0.01 *Yield:* 37%	*TON:* 0.3 ± 0.03 *Yield:* 9%	*TON:* 0.1 ± 0.02 *Yield:* 2%
	50 mol%	*TON:* 1.8 ± 0.01 *Yield:* 89%	*TON:* 1.5 ± 0.01 *Yield:* 74%	*TON:* 0.3 ± 0.01 *Yield:* 13%	*TON:* 0.1 ± 0.01 *Yield:* 2%

Supplementary Figure 17. Reactivity of substrate **1a** using varying levels of catalyst loading (5, 10, 25, and 50 mol%). Displayed are both the obtained product yields of **2a** and TON values. Error is represented as the standard deviation of three independent experiments.

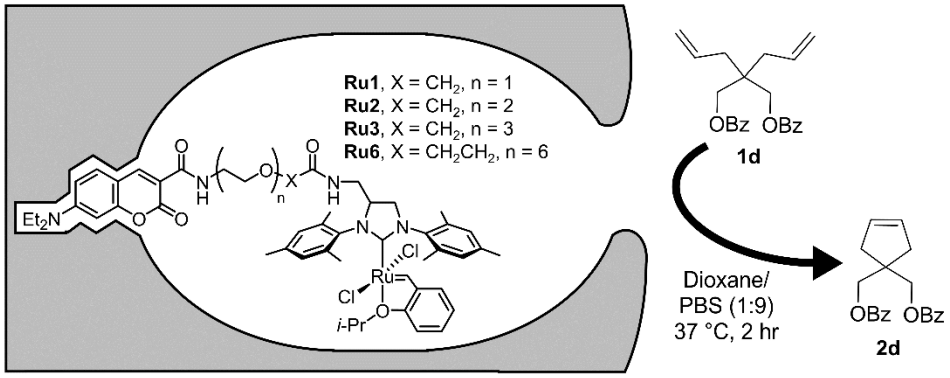

alb-Ru complex

Sub.	Catalyst loading	alb-Ru complex			
		Ru1 (n = 1)	**Ru2** (n = 2)	**Ru3** (n = 3)	**Ru6** (n = 6)
1d	0.5 mol%	*TON:* 24.8 ± 1.47 *Yield:* 12%	*TON:* 3.5 ± 0.31 *Yield:* 2%	*TON:* 0.8 ± 0.06 *Yield:* 0.4%	*TON:* 0.7 ± 0.04 *Yield:* 0.3%
	1 mol%	*TON:* 18.9 ± 0.55 *Yield:* 19%	*TON:* 4.0 ± 0.39 *Yield:* 4%	*TON:* 0.7 ± 0.05 *Yield:* 0.7%	*TON:* 0.7 ± 0.01 *Yield:* 0.7%
	2 mol%	*TON:* 21.9 ± 0.60 *Yield:* 43%	*TON:* 4.7 ± 0.15 *Yield:* 9%	*TON:* 0.6 ± 0.01 *Yield:* 1.1%	*TON:* 0.5 ± 0.01 *Yield:* 0.9%
	4 mol%	*TON:* 15.4 ± 0.94 *Yield:* 61%	*TON:* 3.6 ± 0.02 *Yield:* 14%	*TON:* 0.4 ± 0.02 *Yield:* 1.5%	*TON:* 0.3 ± 0.01 *Yield:* 1.2%

Supplementary Figure 18. Reactivity of substrate **1d** using varying levels of catalyst loading (0.5, 1, 2, and 4 mol%). Displayed are both the obtained product yields of **2d** and TON values. Error is represented as the standard deviation of three independent experiments.

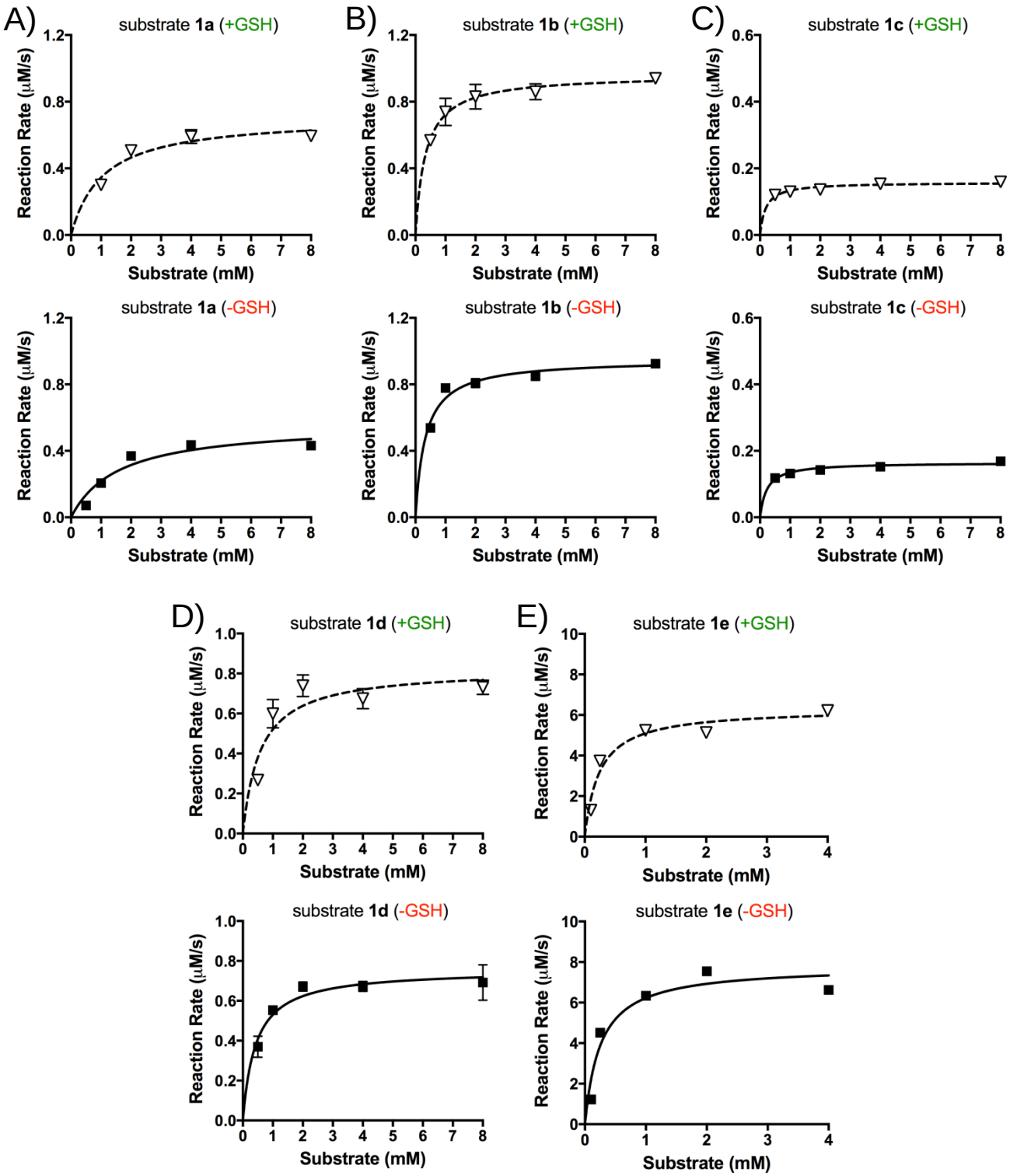

Supplementary Figure 19. Michaelis-Menten plots of the substrates A) **1a**, B) **1b**, C) **1c**, D) **1d**, and E) **1e**, both in the presence of 10 equivalents of glutathione (green title) or absence of glutathione (red title). The concentration of alb-Ru1 used was 10 μM. Error bars represent the standard deviation of three independent experiments.

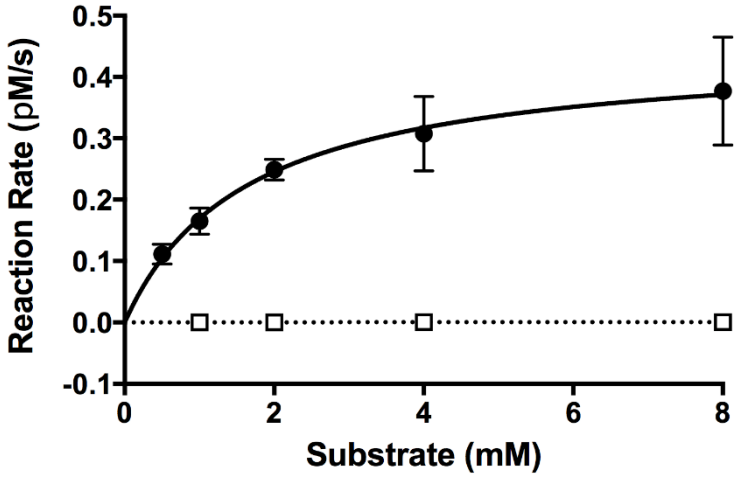

	V_{max} (pM/s)	K_M (mM)	k_{cat} (s^{-1})	k_{cat}/K_M (M^{-1} s^{-1})	R^2
1g	0.001 ± 0.001	5.51 ± 3.44	0.00005 ± 0.00001	0.009 ± 0.006	0.912
1h	0.448 ± 0.047	1.65 ± 0.49	0.02238 ± 0.00236	13.6 ± 4.3	0.899
initial velocity values were obtained in triplicate					

Supplementary Figure 20. Michaelis-Menten plots of the substrates **1g** (dotted line) and **1h** (black line). The concentration of alb-Ru1 used was 20 µM. Reactivity was performed using varying concentrations of substrate with 20 µm of alb-Ru1 in MES buffer pH 6.0. Summarized values are the maximum velocity (V_{max}), substrate affinity (K_M), turnover frequency (k_{cat}), catalytic efficiency (k_{cat}/K_M), and the coefficient of determination (R^2). Error bars represent the standard deviation of three independent experiments.

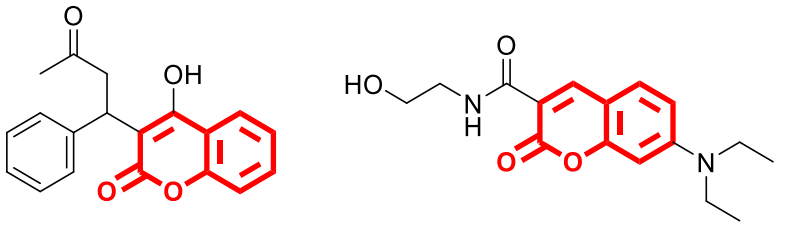

Supplementary Figure 21. Structural comparison between warfarin and DECA. Highlighted in red is the core coumarin ring moiety shared between these compounds. Warfarin is a well-known ligand of the drug site I binding pocket in human serum albumin,[3-4] as confirmed by several PDB crystal structures (ex/ 2BXD, 1H9Z, 1HA2). In this study, ruthenium catalysts are anchored to the albumin protein via a coumarin-based derivative, otherwise referred to as a 7-(diethylamino)coumarin-3-carboxamide moiety (or simply as DECA).

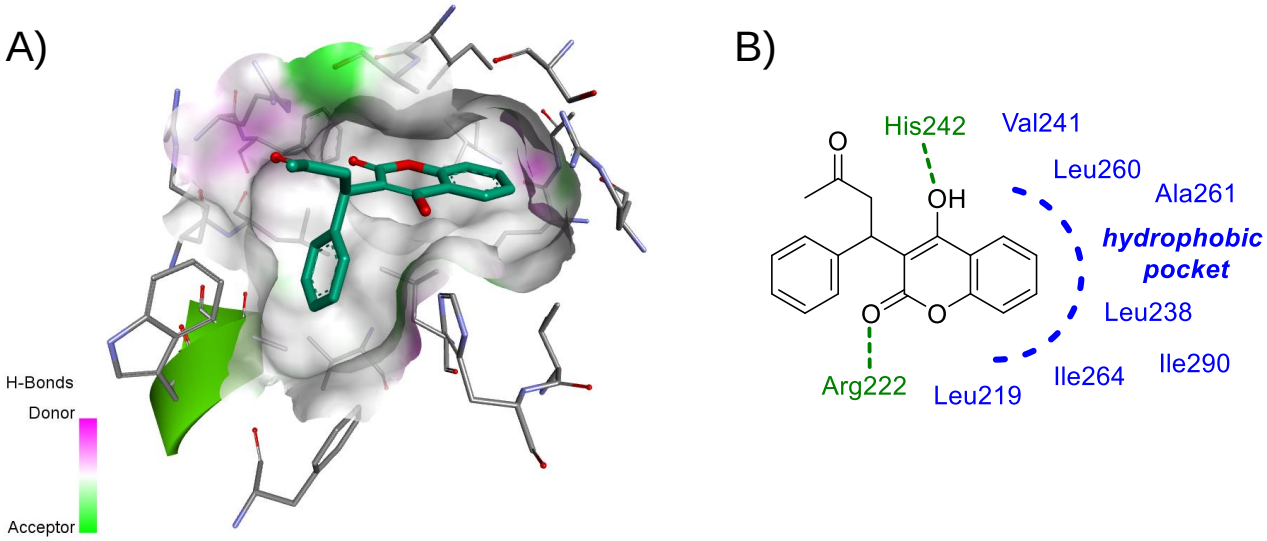

Supplementary Figure 22. Crystallized warfarin in the drug site I binding pocket of albumin (PDB 1H9Z). A) View of the surface and residues around the ligand in the binding pocket. Hydrophobic surfaces are represented in grey, with hydrogen bonding surfaces represented by purple/light green. B) Cartoon representation of the major ligand-protein interactions. Closer analysis of warfarin crystallized with albumin reveals that affinity to the drug site I binding pocket is mainly conferred via hydrophobic interactions. Warfarin is largely surrounded by hydrophobic residues, with the only exceptions being hydrogen bonding interactions with Arg222 and His242.

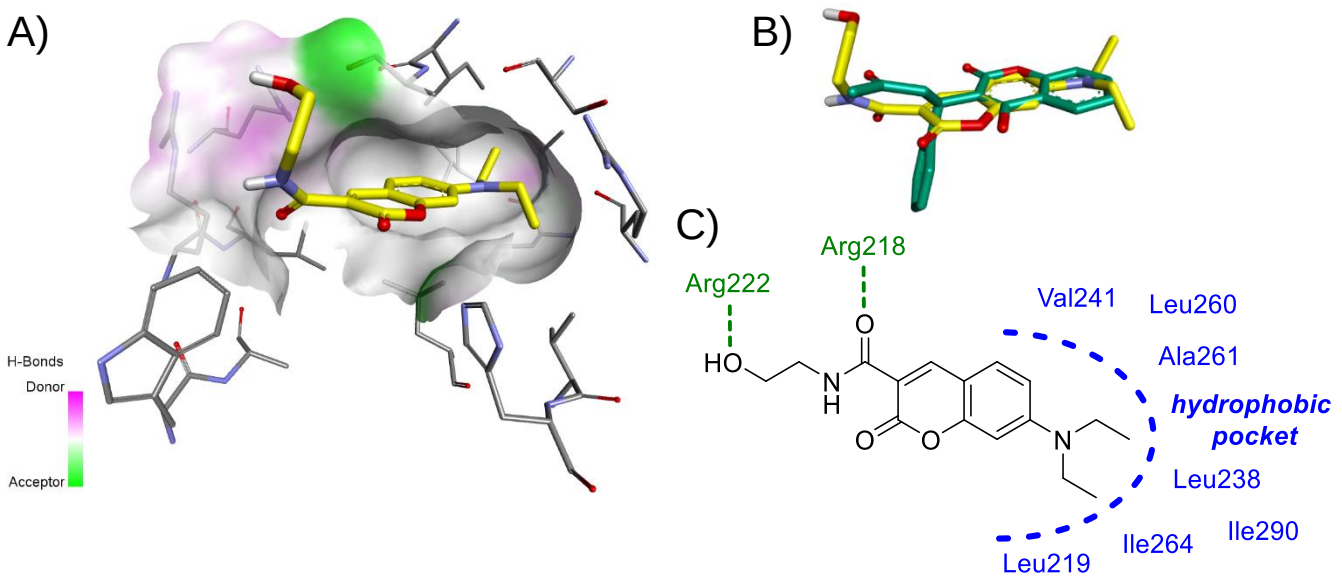

Supplementary Figure 23. Modeled docking of DECA in the drug site I binding pocket of albumin (PDB 1H9Z) with a calculated binding affinity of -6.3 kcal/mol. A) View of the surface and residues around the ligand in the binding pocket. Hydrophobic surfaces are represented in grey, with hydrogen bonding surfaces represented by purple/light green. B) Overlay of DECA (yellow) and warfarin (turquoise) binding configurations. C) Cartoon representation of the major ligand-protein interactions. For these calculations, a grid box of 15×15×15 points centered at 33.91, 14.378, 9.587 (x,y,z) with a spacing of 0.375 Å between grid points was used. As a note, the generated docking configuration aligns well with the co-crystallized warfarin ligand, suggesting a similar binding mechanism based mainly on hydrophobic interactions.

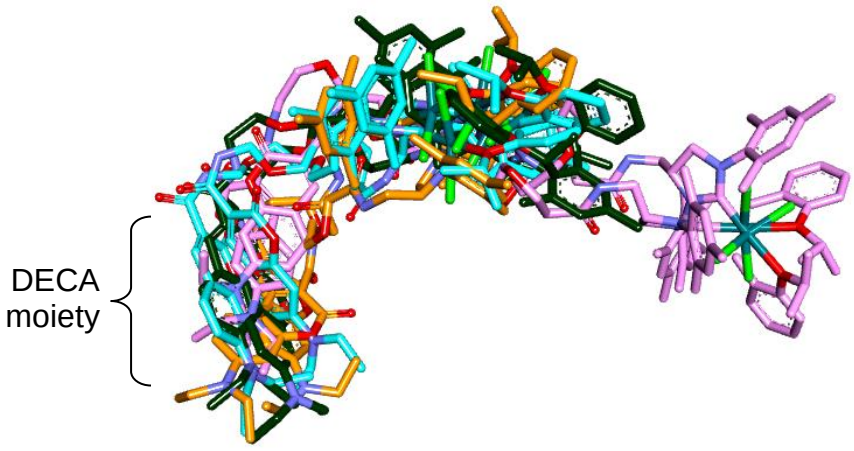

Supplementary Figure 24. Overlay of both R- and S- enantiomers of compounds **Ru1** (orange), **Ru2** (light blue), **Ru3** (dark green), and **Ru6** (pink) binding configurations.

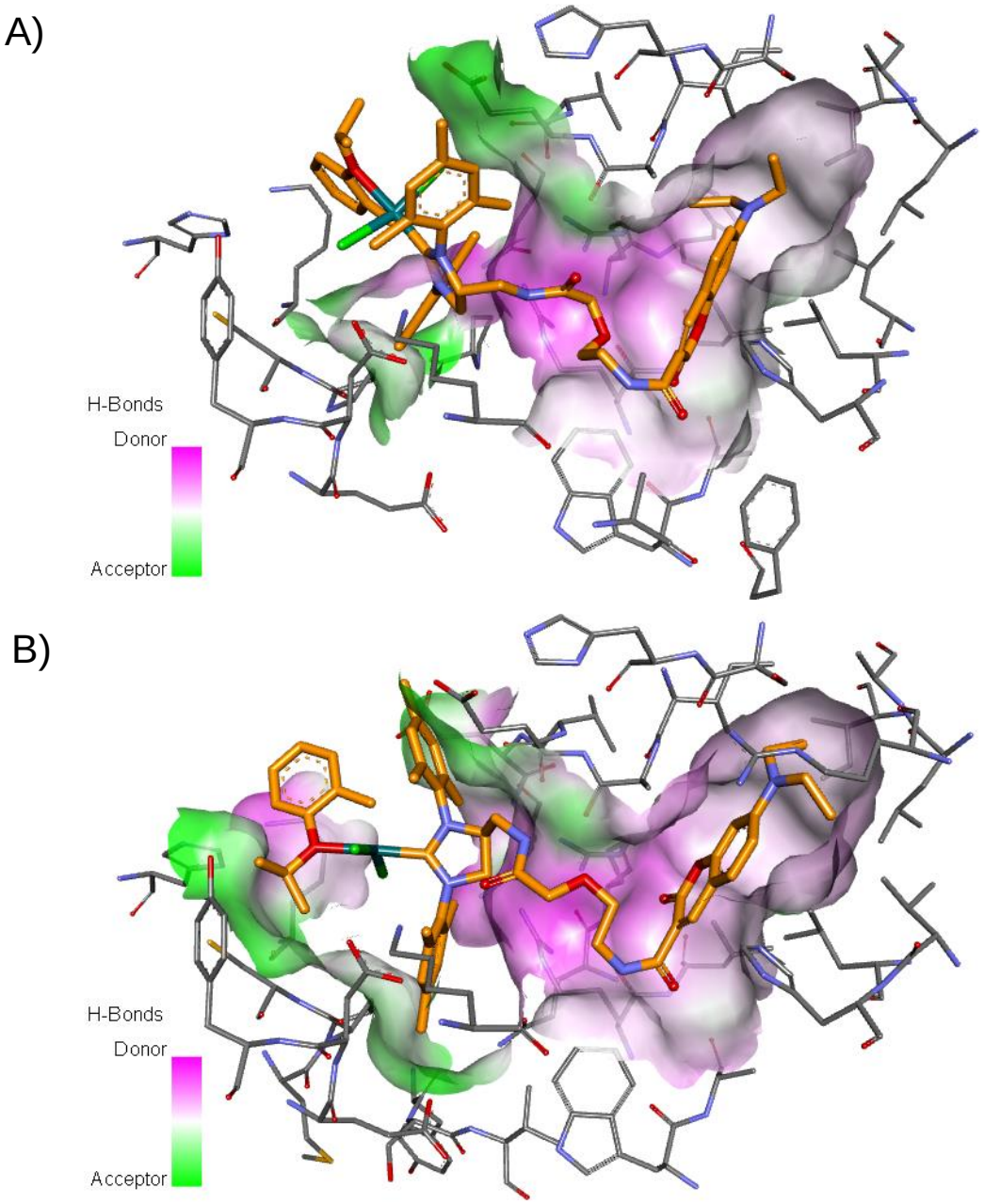

Supplementary Figure 25. Modeled docking of A) R-enantiomer of **Ru1** (orange), and B) S-enantiomer of **Ru1** (orange) with docking scores of -13.430 and -15.305 in the drug site I binding pocket of albumin (PDB 1H9Z). Shown is the view of the surface and residues around the ligand in the binding pocket. Hydrophobic surfaces are represented in grey, with hydrogen bonding surfaces represented by purple/light green. For these calculations, a grid box of 50×50×50 points centered at 28.487, 19.144, 9.787 (x,y,z) with a spacing of 0.375 Å between grid points was used.

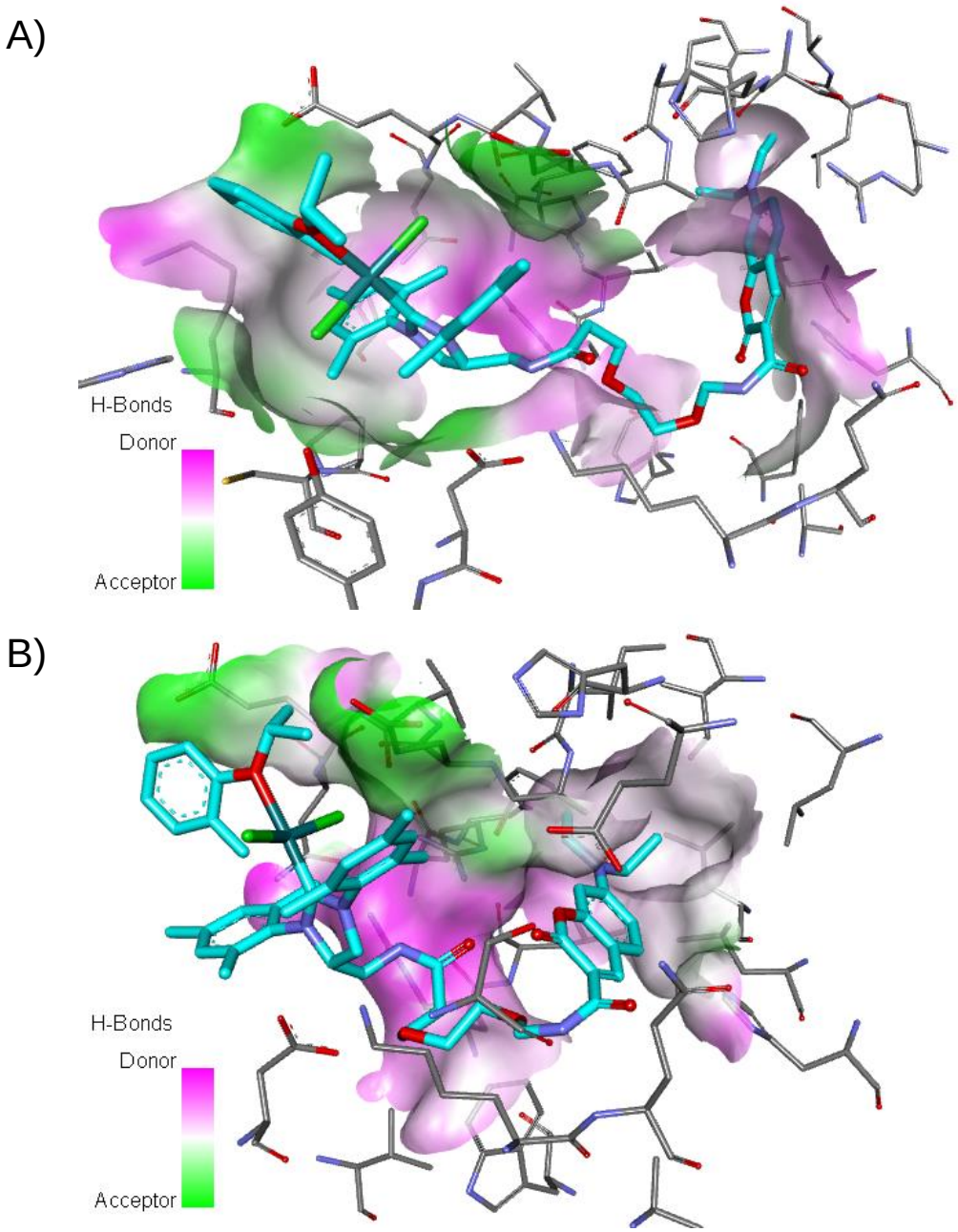

Supplementary Figure 26. Modeled docking of A) R-enantiomer of **Ru2** (light blue), and B) S-enantiomer of **Ru2** (light blue) with docking scores of -11.935 and -15.485 in the drug site I binding pocket of albumin (PDB 1H9Z). Shown is the view of the surface and residues around the ligand in the binding pocket. Hydrophobic surfaces are represented in grey, with hydrogen bonding surfaces represented by purple/light green. For these calculations, a grid box of 50×50×50 points centered at 28.487, 19.144, 9.787 (x,y,z) with a spacing of 0.375 Å between grid points was used.

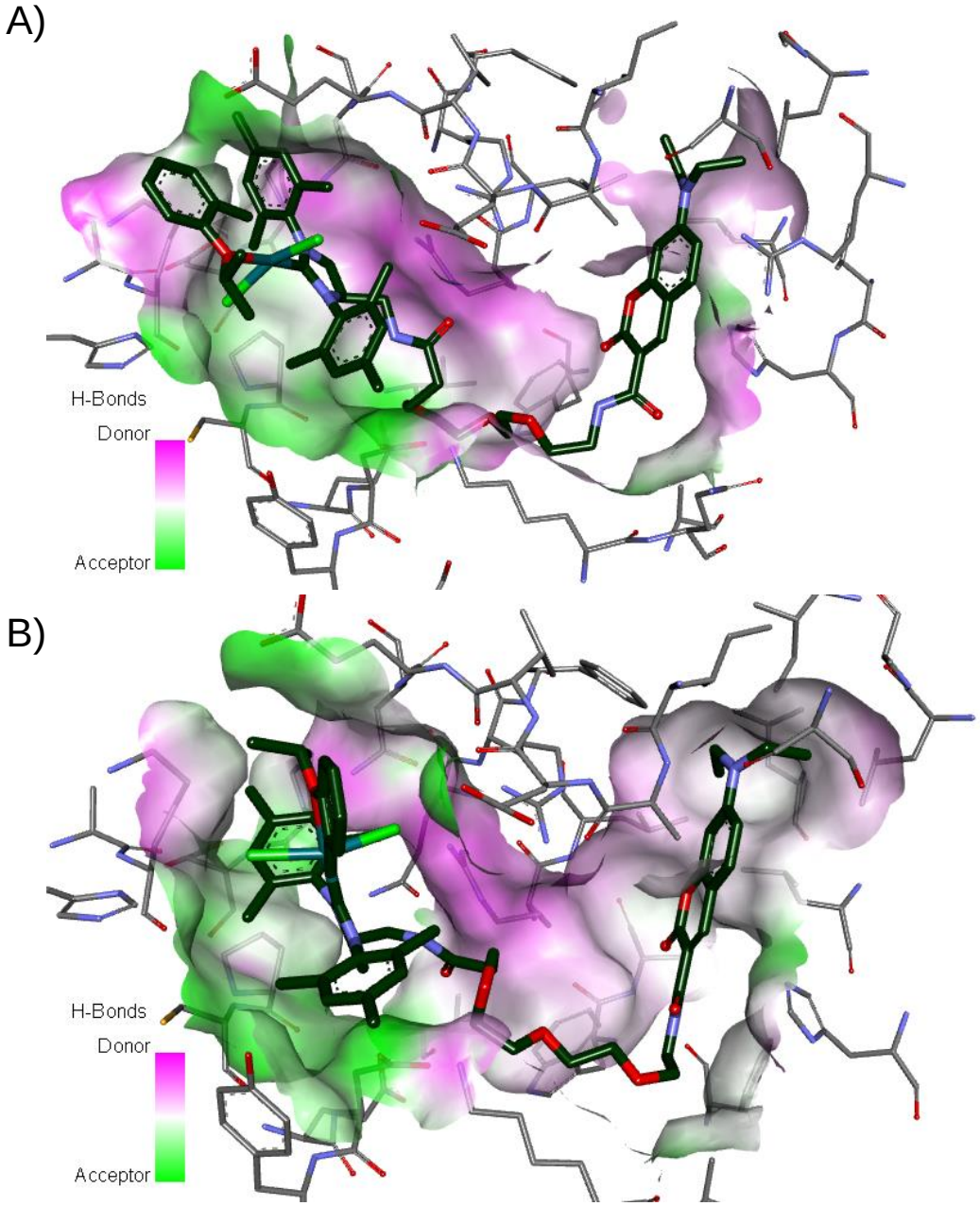

Supplementary Figure 27. Modeled docking of A) R-enantiomer of **Ru3** (dark green), and B) S-enantiomer of **Ru3** (dark green) with docking scores of -11.180 and -16.210 in the drug site I binding pocket of albumin (PDB 1H9Z). Shown is the view of the surface and residues around the ligand in the binding pocket. Hydrophobic surfaces are represented in grey, with hydrogen bonding surfaces represented by purple/light green. For these calculations, a grid box of 50×50×50 points centered at 28.487, 19.144, 9.787 (x,y,z) with a spacing of 0.375 Å between grid points was used.

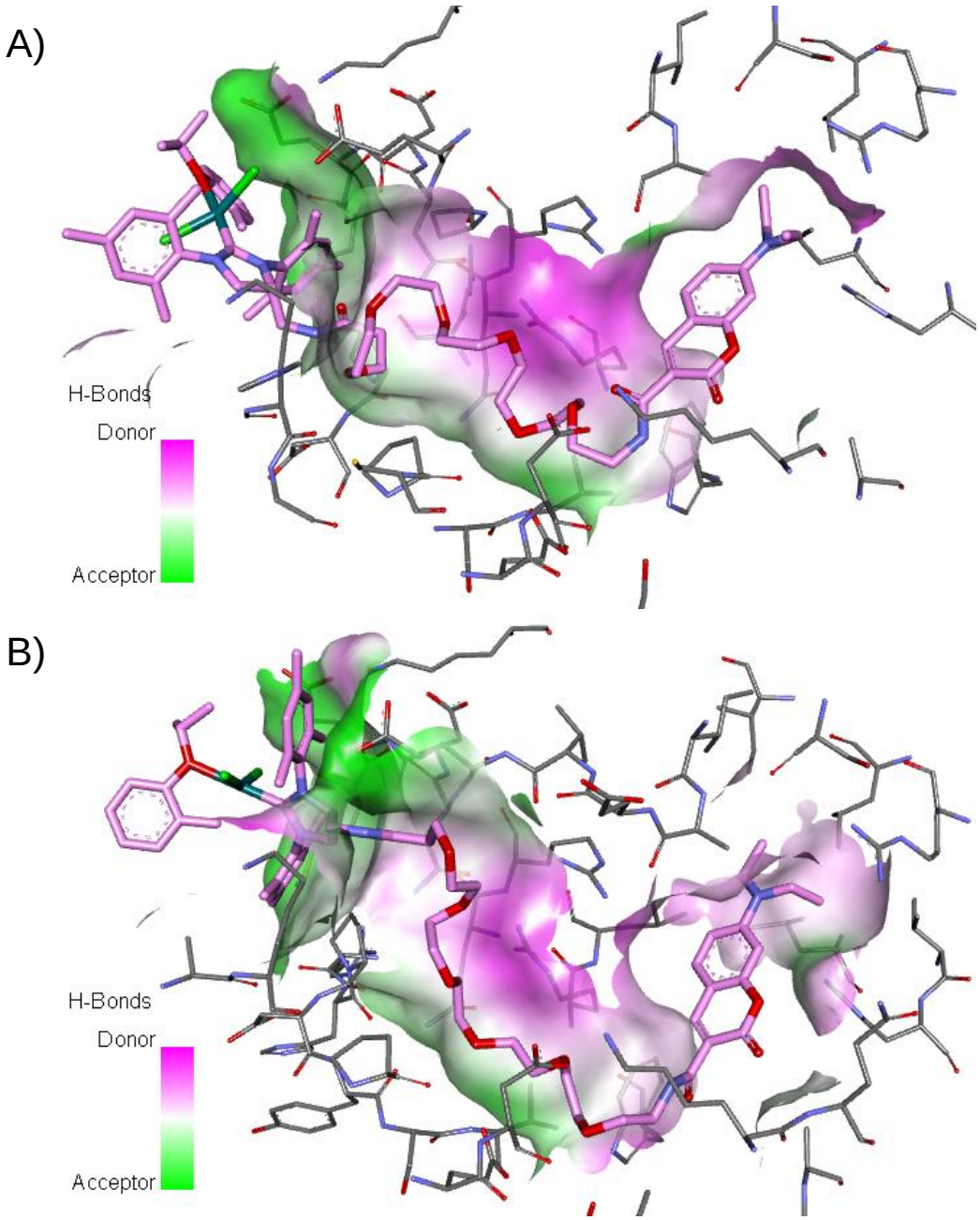

Supplementary Figure 28. Modeled docking of A) R-enantiomer of **Ru6** (pink), and B) S-enantiomer of **Ru6** (pink) with docking scores of -6.376 and -6.474 in the drug site I binding pocket of albumin (PDB 1H9Z). Shown is the view of the surface and residues around the ligand in the binding pocket. Hydrophobic surfaces are represented in grey, with hydrogen bonding surfaces represented by purple/light green. For these calculations, a grid box of 64×64×64 points centered at 23.682, 21.066, 4.422 (x,y,z) with a spacing of 0.375 Å between grid points was used.

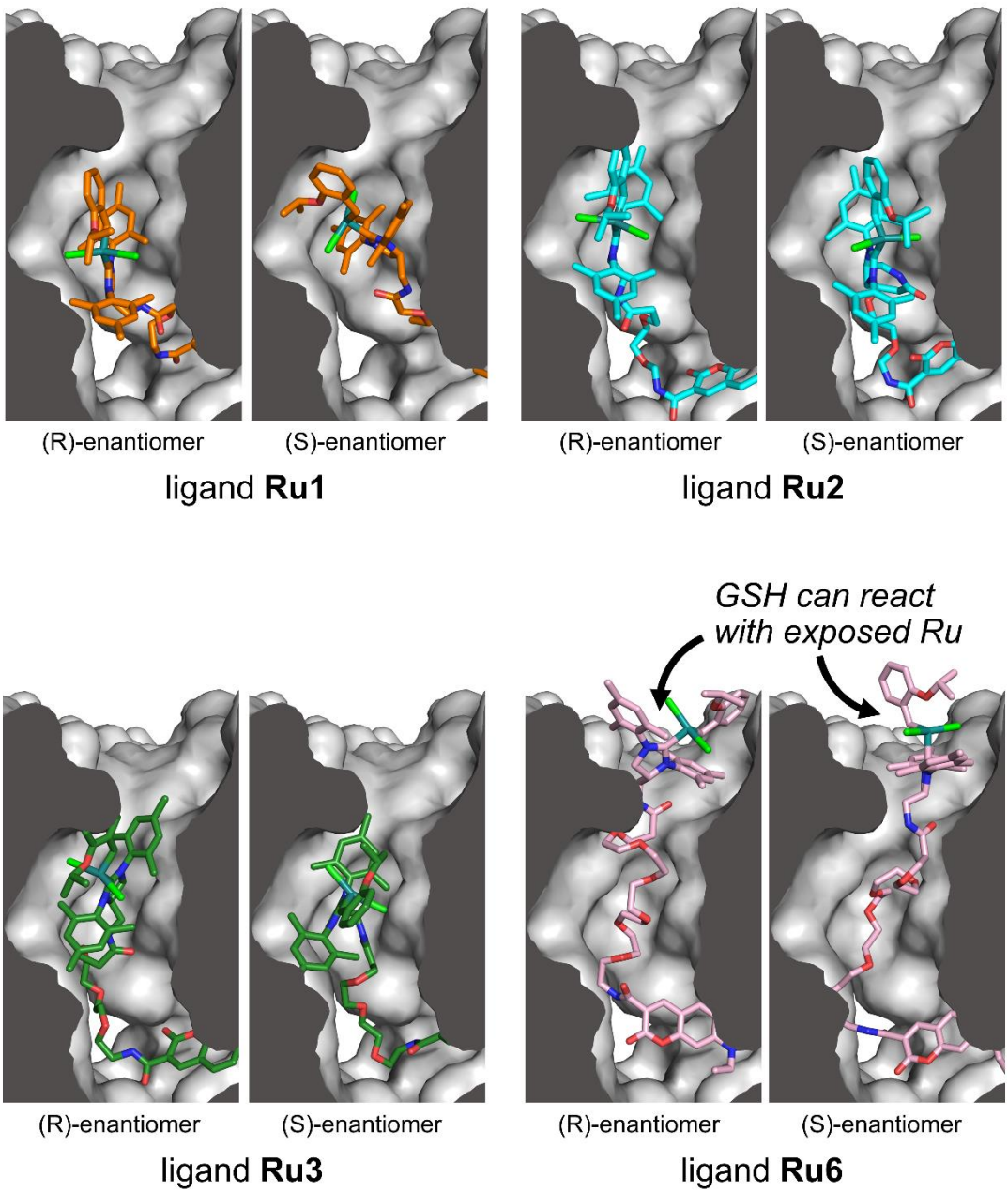

Supplementary Figure 29. Modeling of both (R)- and (S)-enantiomers of **Ru1-3,6** into the drug site I binding pocket of albumin (PDB:1H9Z) with an emphasis on binding conformations shown in a sliced view of the binding pocket.

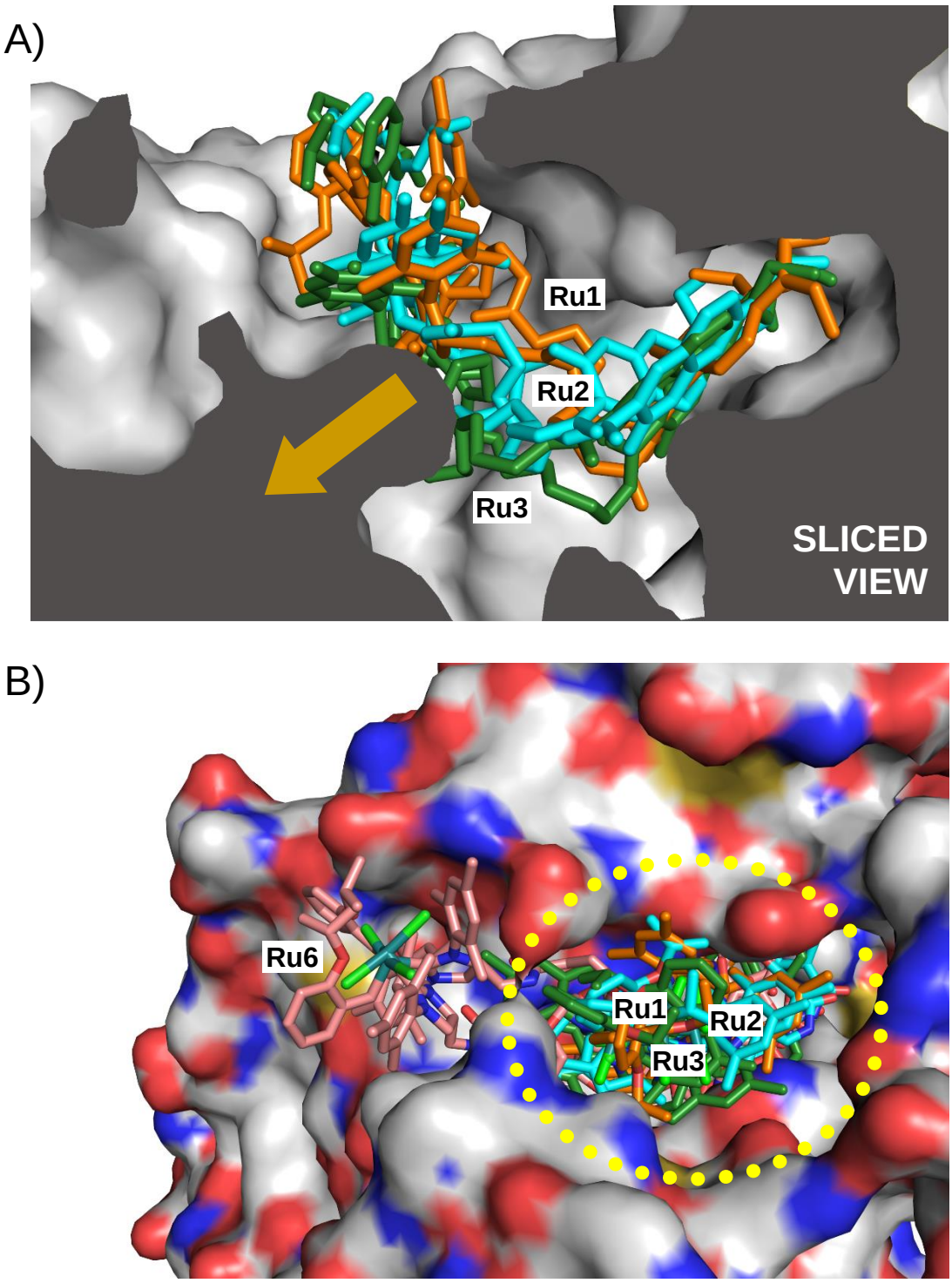

Supplementary Figure 30. Modeling of both (R)- and (S)-enantiomers of **Ru1-3,6** into the drug site I binding pocket of albumin (PDB:1H9Z) with an emphasis on A) the limited space within the binding pocket to accommodate short (**Ru1**) and medium (**Ru2**, **Ru3**) PEG linkers, and B) the view of the binding pocket entrance to highlight the extent of **Ru6** protrusion compared to **Ru1-3**.

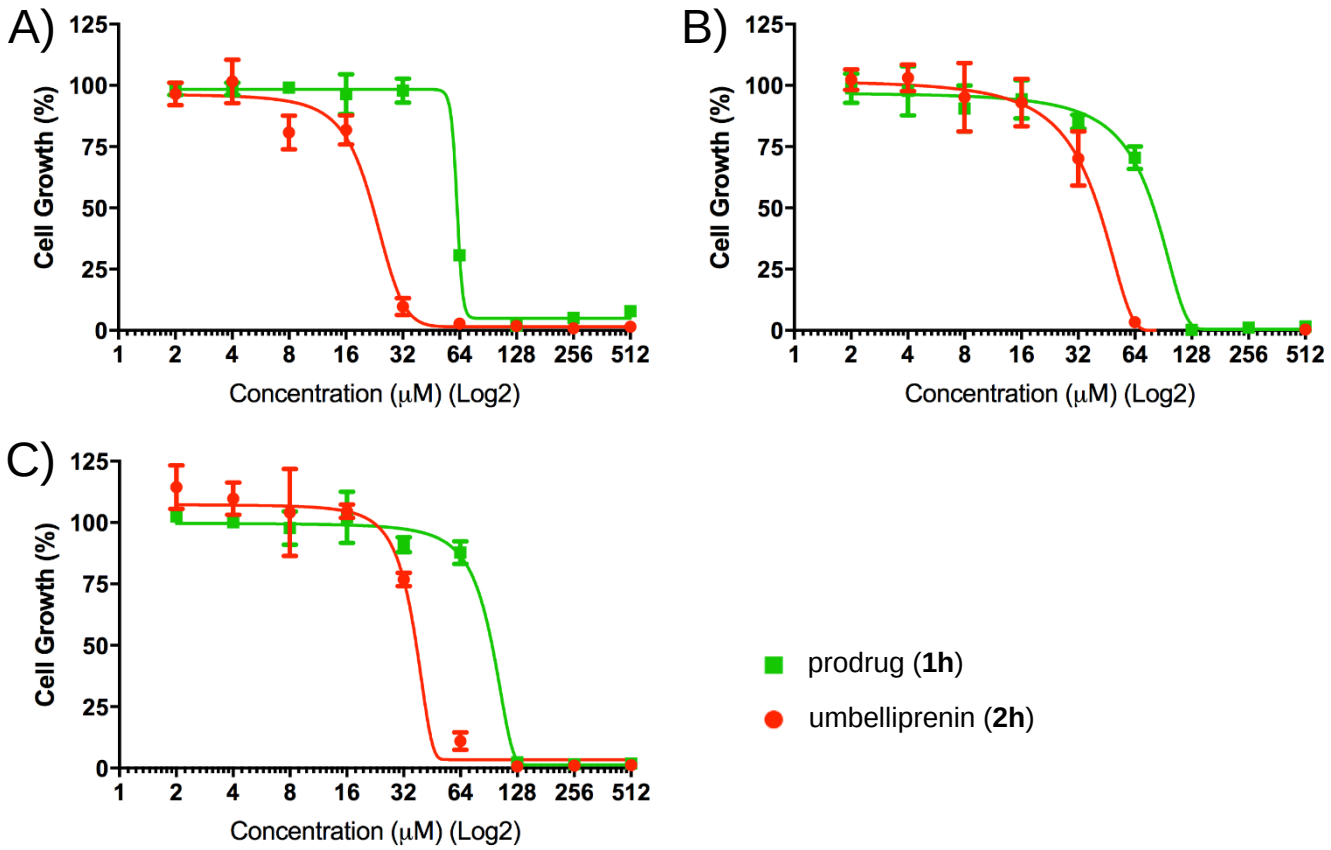

Supplementary Figure 31. Dose response curves of umbelliprenin prodrug **1h** (green square) and umbelliprenin **2h** (red circle) against A) SW620 cells, B) HeLa cells, and C) A549 cells. From this data, prodrug **1h** concentrations for subsequent experiments were chosen to be 64 μM for A549/HeLa cells, and 32 μM for SW620 cells. Error bars represent the standard deviation of three replicate measurements.

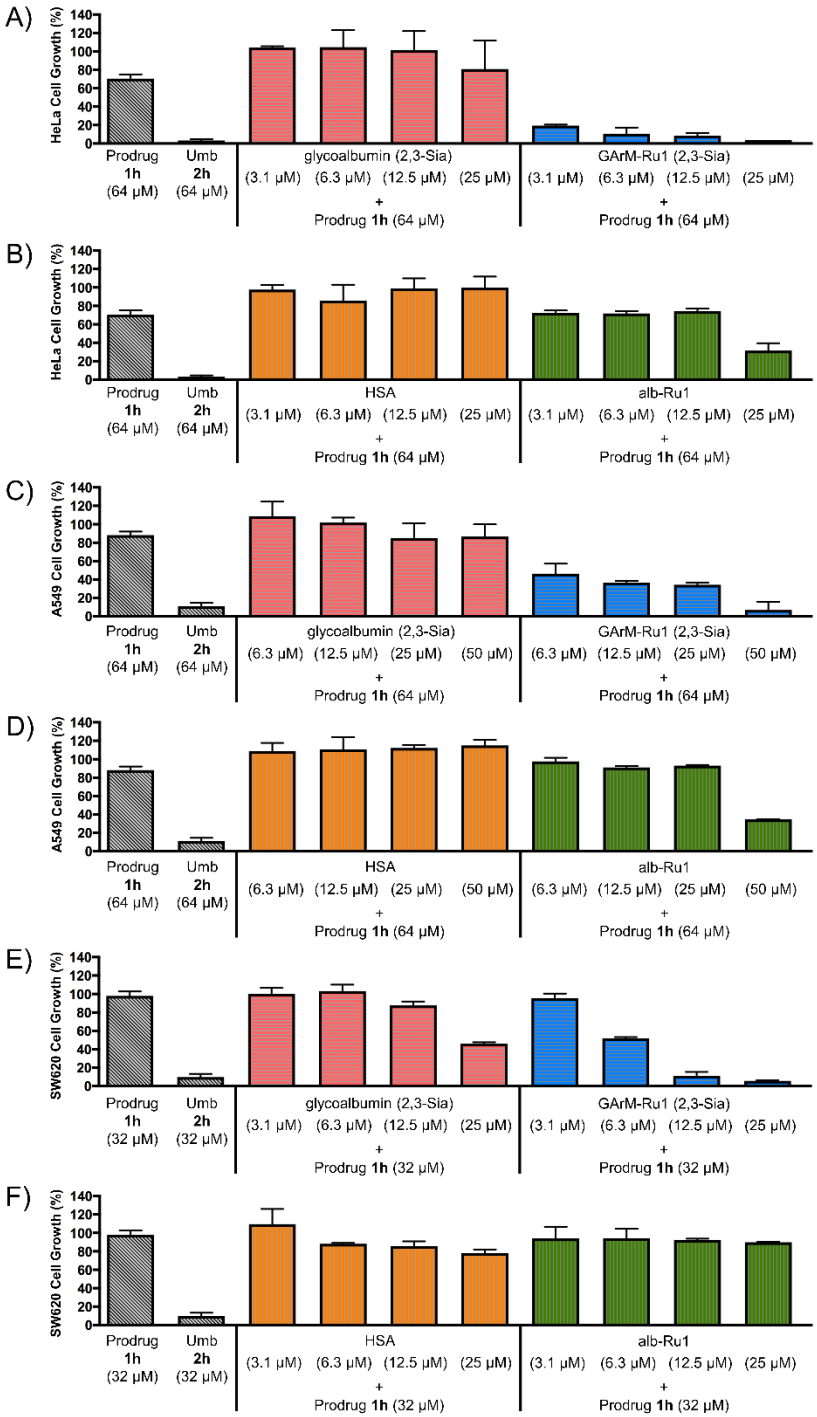

Supplementary Figure 32. Cytotoxicity assays were run using HeLa cancer cells incubated with A) varying concentrations of GArM-Ru1(2,3-Sia) and glycoalbumin(2,3-Sia) with prodrug **1h** (fixed at 64 μM), and B) varying concentrations of alb-Ru1 and HSA with prodrug **1h** (fixed at 64 μM). A549 cancer cells incubated with C) varying concentrations of GArM-Ru1(2,3-Sia) and glycoalbumin(2,3-Sia) with prodrug **1h** (fixed at 64 μM), and D) varying concentrations of alb-Ru1 and HSA with prodrug **1h** (fixed at 64 μM). SW620 cancer cells incubated with E) varying concentrations of GArM-Ru1(2,3-Sia) and glycoalbumin(2,3-Sia) with prodrug **1h** (fixed at 32 μM), and F) varying concentrations of alb-Ru1 and HSA with prodrug **1h** (fixed at 32 μM). Error bars represent the standard deviation of three replicate measurements.

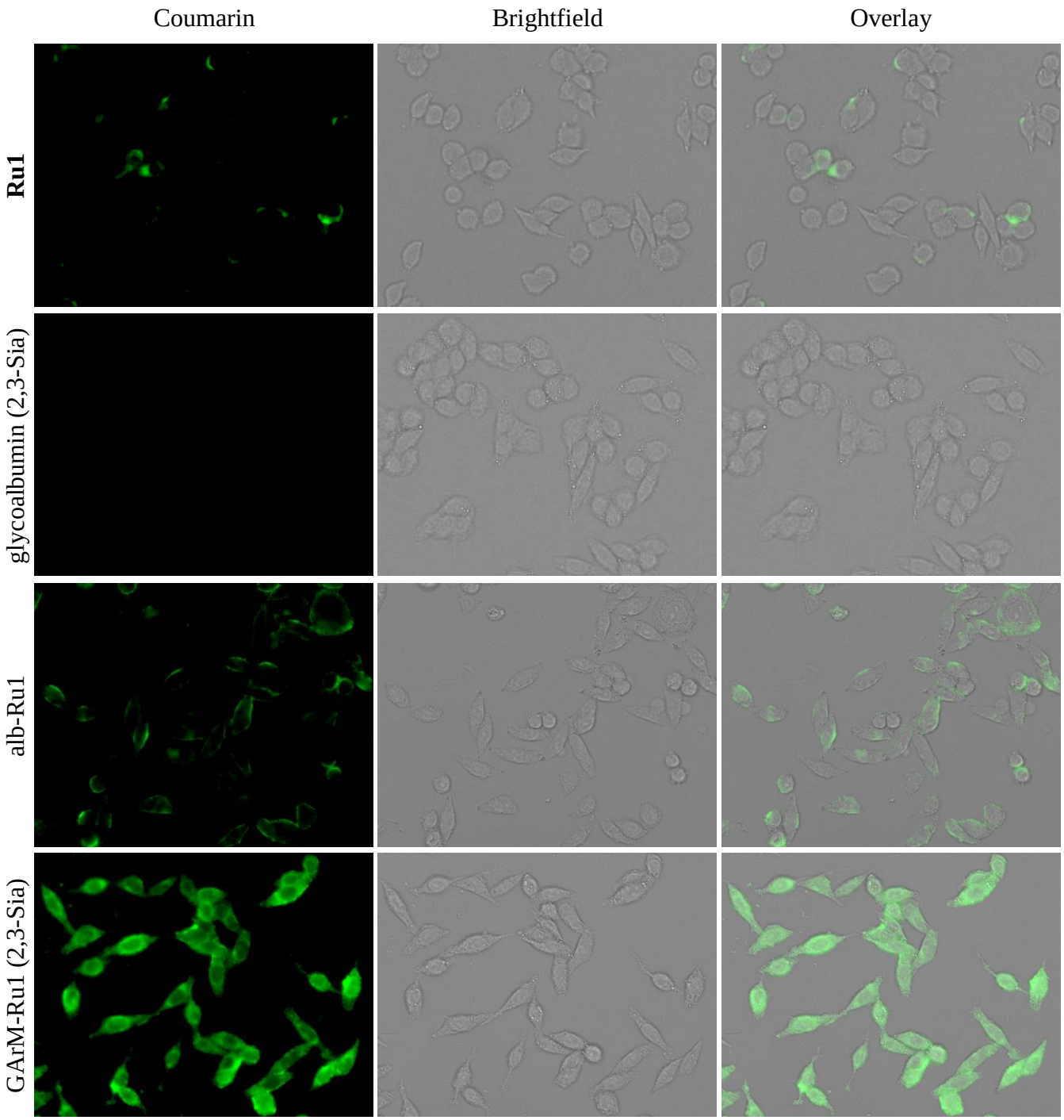

Supplementary Figure 33. SW620 cell imaging results following incubation (3 hr, 37 °C) with either **Ru1**, glycoalbumin (2,3-Sia), alb-Ru1, or GArM-Ru1 (2,3-Sia). Shown are images obtained via coumarin fluorescence (1/20s exposure time), brightfield (1/2000s exposure time), and the combined overlay.

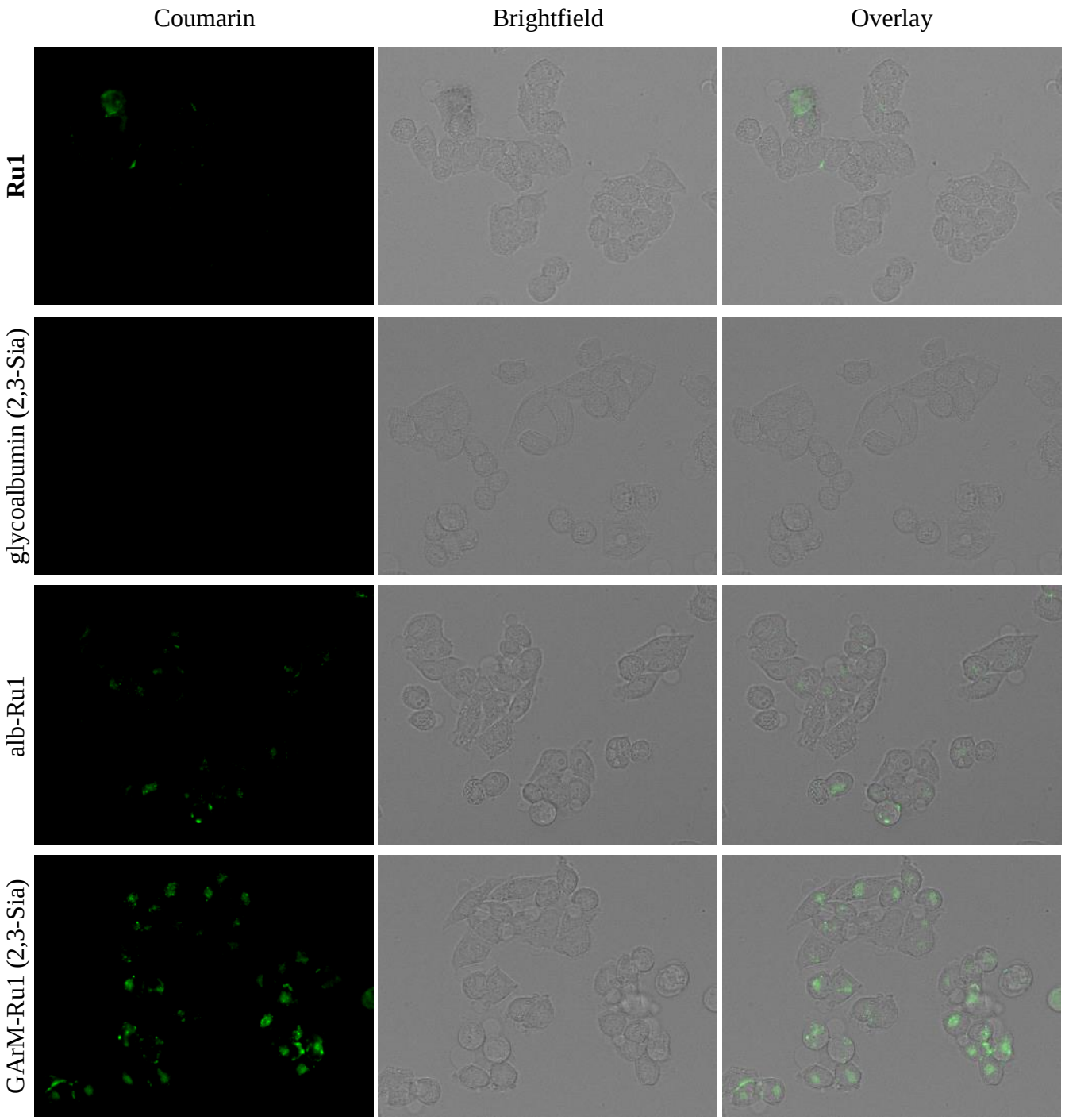

Supplementary Figure 34. HeLa cell imaging results following incubation (3 hr, 37 °C) with either **Ru1**, glycoalbumin (2,3-Sia), alb-Ru1, or GArM-Ru1 (2,3-Sia). Shown are images obtained via coumarin fluorescence (1/20s exposure time), brightfield (1/2000s exposure time), and the combined overlay.

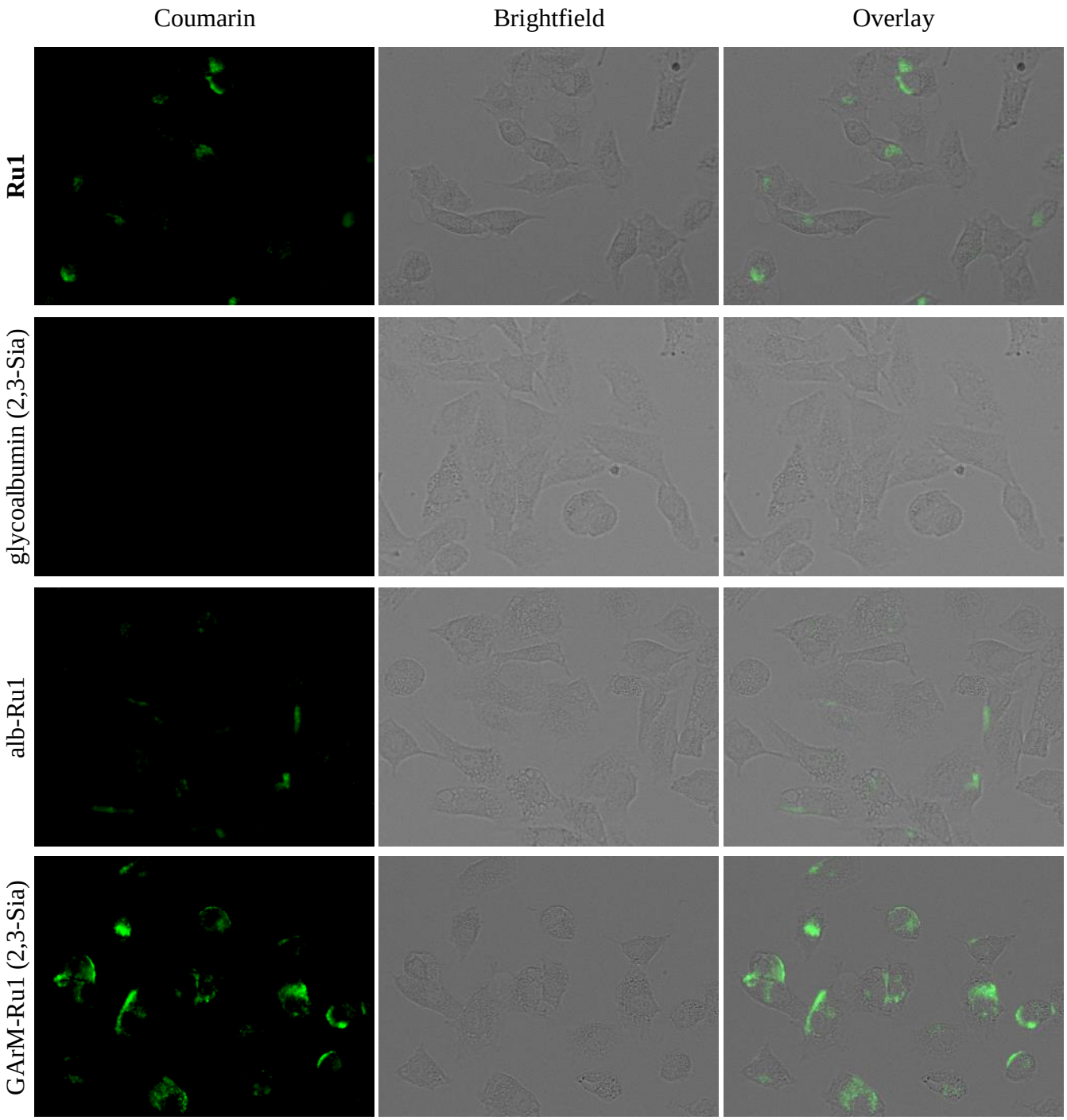

Supplementary Figure 35. A549 cell imaging results following incubation (3 hr, 37 °C) with either **Ru1**, glycoalbumin (2,3-Sia), alb-Ru1, or GArM-Ru1 (2,3-Sia). Shown are images obtained via coumarin fluorescence (1/20s exposure time), brightfield (1/2000s exposure time), and the combined overlay.

Product Structure	Calibration Curve
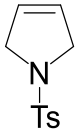 **2a**	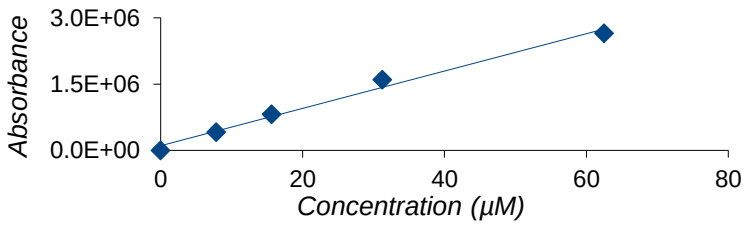

R^2 = 0.9878

	Value	Error (σ)
Slope	422360.5227	27114.6367
Intercept	105982.1917	87341.0244

HPLC Method: 1

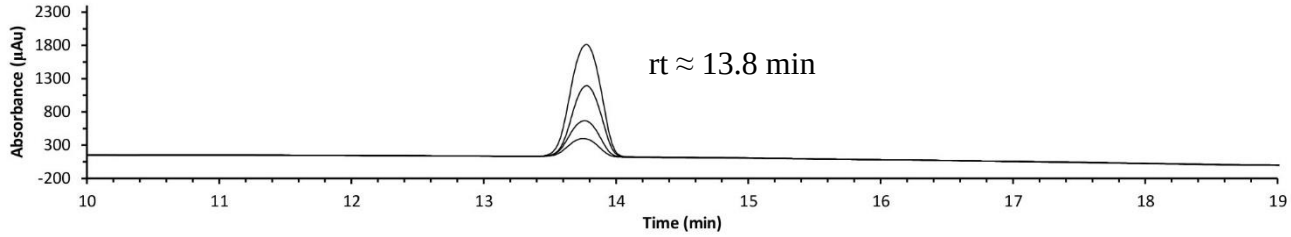

Supplementary Figure 36. HPLC calibration curve of product **2a**

Product Structure	Calibration Curve
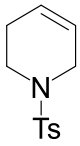 **2b**	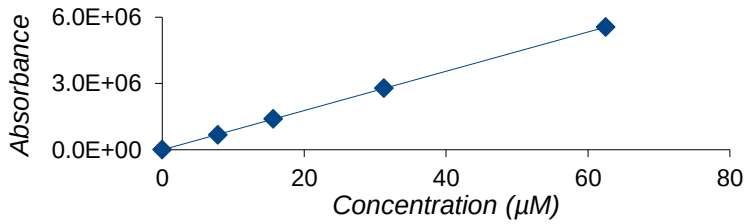

R^2 = 1.0000

	Value	Error (σ)
Slope	889165.8880	3392.2355
Intercept	-2944.4167	10926.9883

HPLC Method: 2

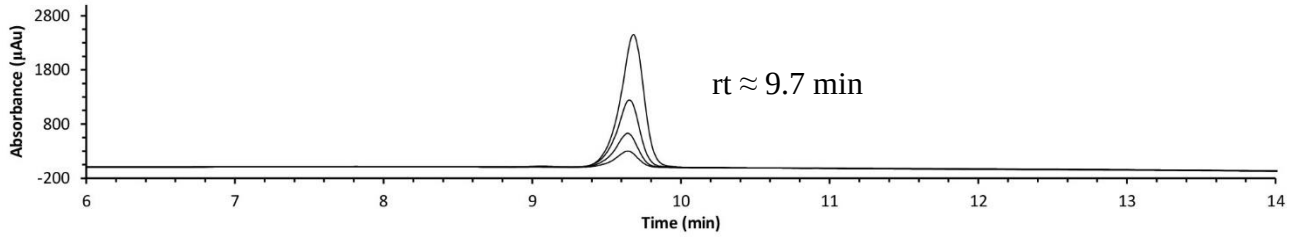

Supplementary Figure 37. HPLC calibration curve of product **2b**

Product Structure	Calibration Curve
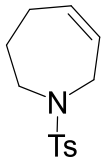 **2c**	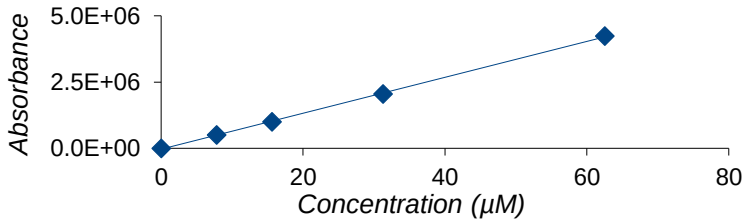
	R^2 = 0.9996

	Value	Error (σ)
Slope	677603.7120	7467.2899
Intercept	-32272.5000	24053.4571

HPLC Method: 2

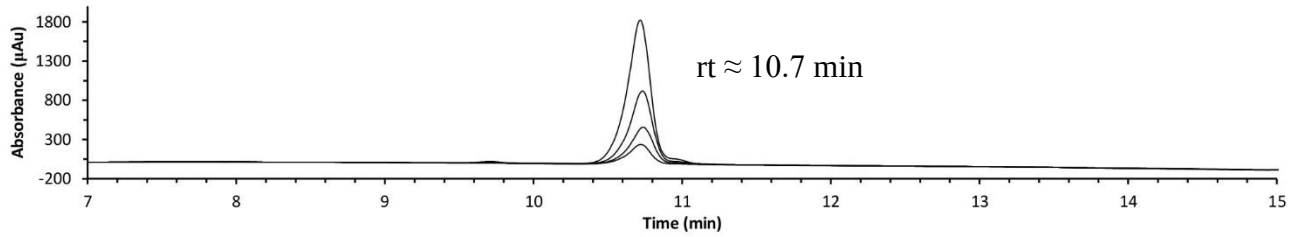

Supplementary Figure 38. HPLC calibration curve of product **2c**

Product Structure	Calibration Curve
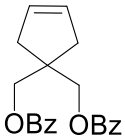 **2d**	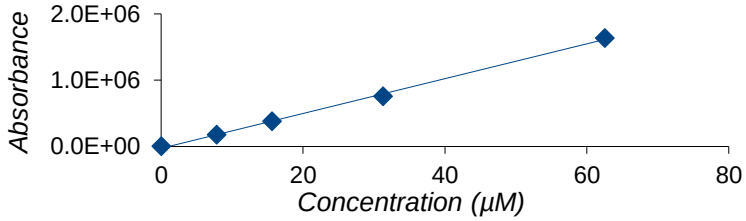
	R^2 = 0.9983

	Value	Error (σ)
Slope	262614.0587	6232.6830
Intercept	-27063.3000	20076.5707

HPLC Method: 3

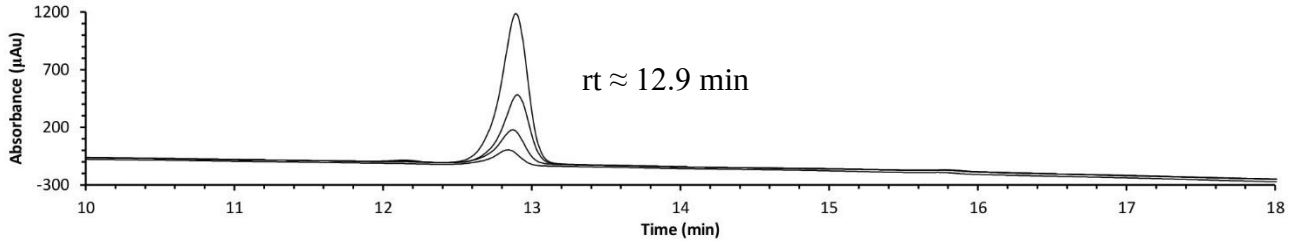

Supplementary Figure 39. HPLC calibration curve of product **2d**

Product Structure	Calibration Curve
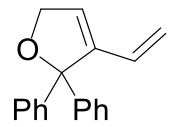 **2e**	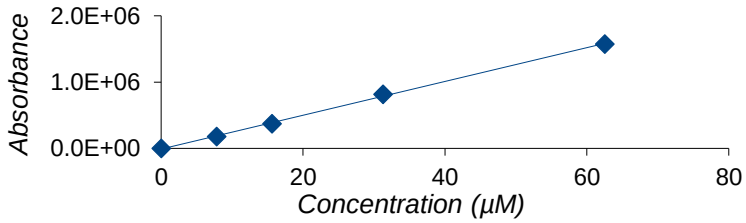

R^2 = **0.9991**	Value	Error (σ)
Slope	254896.4907	4466.3926
Intercept	-9818.5833	14387.0380

HPLC Method: 2

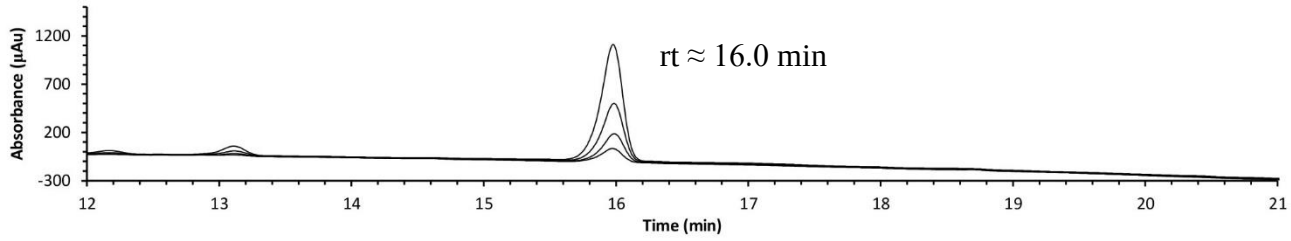

Supplementary Figure 40. HPLC calibration curve of product **2e**

Product Structure	Calibration Curve
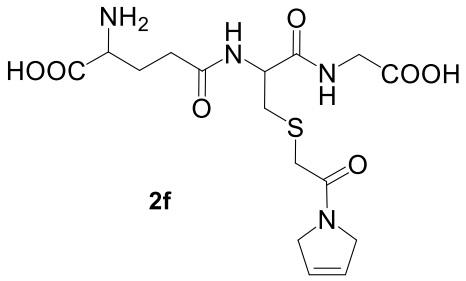 **2f**	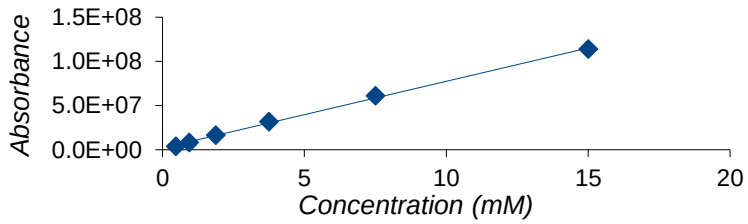

R^2 = **0.9985**	Value	Error (σ)
Slope	75516088.0398	1458400.4789
Intercept	1942473.7512	1031118.9763

HPLC Method: 4

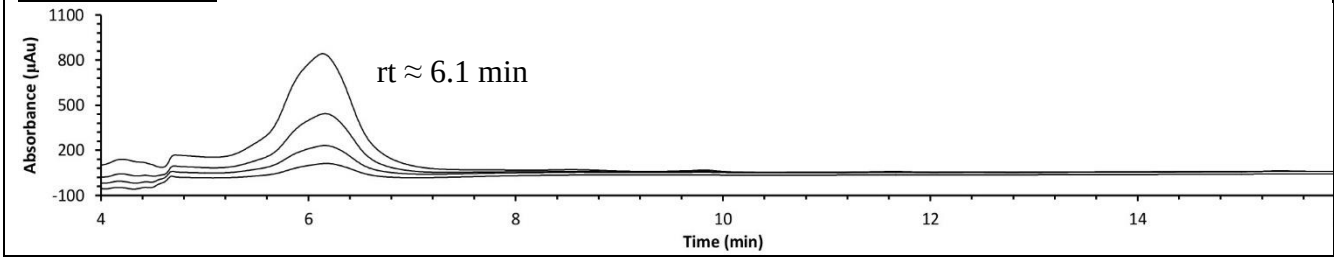

Supplementary Figure 41. HPLC calibration curve of product **2f**

Product Structure	Calibration Curve
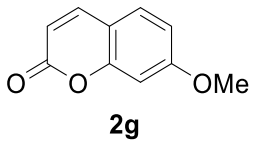 **2g**	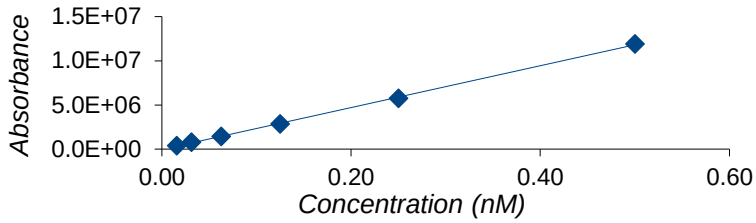

R^2 = **0.9996**	Value	Error (σ)
Slope	236954958692.3	2443087059.1
Intercept	-38468.1	57577.1

HPLC Method: 5 λ_{EX}=325 nm/ λ_{EM}=390 nm

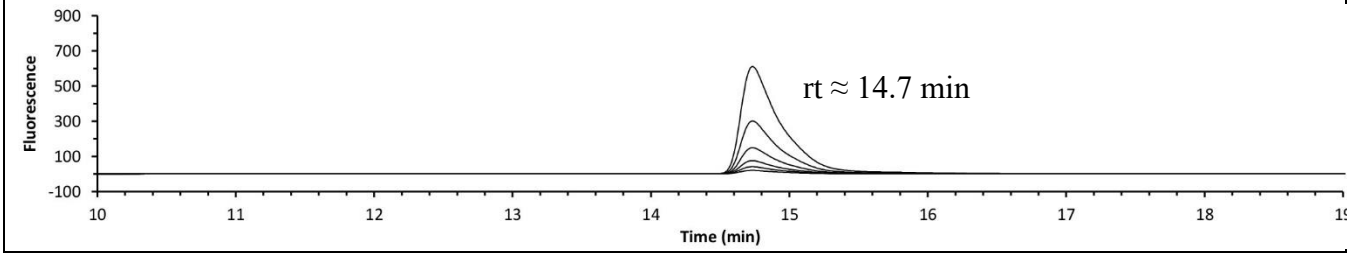

Supplementary Figure 42. HPLC calibration curve of product **2g**

Product Structure	Calibration Curve
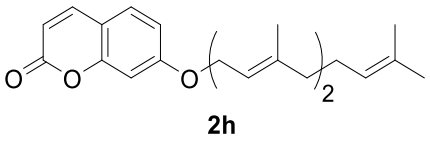 **2h**	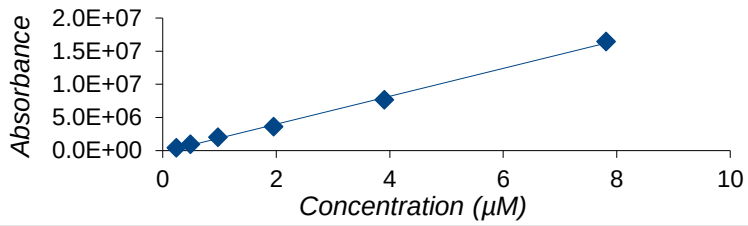

R^2 = **0.9983**	Value	Error (σ)
Slope	21042445.7479	434207.2310
Intercept	-218623.4826	159892.3937

HPLC Method: 6 λ_{EX}=325 nm/ λ_{EM}=390 nm

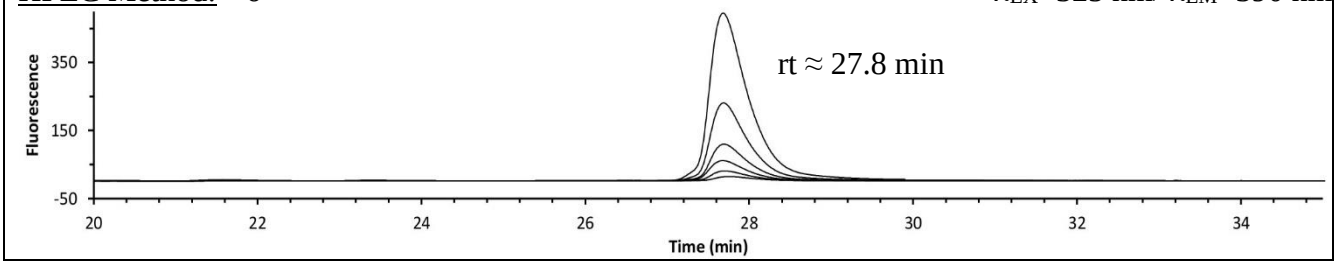

Supplementary Figure 43. HPLC calibration curve of product **2h**

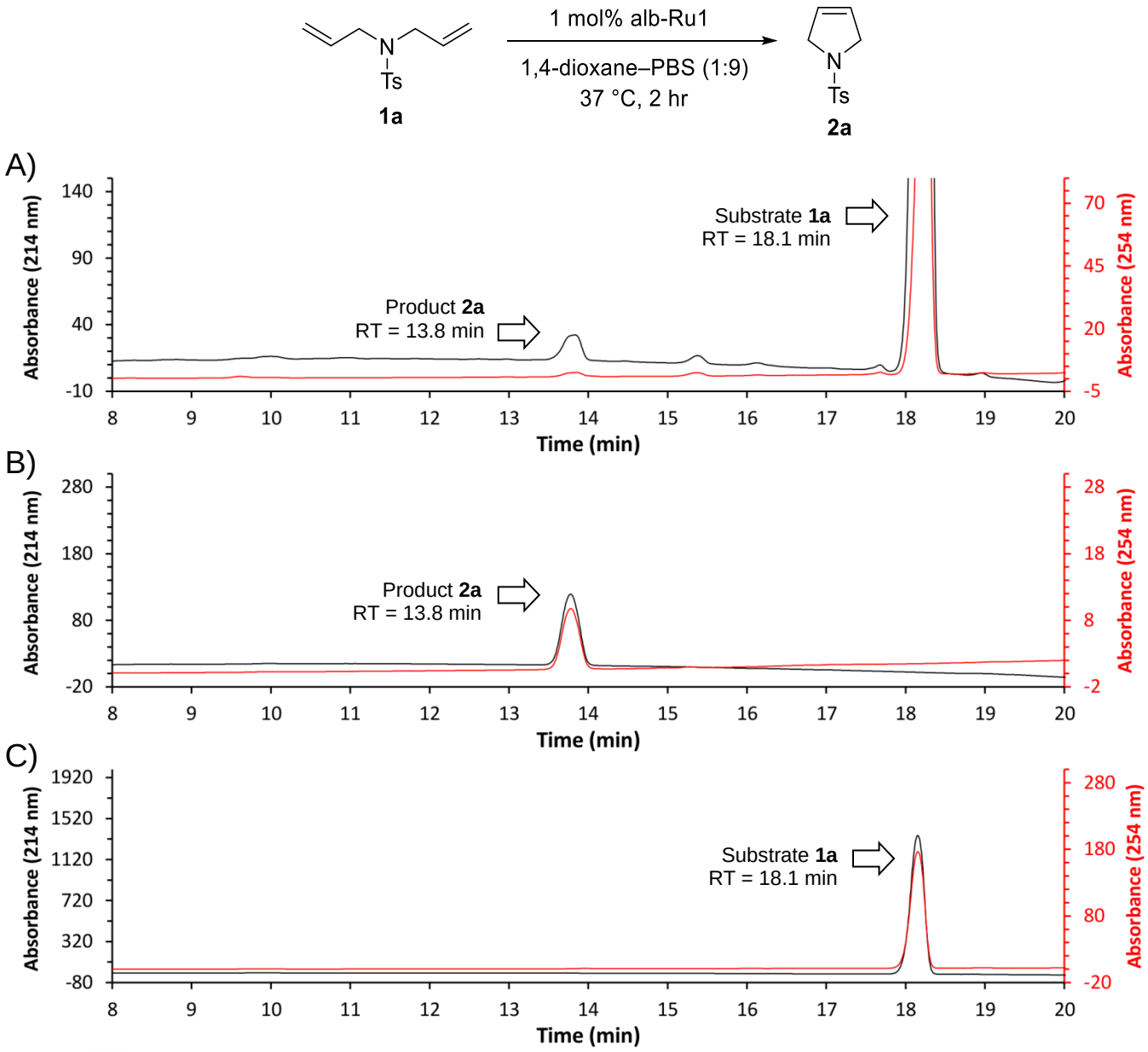

Supplementary Figure 44. Example HPLC traces of A) reaction mixture of **1a** incubated with alb-Ru1. Standard runs of known compounds include B) product **2a** standard, and C) substrate **1a** standard.

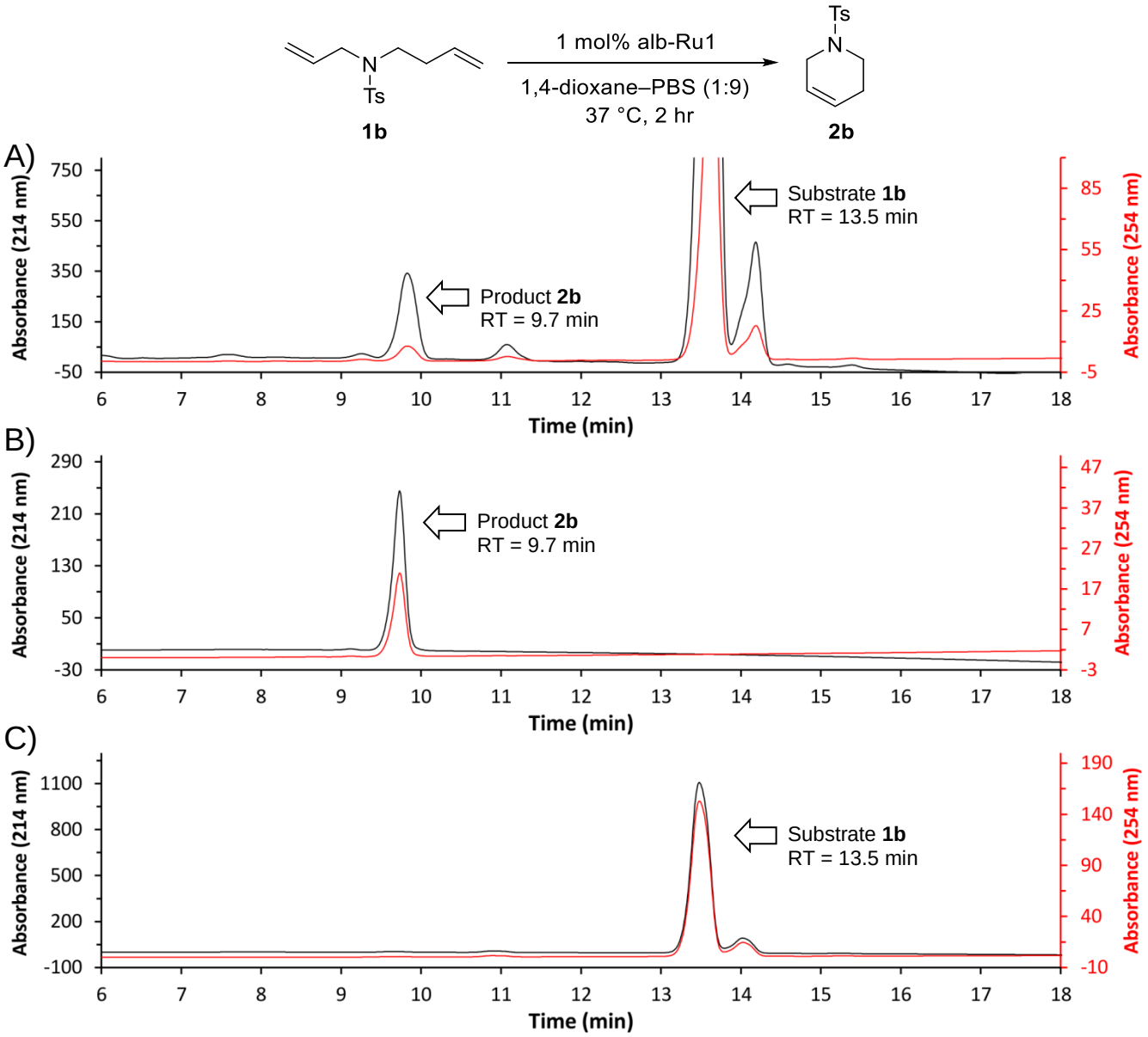

Supplementary Figure 45. Example HPLC traces of A) reaction mixture of **1b** incubated with alb-Ru1. Standard runs of known compounds include B) product **2b** standard, and C) substrate **1b** standard.

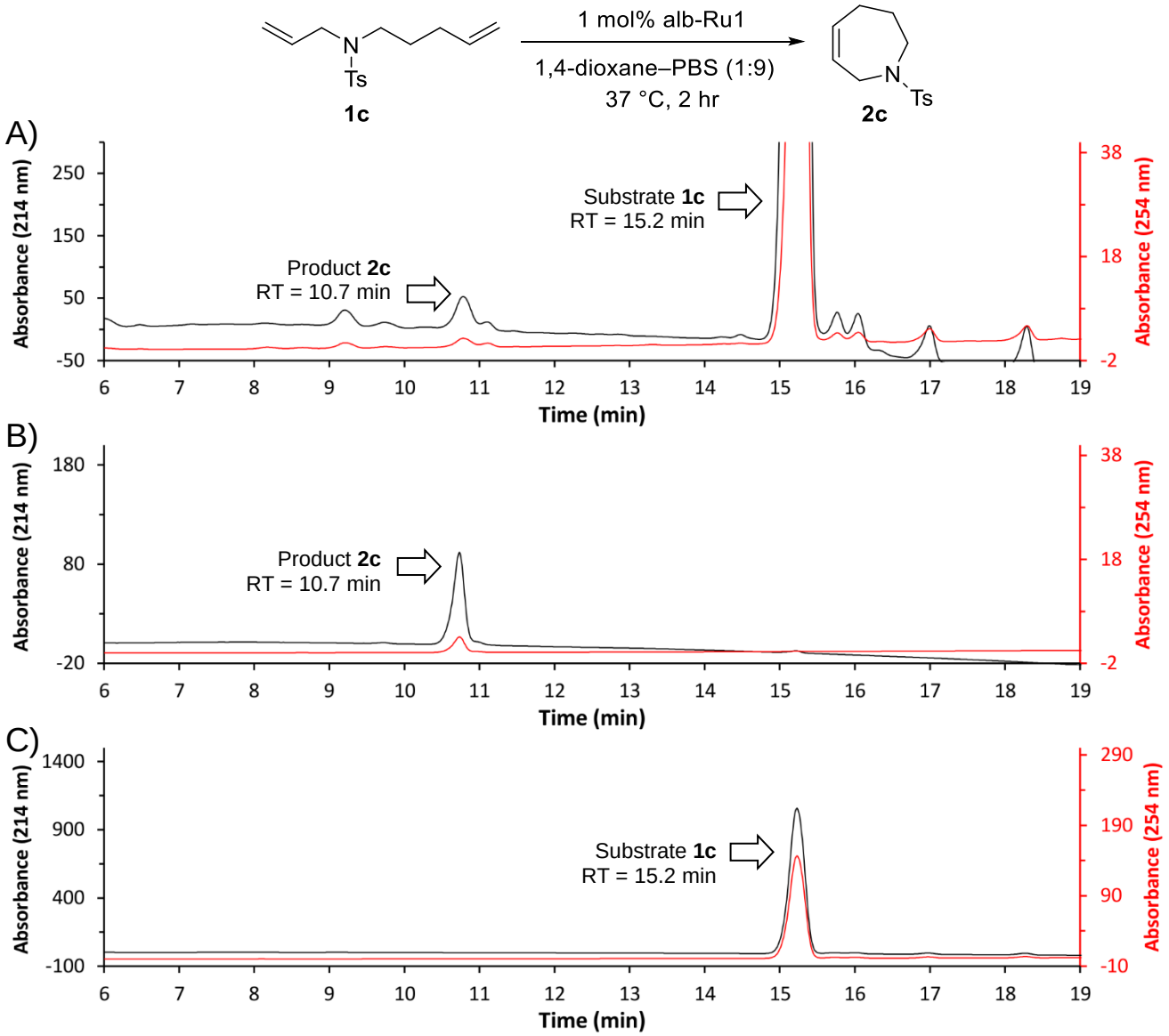

Supplementary Figure 46. Example HPLC traces of A) reaction mixture of **1c** incubated with alb-Ru1. Standard runs of known compounds include B) product **2c** standard, and C) substrate **1c** standard.

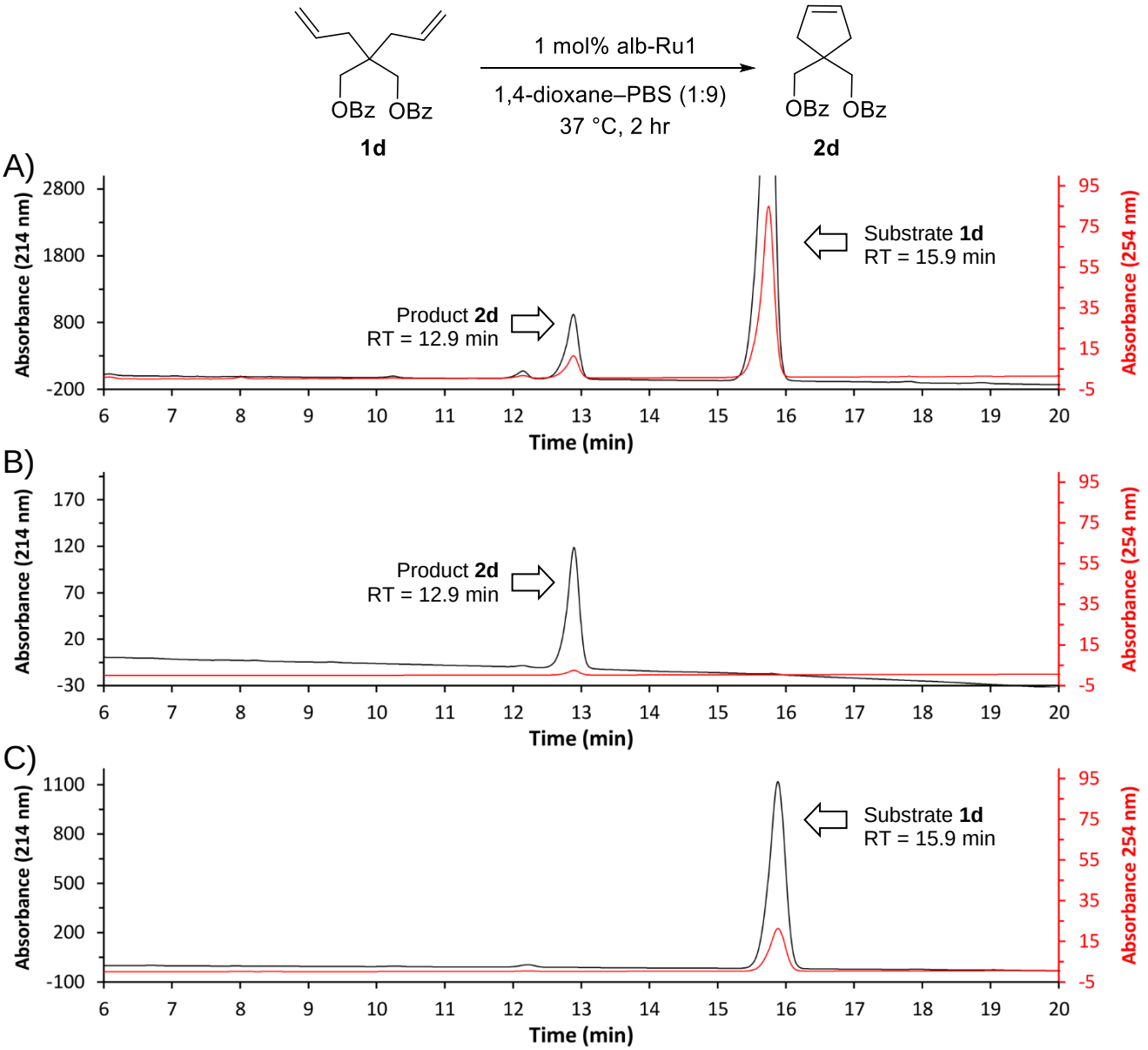

Supplementary Figure 47. Example HPLC traces of A) reaction mixture of **1d** incubated with alb-Ru1. Standard runs of known compounds include B) product **2d** standard, and C) substrate **1d** standard.

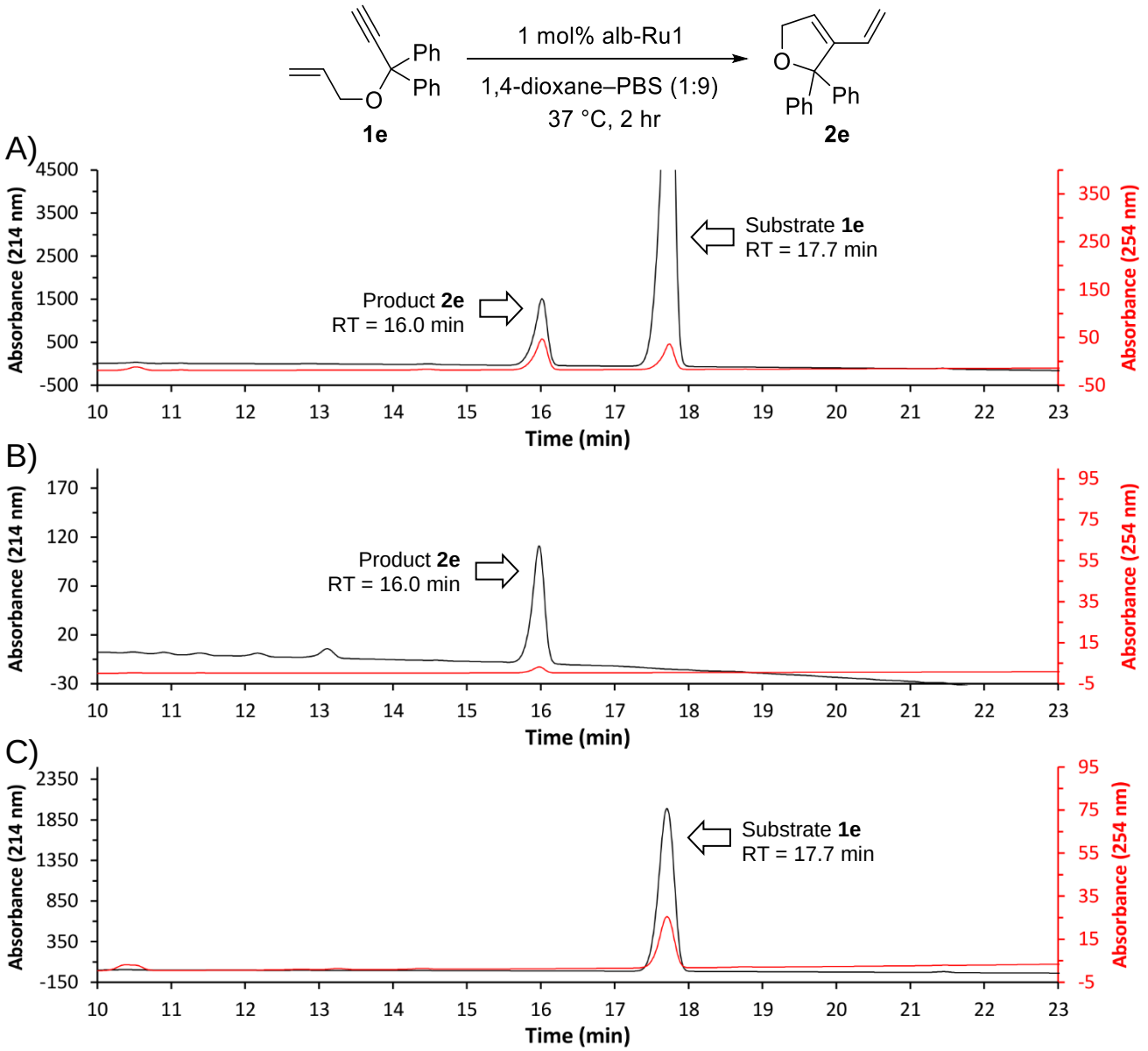

Supplementary Figure 48. Example HPLC traces of A) reaction mixture of **1e** incubated with alb-Ru1. Standard runs of known compounds include B) product **2e** standard, and C) substrate **1e** standard.

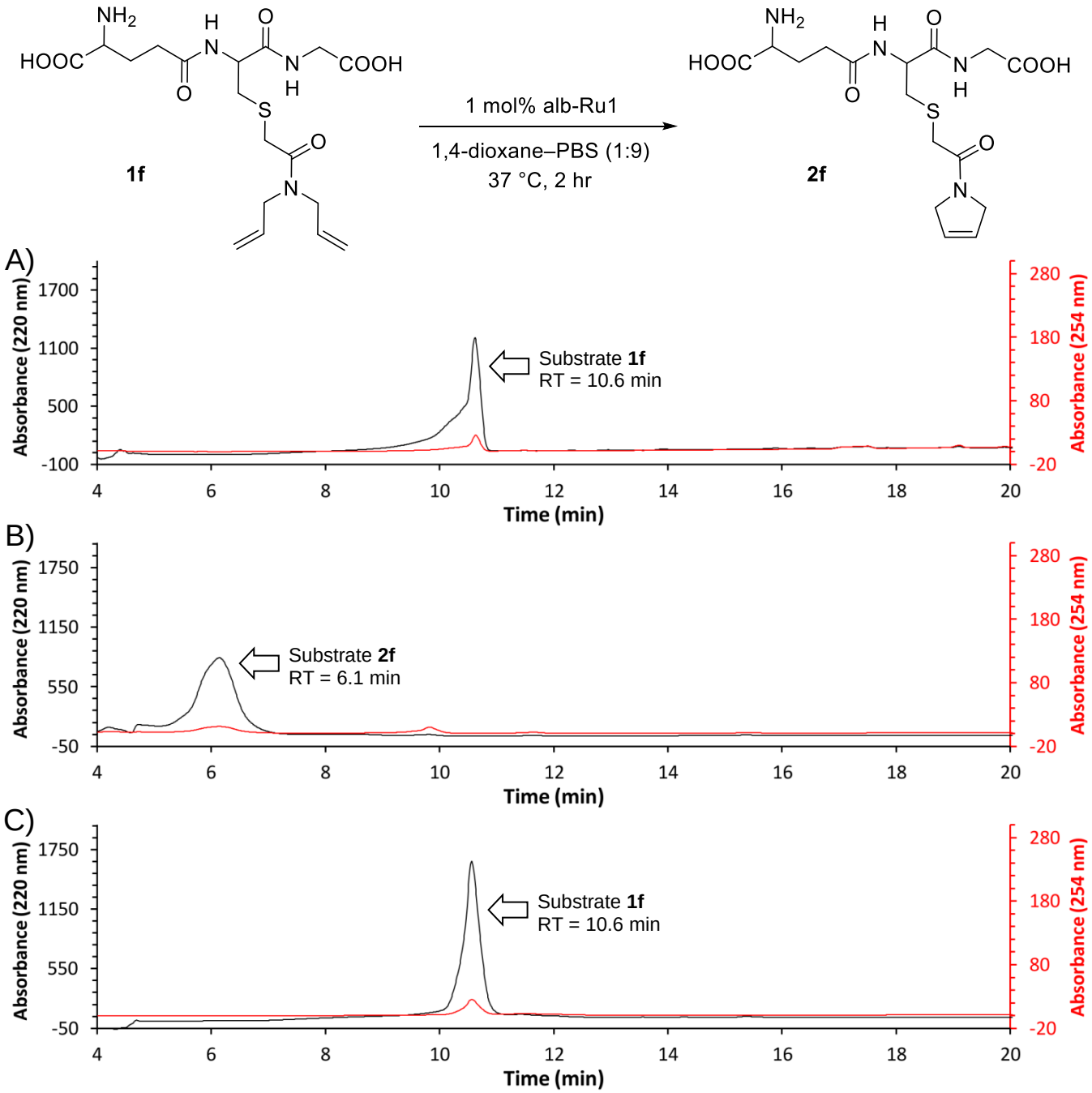

Supplementary Figure 49. Example HPLC traces of A) reaction mixture of **1f** incubated with alb-Ru1. Standard runs of known compounds include B) product **2f** standard, and C) substrate **1f** standard.

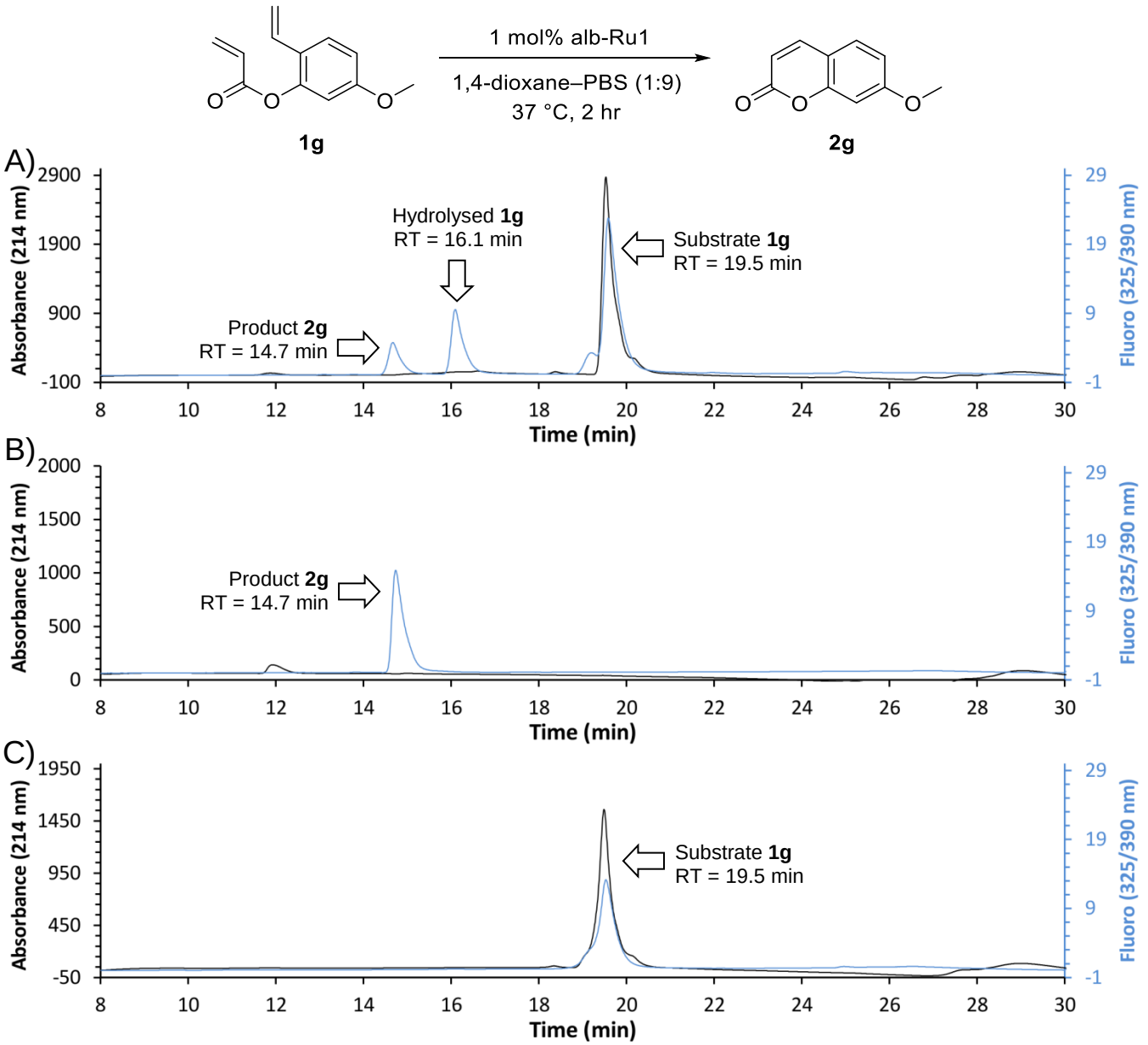

Supplementary Figure 50. Example HPLC traces of A) reaction mixture of **1g** incubated with alb-Ru1. Standard runs of known compounds include B) product **2g** standard, and C) substrate **1g** standard.

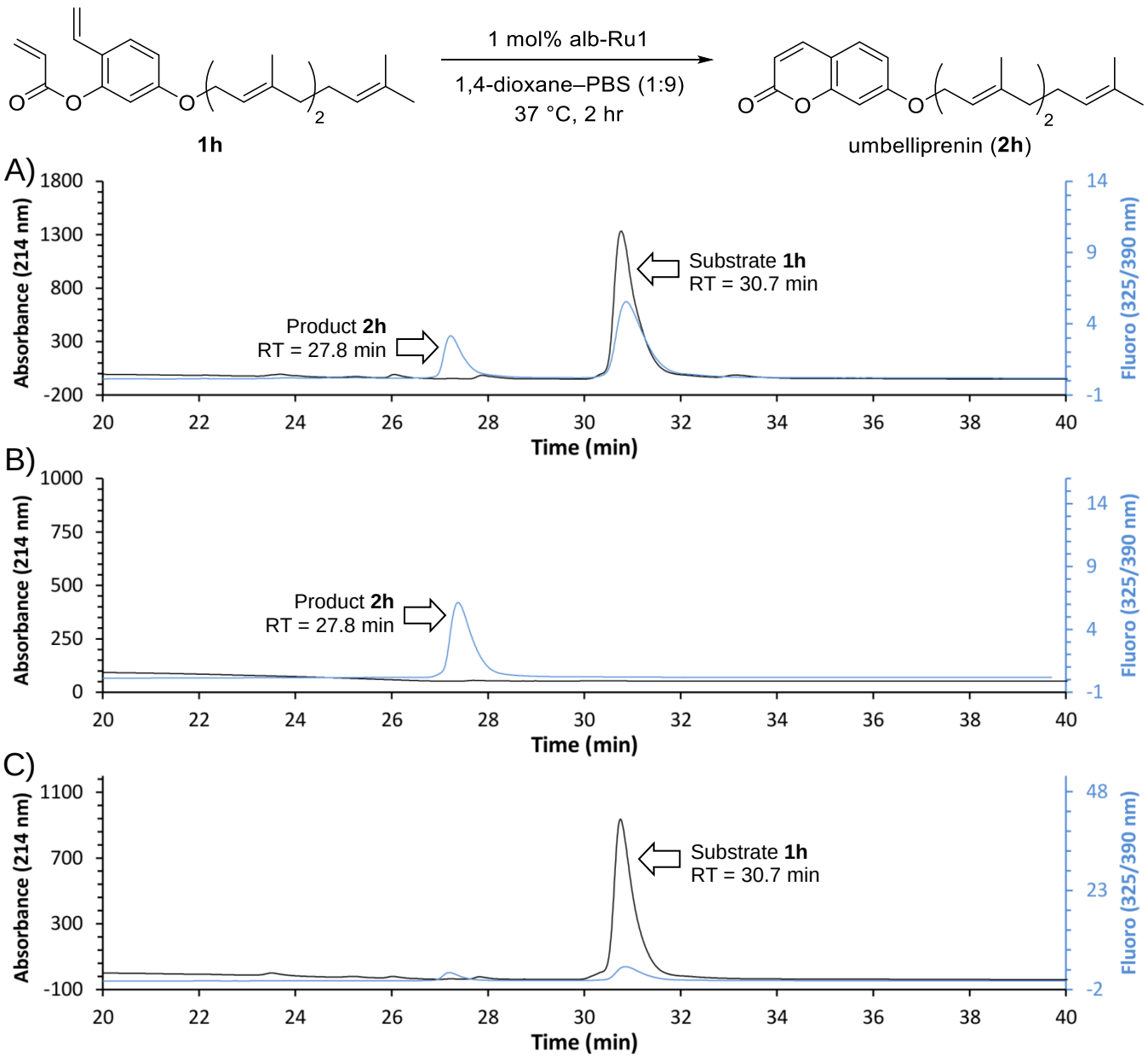

Supplementary Figure 51. Example HPLC traces of A) reaction mixture of **1h** incubated with alb-Ru1. Standard runs of known compounds include B) product **2h** standard, and C) substrate **1h** standard.

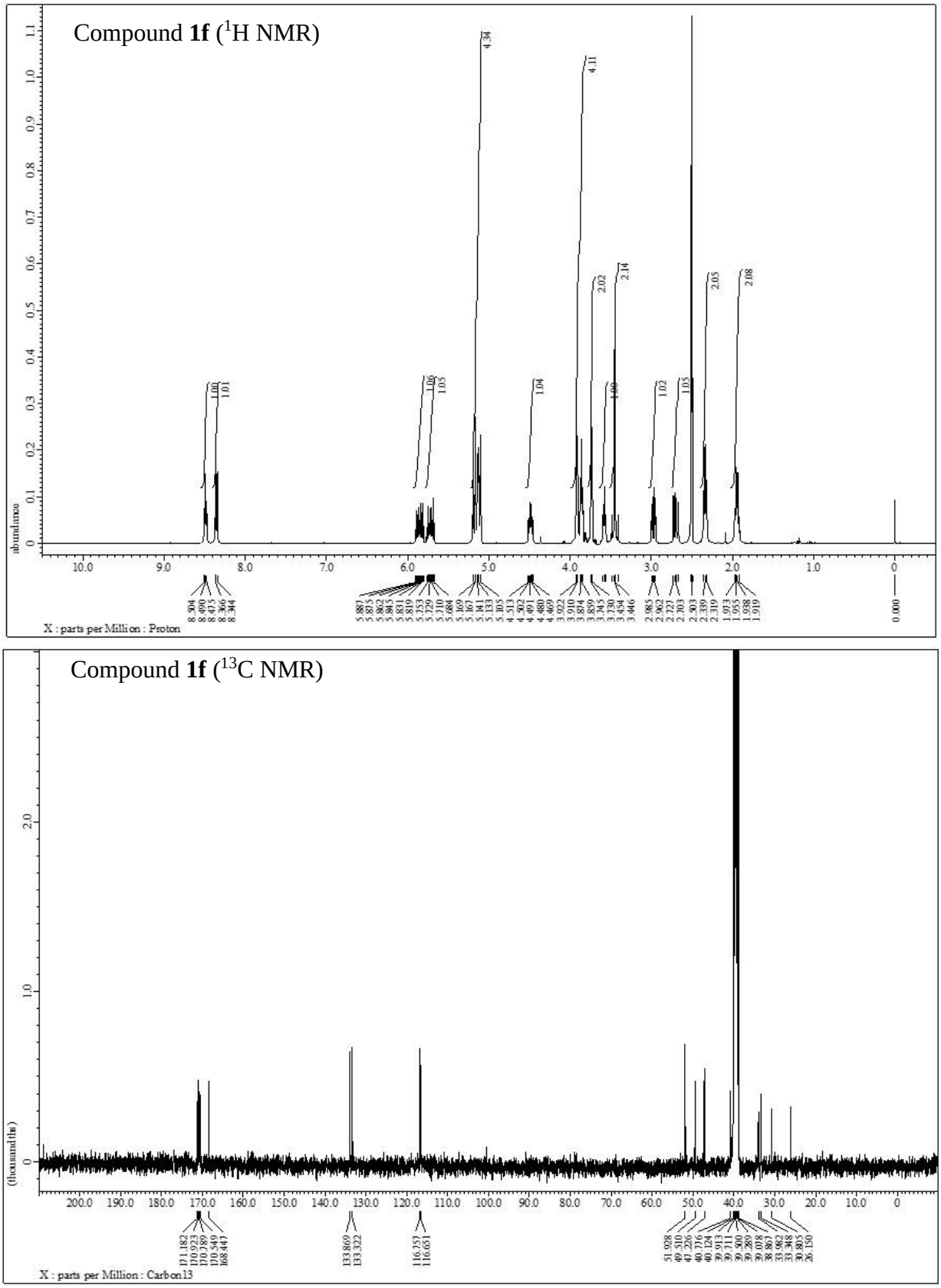

Supplementary Figure 52. NMR spectra of compound **1f**

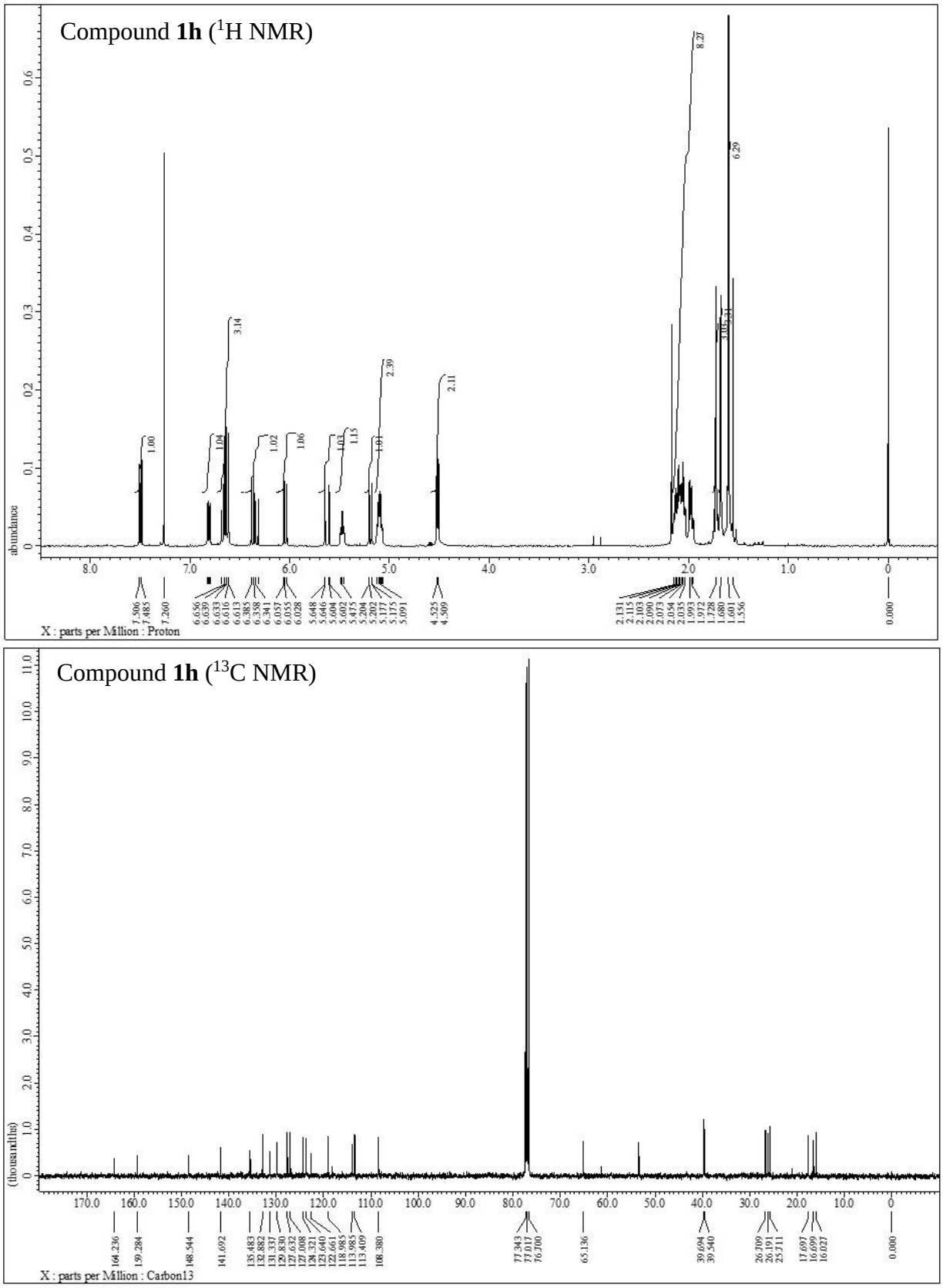

Supplementary Figure 53. NMR spectra of compound **1h**

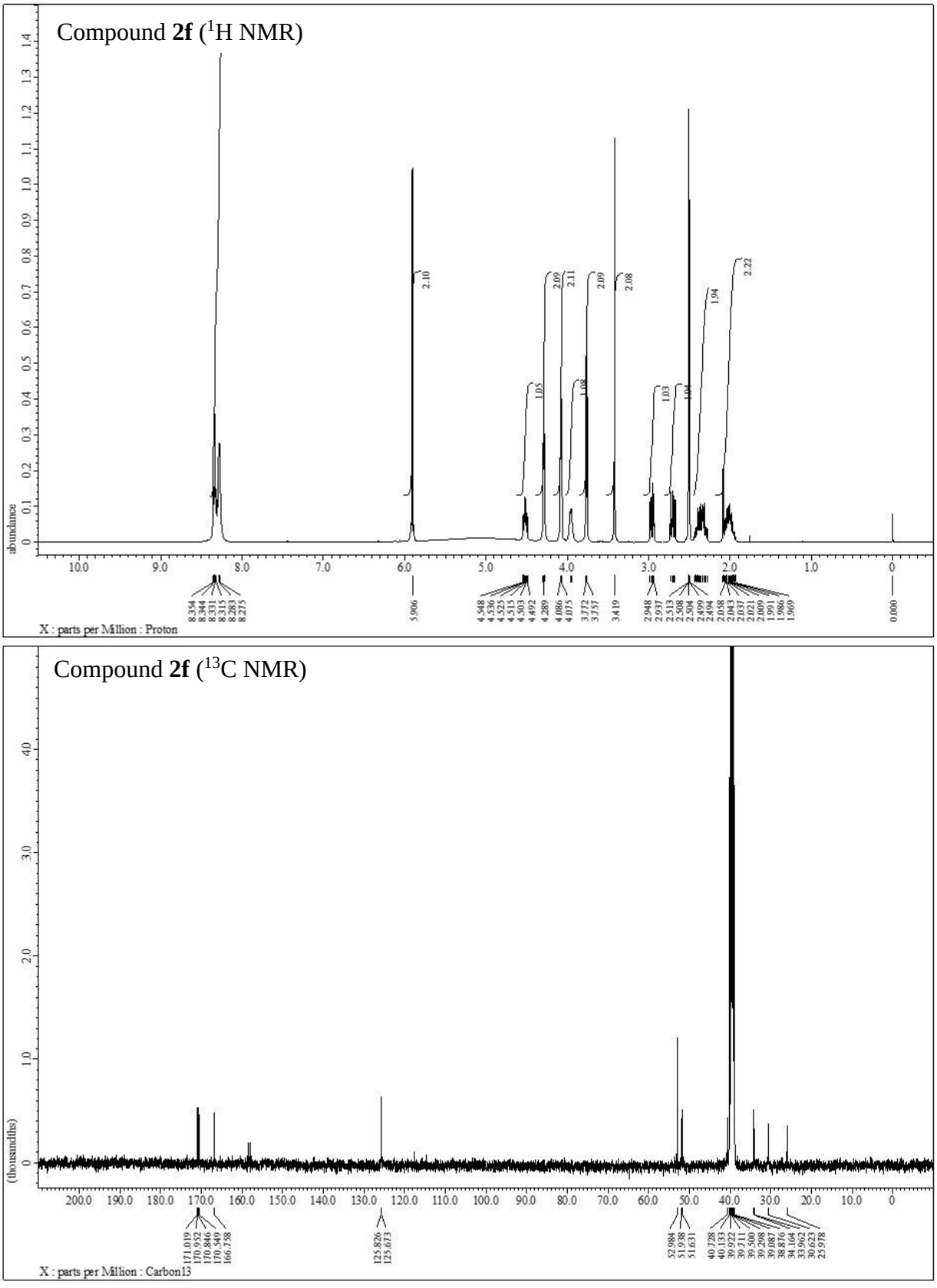

Supplementary Figure 54. NMR spectra of compound **2f**

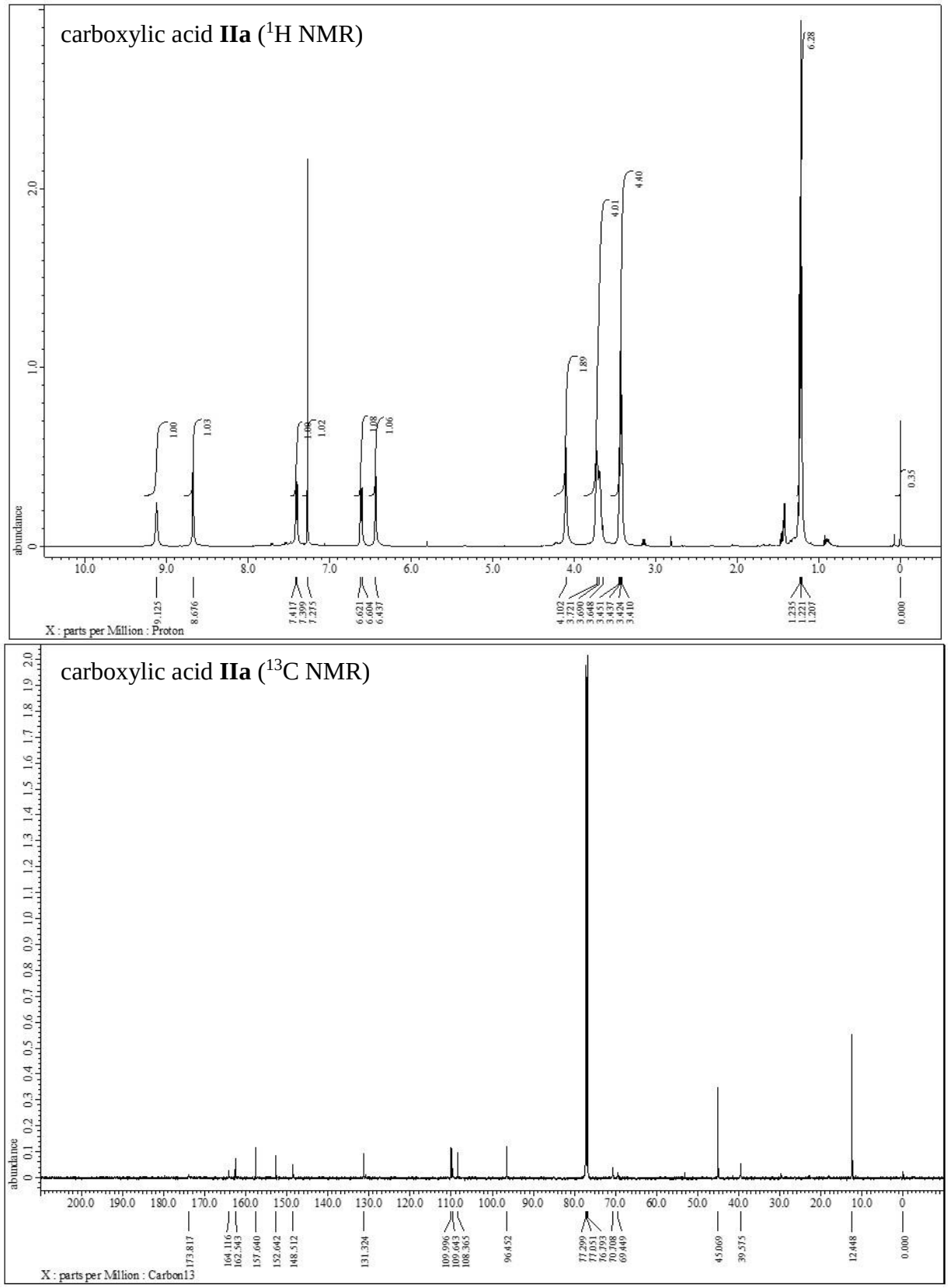

Supplementary Figure 55. NMR spectra of compound **IIa**

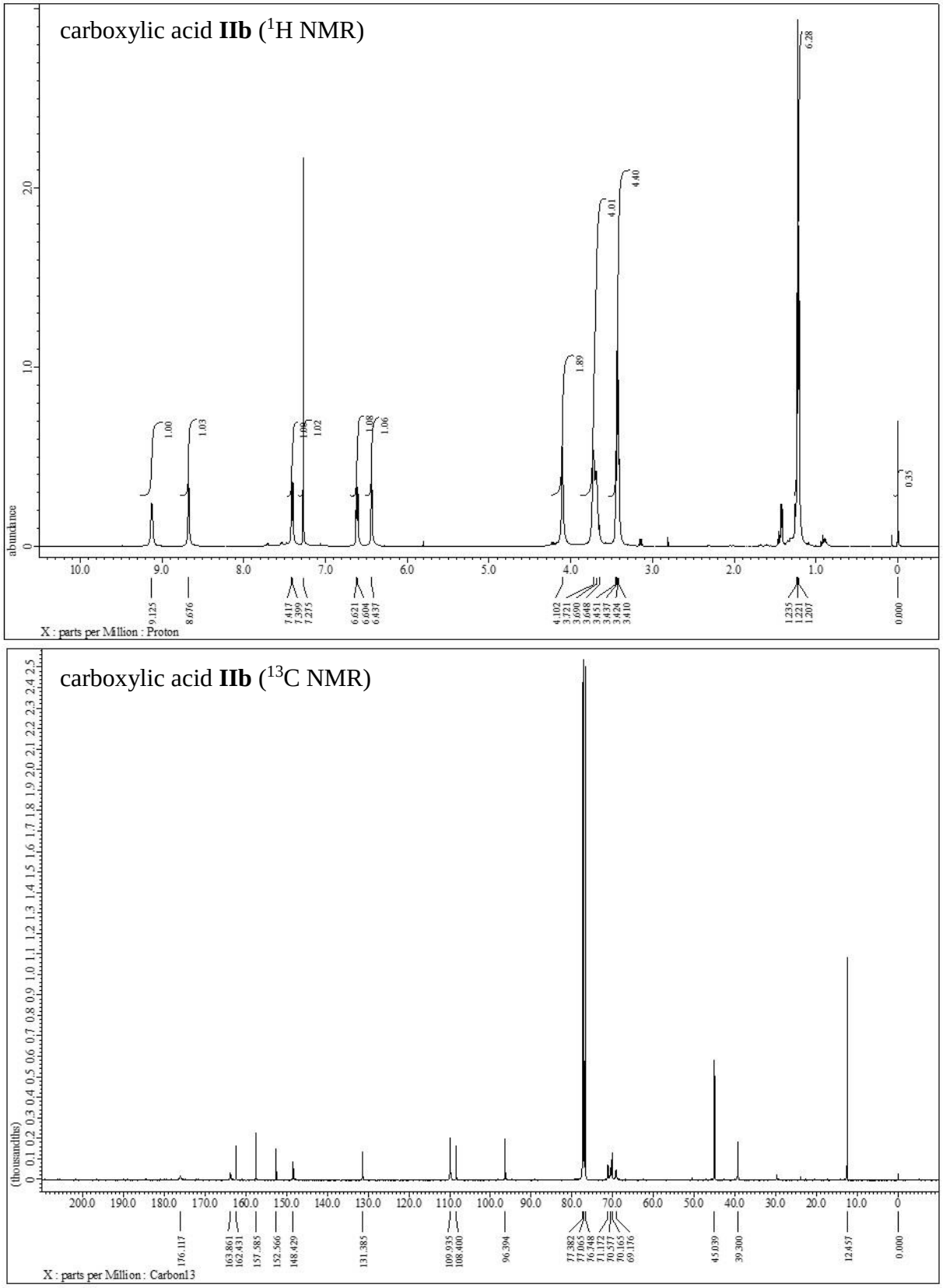

Supplementary Figure 56. NMR spectra of compound **IIb**

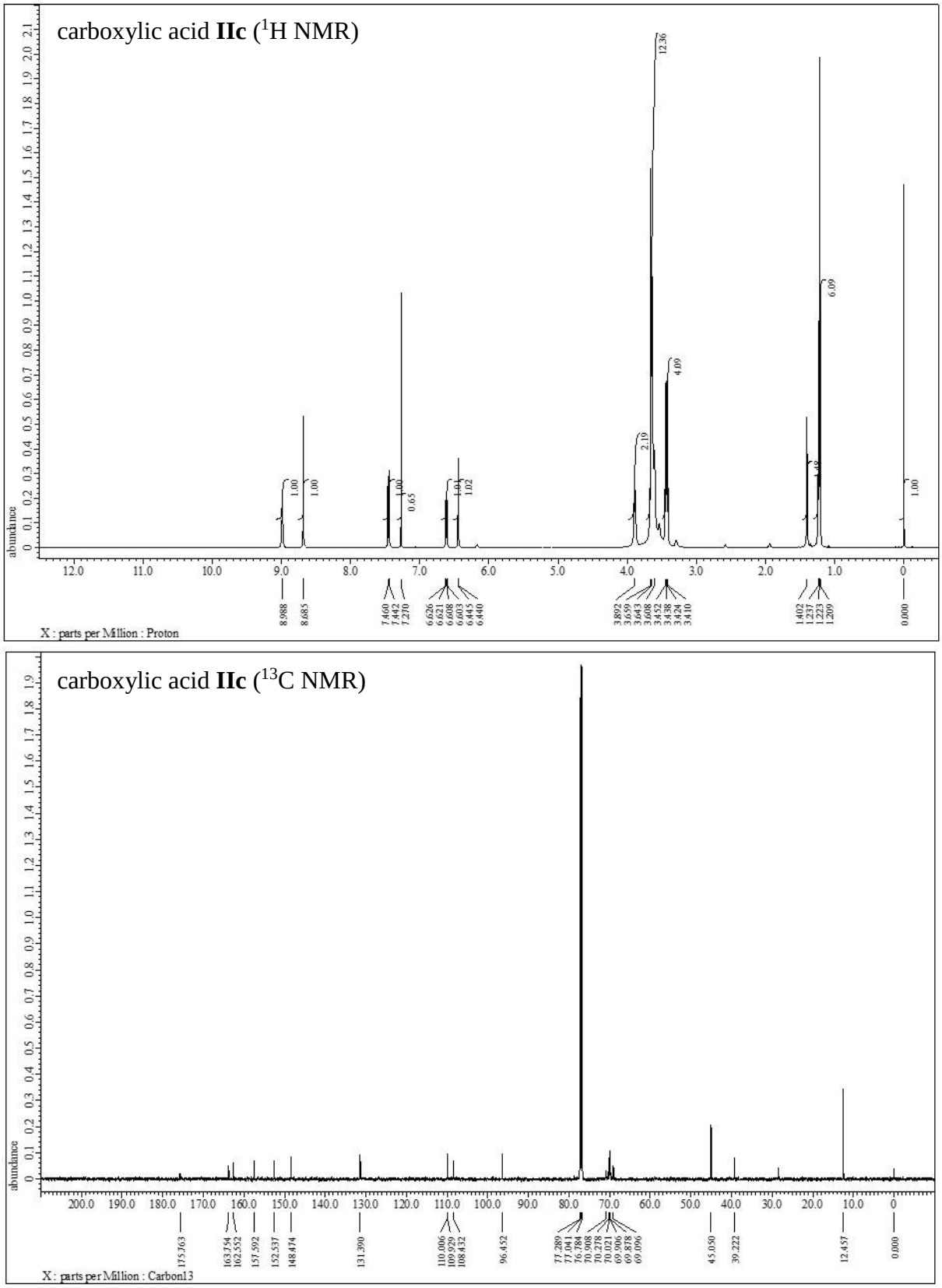

Supplementary Figure 57. NMR spectra of compound **IIc**

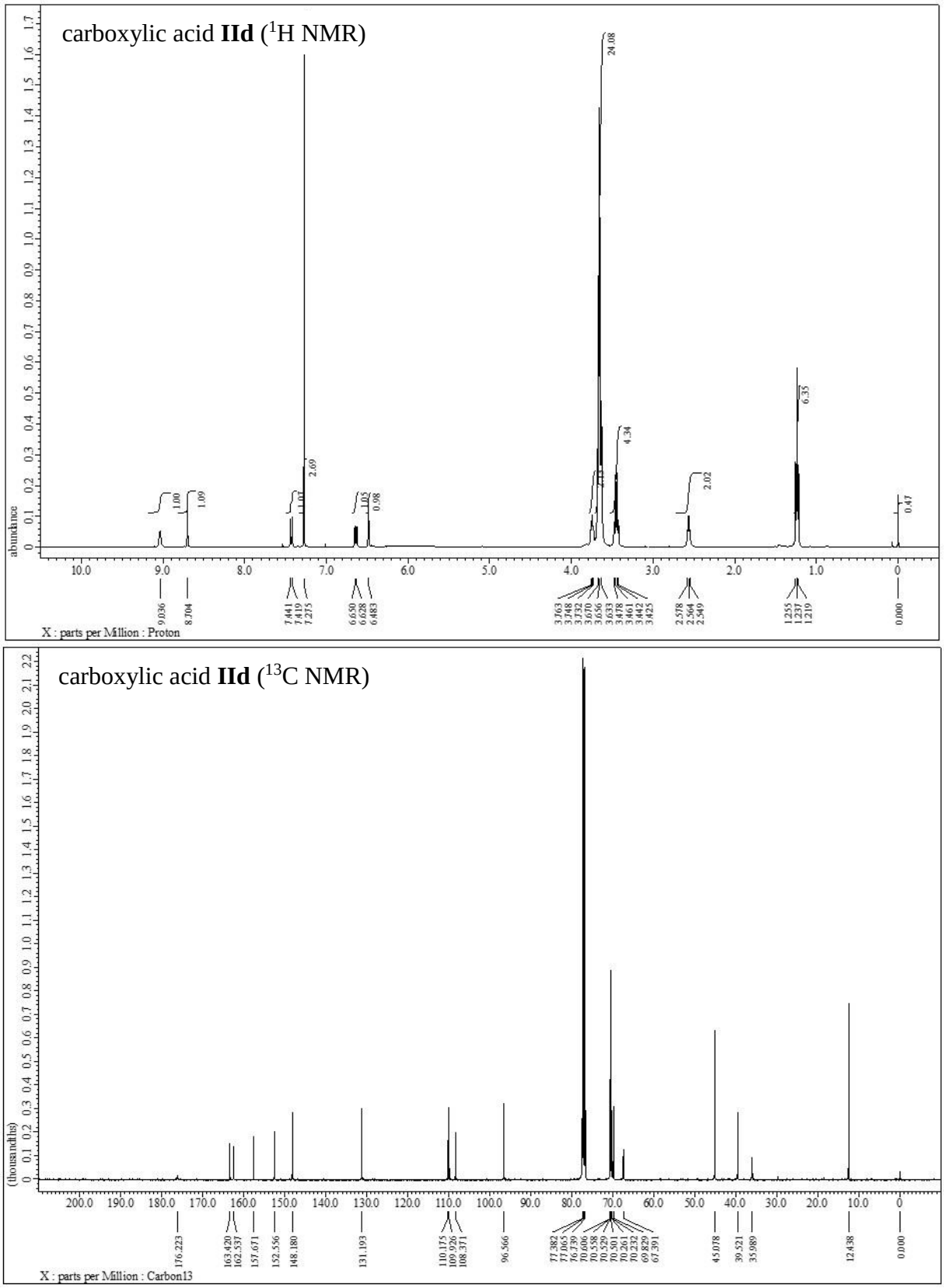

Supplementary Figure 58. NMR spectra of compound **IId**

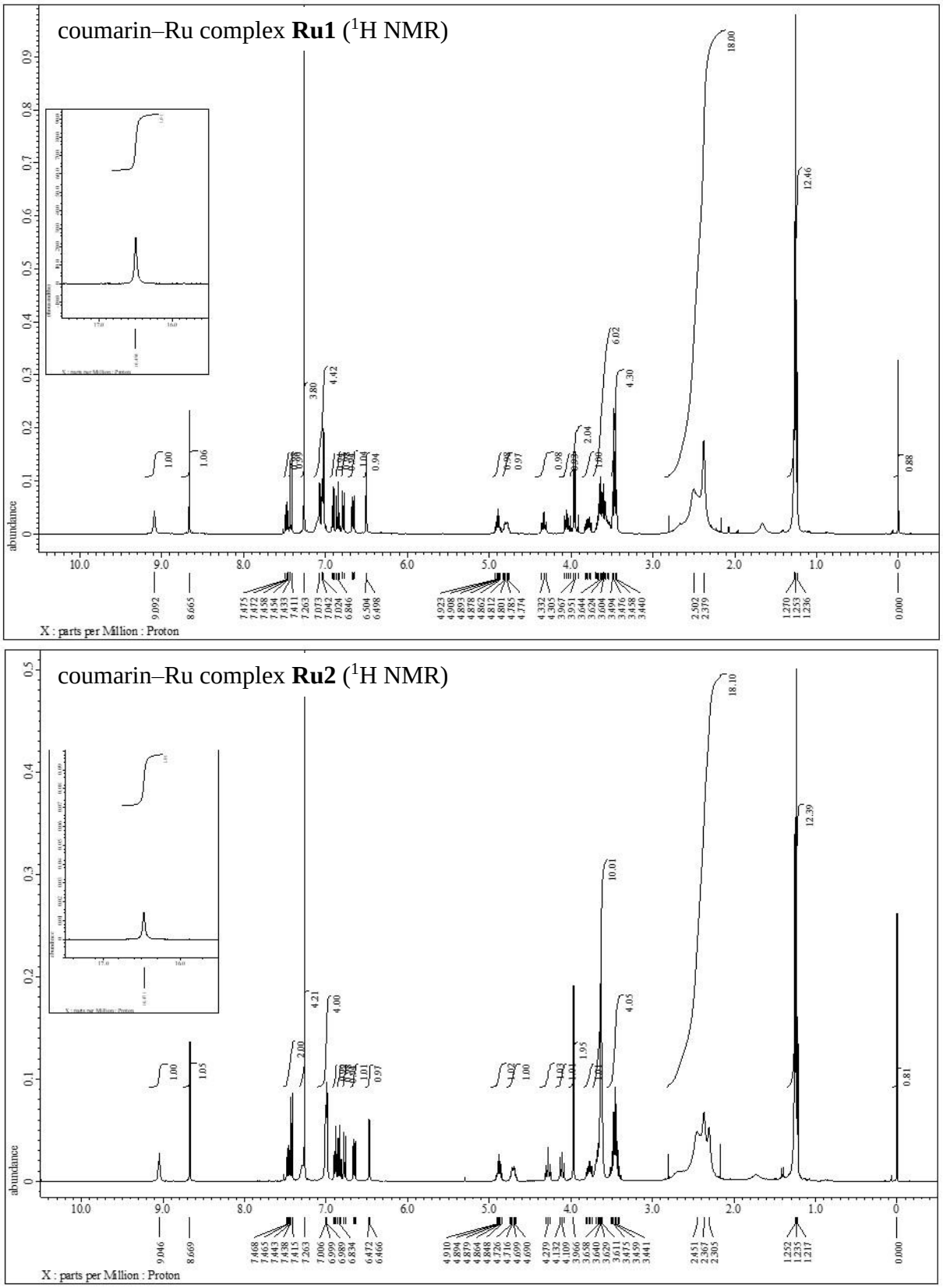

Supplementary Figure 59. NMR spectra of compound **Ru1** and **Ru2**

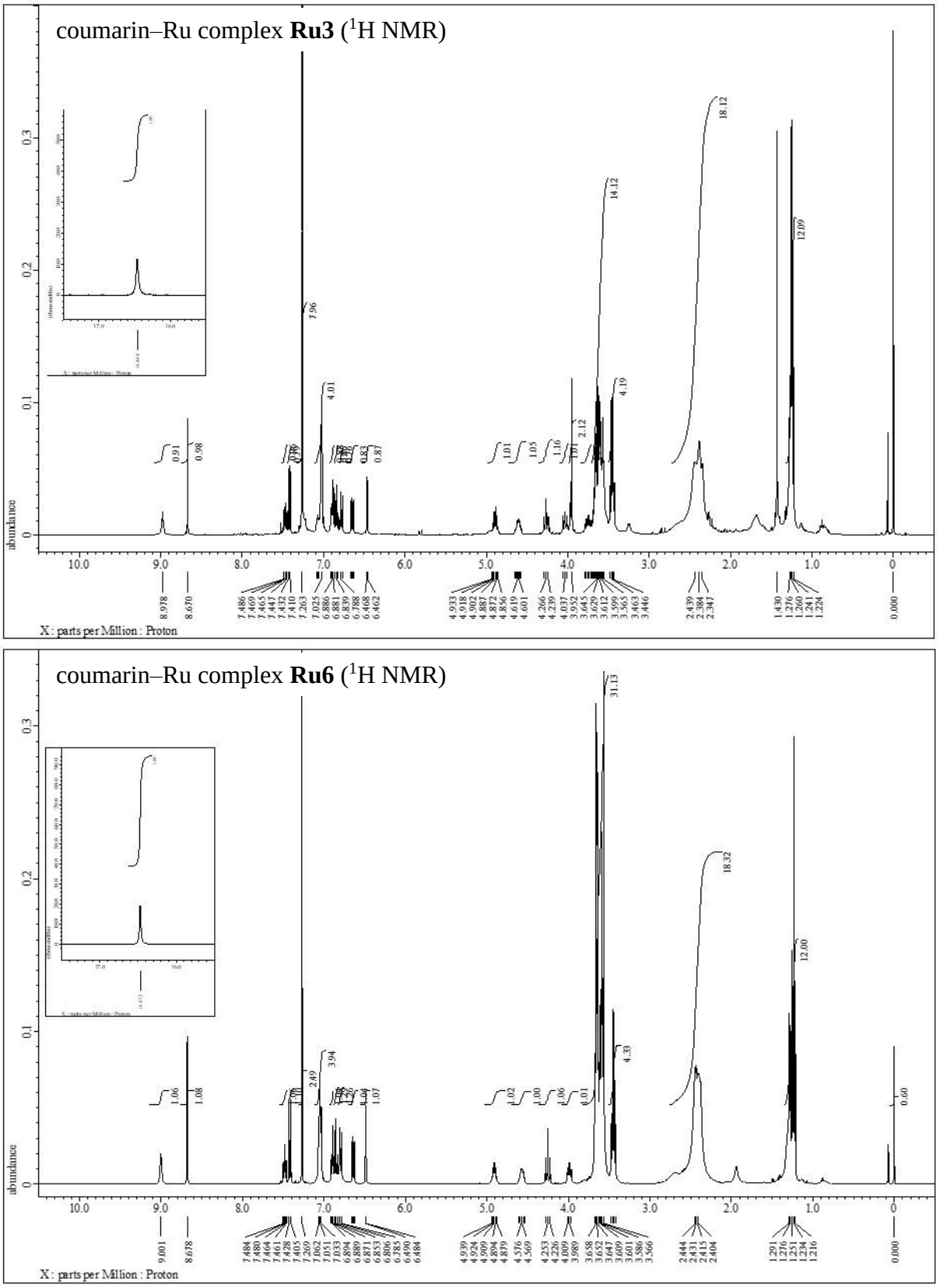

Supplementary Figure 60. NMR spectra of compound **Ru3** and **Ru6**

Supplementary Tables

Supplementary Table 1. Gradient profiles for HPLC purification

	Flow rate (ml/min)	Time (min)	%A (H_2O with 0.1% TFA)	%B (ACN with 0.1% TFA)
Method 1	1.0	0	70	30
		20	10	90
		20.5	70	30
		30	70	30
Method 2	1.0	0	50	50
		20	10	90
		20.5	50	50
		30	50	50
Method 3	1.0	0	35	65
		20	10	90
		20.5	35	65
		30	35	65
Method 4	1.0	0	90	10
		20	10	90
		25	90	10
		30	90	10
Method 5	1.0	0	90	10
		20	1	99
		25	90	10
		30	90	10
Method 6	1.0	0	60	40
		20	10	90
		40	10	90
		45	60	40
		50	60	40

Supplementary Table 2. Michaelis-Menten kinetics for substrates **1a-e** with alb-Ru1 complex both in the absence and presence of 10 equivalents (100 µM) of GSH. Reactivity was performed using varying concentrations of substrate with 10 µm of alb-Ru1. Summarized values are the maximum velocity (V_{max}), substrate affinity (K_M), turnover frequency (k_{cat}), catalytic efficiency (k_{cat}/K_M), and the coefficient of determination (R^2). Error is represented as the standard deviation of three independent experiments.

	V_{max} (µM/s)	K_M (mM)	k_{cat} (s^{-1})	k_{cat}/K_M (M^{-1} s^{-1})	R^2
without glutathione					
1a	0.5652 ± 0.0462	1.5950 ± 0.3724	0.0565 ± 0.0046	35.4 ± 8.8	0.8990
1b	0.9506 ± 0.0210	0.3279 ± 0.0401	0.0951 ± 0.0021	289.9 ± 36.0	0.9122
1c	0.1648 ± 0.0032	0.2231 ± 0.0303	0.0165 ± 0.0003	73.9 ± 10.1	0.8659
1d	0.7561 ± 0.0296	0.4258 ± 0.0806	0.0756 ± 0.0030	177.6 ± 34.3	0.8373
1e	7.802 ± 0.4868	0.2532 ± 0.0679	0.7802 ± 0.0487	3081.4 ± 848.4	0.9085
with glutathione (10 equivalents)					
1a	0.7108 ± 0.0389	1.0620 ± 0.2140	0.0711 ± 0.0039	66.9 ± 14.0	0.8770
1b	0.9619 ± 0.0257	0.3324 ± 0.0488	0.0962 ± 0.0026	289.4 ± 43.2	0.8750
1c	0.1579 ± 0.0031	0.1857 ± 0.0288	0.0158 ± 0.0003	85.0 ± 13.3	0.8224
1d	0.8245 ± 0.0568	0.5831 ± 0.1678	0.0825 ± 0.0057	141.4 ± 41.8	0.7487
1e	6.321 ± 0.3038	0.2409 ± 0.0503	0.6321 ± 0.0304	2623.9 ± 562.2	0.9366
initial velocity values were obtained in triplicate					

Supplementary Table 3. Calculated SASA values of whole ligands **Ru1-3,6**

		SASA (no albumin)	SASA (with albumin)	SASA of buried ligand in protein	Percentage of buried ligand
Ligand **Ru1** (PEG linker = 1)	(R)	1206.38135	29243.03516	850.49146	70.5%
	(S)	1238.15808	29315.96875	829.91302	67.0%
Ligand **Ru2** (PEG linker = 2)	(R)	1307.99536	29226.90820	909.36194	69.5%
	(S)	1205.93164	29219.69727	861.93555	71.5%
Ligand **Ru3** (PEG linker = 3)	(R)	1404.98645	29220.48047	961.07135	68.4%
	(S)	1376.80188	29175.78320	969.32770	70.4%
Ligand **Ru6** (PEG linker = 6)	(R)	1545.66138	29415.67969	933.80920	60.4%
	(S)	1672.71118	29375.95703	1017.19543	60.8%
Values rounded to 5 decimal places. Measurements were carried out with albumin (PDB 1H9Z), which has an individual SASA value of 29737.63672.					

Supplementary Table 4. Calculated SASA of specific atoms of the (R)-enantiomer of ligand **Ru1-3,6**

		Ligand **Ru1** (PEG linker = 1)	Ligand **Ru2** (PEG linker = 2)	Ligand **Ru3** (PEG linker = 3)	Ligand **Ru6** (PEG linker = 6)
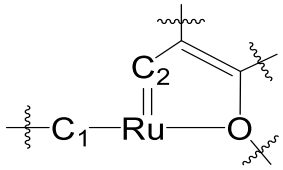	**C_1**	0	0	0	3.019
	Ru	0	0	0.503	3.522
	C_2	0	0.503	13.083	28.178
	O	0	0	0.942	0.942

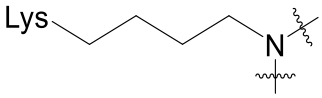		*Lys73*	*Lys195*	*Lys199*	*Lys351*
	N	19.970	29.225	26.165	13.151
		Lys402	*Lys439*	*Lys525*	*Lys541*
	N	36.044	43.350	48.708	19.483

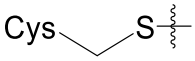		*Cys34*
	S	10.264

Supplementary Table 5. Measured fluorescence values and total cell counts (manually tallied) obtained for the calculation of fluorescence per cell. For each cell line and condition, a minimum of 3 images were taken at random locations.

	SW620			HeLa			A549		
	FL	cell count	FL / cell	FL	cell count	FL / cell	FL	cell count	FL / cell
Ru1	2203738	243	9069	367054	152	2415	469089	164	2860
	2015232	259	7781	321425	143	2248	531434	146	3640
	2188536	252	8685	337878	120	2816	486749	130	3744
			8511			**2493**			**3415**
glycoalbumin (2,3-Sia)	441533	172	2567	170608	206	828	188336	116	1624
	282156	130	2170	127667	148	863	321067	242	1327
	357477	153	2336	45138	100	451	597290	254	2352
			2358			**714**			**1767**
alb-Ru1	0	197	0	0	182	0	0	192	0
	0	213	0	0	113	0	0	187	0
	0	185	0	0	240	0	0	141	0
			0			**0**			**0**
GArM-Ru1 (2,3-Sia)	194745	98	1987	243481	258	944	199105	75	2655
	438549	173	2535	240493	240	1002	319371	112	2852
	260567	103	2530	198329	166	1195	201588	100	2016
			2351			**1047**			**2507**
FL = fluorescence									

Supplementary Methods

Binding Stoichiometry

To determine the stoichiometry of binding between HSA and catalysts **Ru1-3,6**, the Encinas─Lissi method was employed to characterize the stoichiometry of the binding step (n). The premise behind this approach is to carry out Stern-Volmer plots, as defined in Supplementary Equation 1, at several protein concentrations. For this equation, K_{SV} is the Stern-Volmer quenching constant, LIG_{tot} is the total ligand/quencher concentration, F_0 is the fluorescent intensity without a quencher, and F is the fluorescent intensity with a quencher.

$$\frac{F_0}{F} = 1 + K_{SV}(LIG_{tot}) \quad (1)$$

To begin, albumin under various concentrations was incubated with varying concentrations of compounds **Ru1-3,6** in 10% dioxane/PBS buffer for 1 hr at 37 °C. The resultant fluorescence measurements (Supplementary Figure 9) show greater quenching correlated to higher ligand concentrations. Using Supplementary Equation 1, this data can be transformed to fit Stern-Volmer plots (Supplementary Figure 10). As a note, all data sets were obtained separately under *Before Purification* and *After Purification* conditions in order to quantify the loss of ligand-binding due to spin-column filtration. For the *Before Purification* condition, mixtures were first cooled to room temperature and then aliquots (100 µl) were pipetted into 96-well microtiter plates for analysis. For the *After Purification* condition, mixtures cooled to room temperature were concentrated using Amicon® Ultra Centrifugal Filters (30 kDa) and washed (3×) with PBS buffer. Samples were then diluted to an appropriate volume and aliquoted (100 µl) into 96-well microtiter plates for analysis.

From the Stern-Volmer plots of Supplementary Figure 10, a set of LIG_{total} values can be obtained at different protein concentrations for any given (F^0/F) ratio, which is represented by the horizontal bars. Another means to define LIG_{total} is given by Supplementary Equation 2, which states it as the sum of unbound ligand (LIG_{free}) and bound ligand (LIG_{bound}) concentrations.

$$LIG_{tot} = LIG_{free} + LIG_{bound} \quad (2)$$

Supplementary Equation 2 can be further rewritten as Supplementary Equation 3, which redefines LIG_{bound} to incorporate the concentration of albumin protein (HSA) with the value of n, which is the ratio of ligand moles bound per moles of HSA protein.

$$LIG_{tot} = LIG_{free} + n[HSA] \quad (3)$$

Using Supplementary Equation 3, a plot LIG_{total} vs. [HSA] should theoretically give the value of n from the slope and the value of LIG_{free} from the y-intercept. Given that for 1:1 ligand-to-protein complexes, the value of n should be equal to 1, the plots shown in Supplementary Figure 11 were constructed for compounds **Ru1-3,6** at F^0/F ratios calculated to produce n values of 1. These plots theoretically give the necessary total ligand concentrations to ensure 1:1 ligand-to-protein complexes within a certain protein range. Using this data as a guide, reagent ratios used in the preparation of the protein-ruthenium catalyst complexes were adjusted accordingly.

Preparation of Substrates and Catalysts

General Procedure A: Synthesis of coumarin-linked carboxylic acid **IIa-d**

To a solution of *N*-succinimidyl 7-(diethylamino)coumarin-3-carboxylate **I** (1 equiv) and corresponding amine (1.1 equiv) in CH_2Cl_2 (3 mL) was added *N,N*-diisopropylethylamine (3 equiv) at 25 °C. After stirring for 16 h, the reaction was stopped by addition of 1 M aq. HCl. The product was then extracted with CH_2Cl_2 (×3), and the combined organic extracts were washed with brine, dried (Na_2SO_4), and concentrated *in vacuo*. The residue was purified by silica-gel flash column chromatography as indicated to give compounds **IIa-d**.

General Procedure B: Synthesis of coumarin-linked ruthenium complexes **Ru1-3,6**

The ruthenium complex **III** was prepared according to literature.[5-7] A solution of ruthenium complex **III** (80.0 mg, 0.106 mmol) in CH_2Cl_2 (3 mL) was bubbled with HCl gas at 25 °C. The gaseous HCl was generated by dropwise addition of conc. H_2SO_4 to NH_4Cl. After stirring for 45 min, CH_2Cl_2 (1 mL) was added to the reaction with a syringe and was continued to be stirred at the same temperature. After a further 15 min, the reaction was concentrated *in vacuo* to give amine **IV**, which was used in the next reaction without further purification. HRMS (ESI) *m*/*z* 620.1979 (620.1981 calcd for $C_{31}H_{41}ClN_3ORu$, $[M–Cl]^+$).

In another flask, a solution of carboxylic acid **IIa** (1.1 equiv) and the coupling agent HCTU (1.3 equiv) in CH_2Cl_2 (1 mL) was stirred at 25 °C for 30 min. To this reaction was added **IV** (1 equiv) in CH_2Cl_2 (1 mL) followed by *N,N*-diisopropylethylamine (10 equiv) at the same temperature. After stirring for 6 h, the reaction was stopped by adding 1 M aq. HCl. The product was extracted with CH_2Cl_2 (×3), and the combined organic extracts were washed with sat. aq. $NaHCO_3$ and brine, dried (Na_2SO_4), and concentrated *in vacuo*. The residue was purified by silica-gel flash column chromatography as indicated to give coumarin–Ru complex **Ru1-3,6**.

General Procedure C: Synthesis of ring-closing metathesis products **2a-e**

The Hoveyda-Grubbs Generation II solution (100 mM stock) was prepared by dissolving the catalyst (7.01 μmol) in CH_2Cl_2 (70 μL). Substrate solutions of **1a-e** (100 mM stock) were then prepared and and mixed with the Hoveyda-Grubbs catalyst solution (5 mol%), followed by incubation in a shaker for 24 h at 37 °C.

Preparation of **IIa**

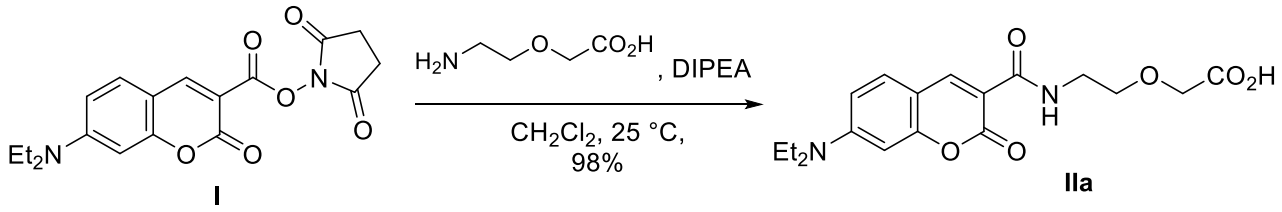

Prepared according to General Procedure A. Compound **I** (100 mg, 0.279 mmol), 5-amino-3-oxapentanoic acid (36.6 mg, 0.307 mmol) and *N*,*N*-diisopropylethylamine (110 mg, 0.851 mmol) gave, after purification by silica-gel flash column chromatography ($CHCl_3$/MeOH = 9/1 → 8/2 → $CHCl_3$/MeOH/AcOH = 79/20/1), the desired carboxylic acid **IIa** (100 mg, 98.9%) as a yellow solid.

^{1}H-NMR (500 MHz, $CDCl_3$, δ) 1.22 (t, 6H, *J* = 6.9 Hz), 3.41 (q, 4H, *J* = 6.9 Hz), 3.64–3.72 (m, 4H), 4.10 (s, 2H), 6.44 (s, 1H, *J* = 2.3 Hz), 6.61 (d, 1H, *J* = 8.8 Hz), 7.41 (d, 1H, *J* = 8.8 Hz), 8.68 (s, 1H), 9.13 (s, 1H);

^{13}C-NMR (125 MHz, $CDCl_3$, δ) 12.4 (2C), 39.6, 45.1 (2C), 69.4, 70.7, 96.5, 108.4, 109.6, 110.0, 131.3, 148.5, 152.6, 157.6, 162.5, 164.1, 173.8;

HRMS (ESI) *m*/*z* 363.1555 (363.1551 calcd for $C_{18}H_{23}N_2O_6$, $[M+H]^+$).

Preparation of **IIb**

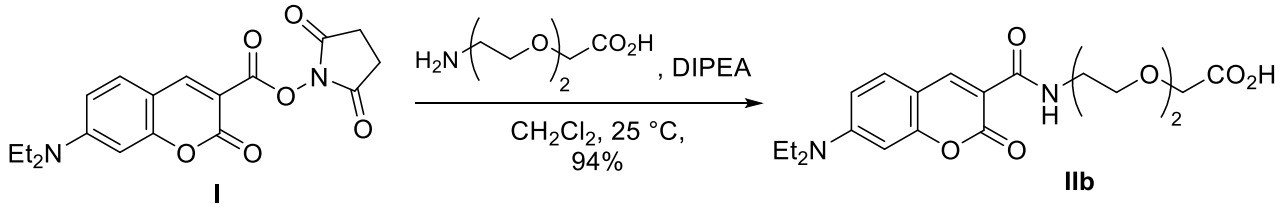

Prepared according to General Procedure A. Compound **I** (108 mg, 0.301 mmol), 8-amino-3,6-dioxaoctanoic acid (54.1 mg, 0.332 mmol) and *N*,*N*-diisopropylethylamine (116 mg, 0.898 mmol) in CH_2Cl_2 (3 mL) gave, after purification by silica-gel flash column chromatography ($CHCl_3$/MeOH = 9/1 → 8/2 → $CHCl_3$/MeOH/AcOH = 79/20/1), the desired carboxylic acid **IIb** (115 mg, 94.0%) as a yellow solid.

^{1}H-NMR (400 MHz, $CDCl_3$, δ) 1.21 (t, 6H, *J* = 7.0 Hz), 3.42 (q, 4H, *J* = 7.0 Hz), 3.64–3.71 (m, 8H), 4.00 (s, 2H), 6.40 (br s, 1H), 6.60 (dd, 1H, J_1 = 2.1 Hz, J_2 = 8.8 Hz), 7.43 (d, 1H, *J* = 8.8 Hz), 8.65 (s, 1H), 9.02 (s, 1H);

^{13}C-NMR (100 MHz, $CDCl_3$, δ) 12.5 (2C), 39.3, 45.0 (2C), 69.2, 70.2, 70.6, 71.2, 96.4, 108.4, 109.9 (2C), 131.4, 148.4, 152.6, 157.6, 162.4, 163.9, 176.1;

HRMS (ESI) *m*/*z* 407.1822 (407.1813 calcd for $C_{20}H_{27}N_2O_7$, $[M+H]^+$).

Preparation of 11-amino-3,6,9-trioxaundecanoic acid

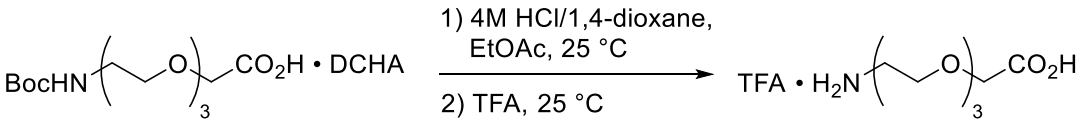

To a solution of *tert*-butyloxycarbonyl-11-amino-3,6,9-trioxaundecanoic acid • dicyclohexylamine (500 mg, 1.02 mmol) in EtOAc (10 mL) was added 4M HCl in 1,4-dioxane (280 µL, 1.12 mmol) at 25 °C. After stirring for 4 h, the mixture was filtered through a Hirsch funnel to remove white solids and the filtrate was concentrated *in vacuo*. The residue was dissolved in TFA (300 µL) and the mixture was stirred at 25 °C for 15 min. After removal of excess TFA by flushing nitrogen gas, the residue was dissolved in water and lyophilized to give 11-Amino-3,6,9-trioxaundecanoic acid • TFA (301 mg, 97.0%) as colorless oil. Characterization matched a previous report of this known compound.[8]

Preparation of **IIc**

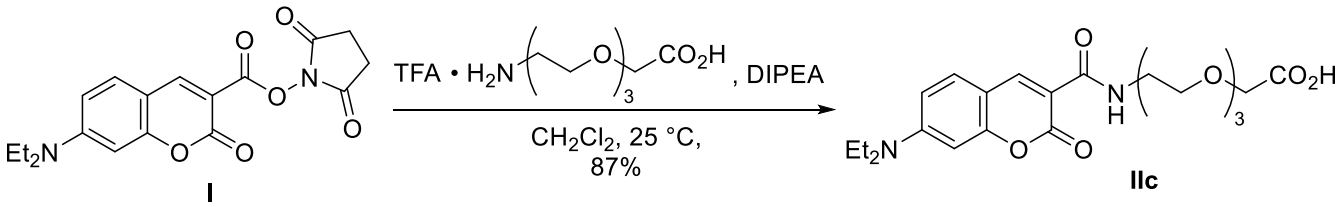

Prepared according to General Procedure A. Compound **I** (105 mg, 0.293 mmol), 11-amino-3,6,9-trioxaundecanoic acid • TFA (98.0 mg, 0.322 mmol) and *N*,*N*-diisopropylethylamine (227 mg, 1.76 mmol) gave, after purification by silica-gel flash column chromatography ($CHCl_3$/MeOH = 9/1 → 8/2 → $CHCl_3$/MeOH/AcOH = 69/30/1), the desired carboxylic acid **IIc** (115 mg, 87.0%) as a yellow solid.

^{1}H-NMR (500 MHz, $CDCl_3$, δ) 1.22 (t, 6H, J = 7.2 Hz), 3.43 (q, 4H, $_J$ = 7.2 Hz), 3.60–3.67 (m, 12H), 3.89 (s, 2H), 6.44 (d, 1H, J = 2.3 Hz), 6.61 (dd, 1H, J_1 = 2.3 Hz, J_2 = 9.0 Hz), 7.45 (d, 1H, J = 9.0 Hz), 8.68 (s, 1H), 8.99 (s, 1H);

^{13}C-NMR (125 MHz, $CDCl_3$, δ) 12.5 (2C), 39.2, 45.1 (2C), 69.1, 69.87, 69.90, 70.0, 70.3, 70.9, 96.5, 108.4, 109.9, 110.0, 131.4, 148.5, 152.5, 157.6, 162.6, 163.8, 175.8;

HRMS (ESI) *m/z* 451.2076 (451.2075 calcd for $C_{22}H_{31}N_2O_8$, $[M+H]^+$)

Preparation of **IId**

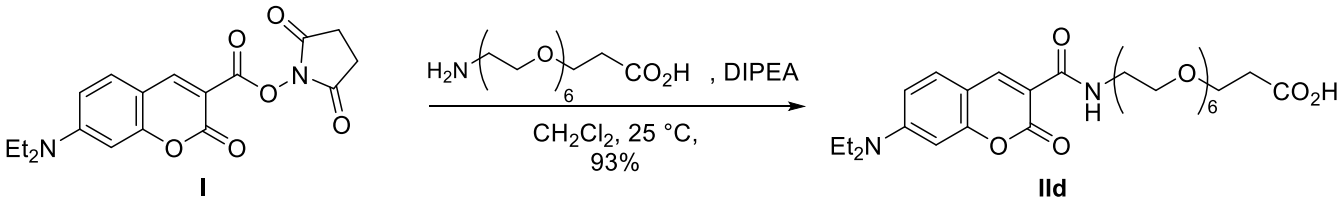

Prepared according to General Procedure A. Compound **I** (101 mg, 0.282 mmol), 21-amino-4,7,10,13,16,19-hexaoxahenicosanoic acid (110 mg, 0.311 mmol) and *N*,*N*-diisopropylethylamine (110 mg, 0.851 mmol) gave, after purification by silica-gel flash column chromatography ($CHCl_3$/MeOH = 9/1 → 8/2 → $CHCl_3$/MeOH/AcOH = 79/20/1), the desired carboxylic acid **IId** (157 mg, 93.3%) as a yellow oil.

^{1}H-NMR (400 MHz, $CDCl_3$, δ) 1.24 (t, 6H, *J* = 7.1 Hz), 2.56 (t, 2H, *J* = 6.1 Hz), 3.45 (q, 4H, *J* = 7.1 Hz), 3.62–3.68 (m, 24H), 3.75 (t, 2H, *J* = 6.1 Hz), 6.48 (s, 1H), 6.64 (d, 1H, *J* = 8.8 Hz), 7.43 (d, 1H, *J* = 8.8 Hz), 8.70 (s, 1H), 9.04 (s, 1H);

^{13}C-NMR (100 MHz, $CDCl_3$, δ) 12.4 (2C), 36.0, 39.5, 45.1 (2C), 67.4, 69.8, 70.2, 70.3, 70.5–70.6 (8C), 96.6, 108.4, 109.9, 110.2, 131.2, 148.2, 152.6, 157.7, 162.5, 163.4, 176.2;

HRMS (ESI) *m*/*z* 597.3035 (597.3018 calcd for $C_{29}H_{45}N_2O_{11}$, $[M+H]^+$).

Preparation of **Ru1**

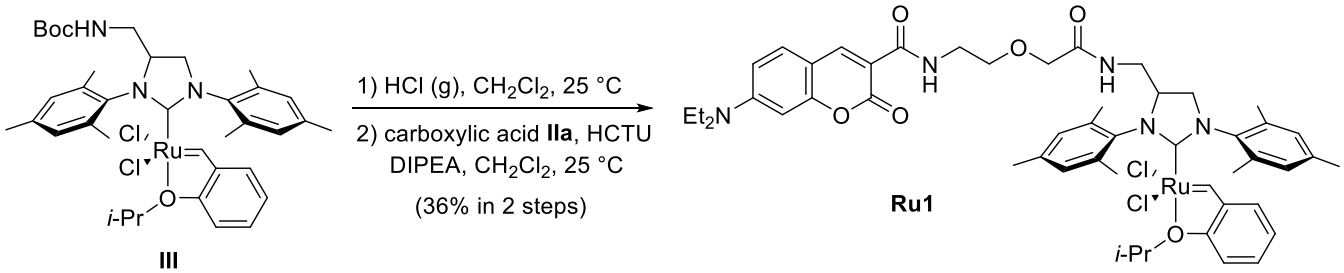

Prepared according to General Procedure B. Ruthenium complex **III** (80.1 mg, 0.106 mmol), carboxylic acid **IIa** (42.4 mg, 0.117 mmol), HCTU (57.6 mg, 0.139 mmol) and *N*,*N*-diisopropylethylamine (137 mg, 1.06 mmol) gave, after purification by silica-gel flash column chromatography (cyclohexane/EtOAc/$CHCl_3$/MeOH = 40/40/15/5), the desired coumarin–Ru complex **Ru1** (37.7 mg, 35.6%) as a green solid.

^{1}H-NMR (400 MHz, $CDCl_3$, δ) 1.24–1.27 (m, 12H), 2.37–2.51 (br m, 18H), 3.47 (q, 4H, *J* = 7.1 Hz), 3.53–3.71 (m, 6H), 3.79 (m, 1H), 3.93 (d, 1H, *J* = 15.3 Hz), 3.99 (d, 1H, *J* = 15.3 Hz), 4.05 (dd, 1H, J_1 = J_2 = 10.0 Hz), 4.33 (dd, 1H, J_1 = J_2 = 10.0 Hz), 4.75–4.84 (br m, 1H), 4.89 (sept, 1H, *J* = 6.1 Hz), 6.50 (d, 1H, *J* = 2.3 Hz), 6.66 (dd, 1H, J_1 = 2.3 Hz, J_2 = 9.1 Hz), 6.78 (d, 1H, *J* = 7.7 Hz), 6.85 (dd, 1H, J_1 = J_2 = 7.7 Hz), 6.91 (dd, 1H, J_1 = 1.7 Hz, J_2 = 7.7 Hz), 7.02 (s, overlapped, 2H), 7.04 (s, 1H), 7.07 (s, 1H), 7.42 (d, 1H, *J* = 9.1 Hz), 7.48 (ddd, 1H, J_1 = 1.7 Hz, J_2 = J_3 = 7.7 Hz), 8.67 (s, 1H), 9.09 (s, 1H), 16.50 (s. 1H);

HRMS (ESI) *m*/*z* 964.3355 (964.3359 calcd for $C_{50}H_{61}ClN_5O_6Ru$, $[M–Cl]^+$).

Preparation of **Ru2**

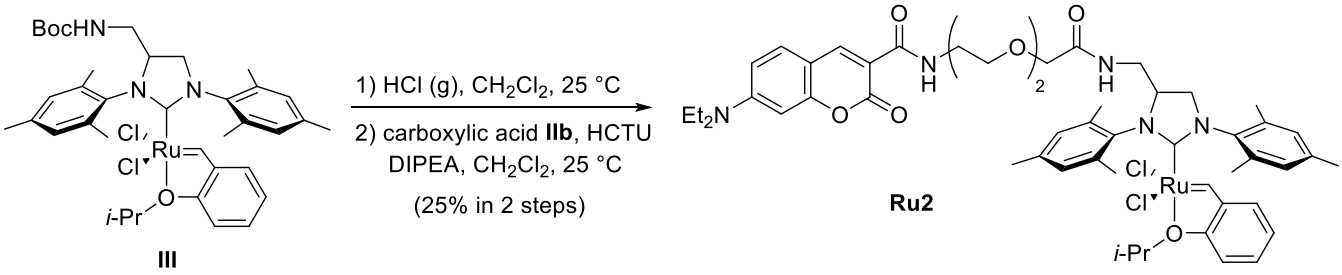

Prepared according to General Procedure B. Ruthenium complex **III** (80.1 mg, 0.106 mmol), carboxylic acid **IIb** (47.4 mg, 0.117 mmol), HCTU (57.1 mg, 0.138 mmol) and *N*,*N*-diisopropylethylamine (137 mg, 1.06 mmol) gave, after purification by silica-gel flash column chromatography (cyclohexane/EtOAc/$CHCl_3$/MeOH = 40/40/15/5), the desired coumarin–Ru complex **Ru2** (27.9 mg, 25.2%) as a green solid.

^{1}H-NMR (400 MHz, $CDCl_3$, δ) 1.22–1.26 (m, 12H), 2.26–2.46 (br m, 18H), 3.38–3.54 (m, 4H), 3.61–3.70 (m, 10H), 3.74–3.82 (m, 1H), 3.97 (s, 2H), 4.11 (dd, 1H, $J_1 = J_2 = 10.3$ Hz), 4.28 (dd, 1H, $J_1 = J_2 = 10.3$ Hz), 4.66–4.75 (br m, 1H), 4.88 (sept, 1H, $J = 6.1$ Hz), 6.47 (d, 1H, $J = 2.3$ Hz), 6.65 (dd, 1H, $J_1 = 2.3$ Hz, $J_2 = 9.0$ Hz), 6.77 (d, 1H, $J = 7.6$ Hz), 6.83 (dd, 1H, $J_1 = J_2 = 7.6$ Hz), 6.89 (dd, 1H, $J_1 = 1.9$ Hz, $J_2 = 7.6$ Hz), 6.98–7.01 (br m, 4H), 7.43 (d, 1H, $J = 9.0$ Hz), 7.47 (ddd, 1H, $J_1 = 1.9$ Hz, $J_2 = J_3 = 7.6$ Hz), 8.67 (s, 1H), 9.05 (s, 1H), 16.47 (s. 1H);

HRMS (ESI) *m*/*z* 1008.3613 (1008.3622 calcd for $C_{52}H_{65}ClN_5O_7Ru$, $[M–Cl]^+$).

Preparation of **Ru3**

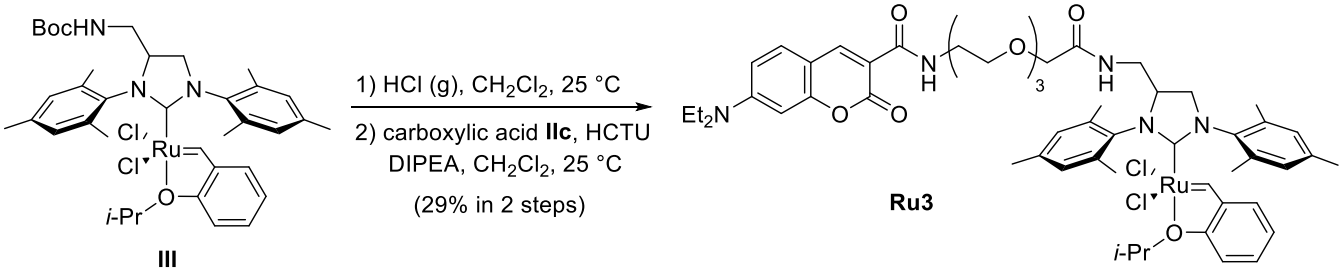

Prepared according to General Procedure B. Ruthenium complex **III** (28.8 mg, 38.1 µmol), carboxylic acid **IIc** (18.9 mg, 42.0 µmol), HCTU (21.3 mg, 51.5 µmol) and *N*,*N*-diisopropylethylamine (49.7 µg, 385 µmol) gave, after purification by silica-gel flash column chromatography (cyclohexane/EtOAc/$CHCl_3$/MeOH = 40/40/15/5), the desired coumarin–Ru complex **Ru3** (12.0 mg, 28.9%) as a green solid.

^{1}H-NMR (400 MHz, $CDCl_3$, δ) 1.22–1.28 (m, 12H), 2.34–2.44 (br m, 18H), 3.46 (q, 4H, $J = 7.2$ Hz), 3.55–3.70 (m, 14H), 3.71–3.80 (m, 1H), 3.95 (s, 2H), 4.04 (dd, 1H, $J_1 = J_2 = 10.7$ Hz), 4.27 (dd, 1H, $J_1 = J_2 = 10.7$ Hz), 4.57–4.65 (m, 1H), 4.89 (sept, 1H, $J = 6.2$ Hz), 6.47 (d, 1H, $J = 2.3$ Hz), 6.65 (dd, 1H, $J_1 = 2.3$ Hz, $J_2 = 8.8$ Hz), 6.79 (d, 1H, $J = 7.7$ Hz), 6.84 (dd, 1H, $J_1 = J_2 = 7.6$ Hz), 6.89 (dd, 1H, $J_1 = 1.9$ Hz, $J_2 = 7.6$ Hz), 7.01–7.05 (br m, 4H), 7.42 (d, 1H, $J = 8.8$ Hz), 7.47 (ddd, 1H, $J_1 = 1.9$ Hz, $J_2 = J_3 = 7.6$ Hz), 8.67 (s, 1H), 8.98 (s, 1H), 16.47 (s. 1H);

HRMS (ESI) *m*/*z* 1088.3661 (1088.3648 calcd for $C_{54}H_{70}Cl_2N_5O_8Ru$, $[M+H]^+$).

Preparation of **Ru6**

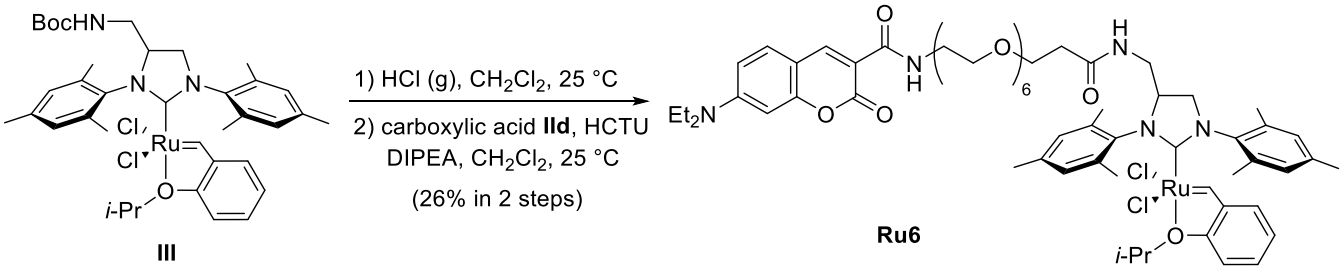

Prepared according to General Procedure B. Ruthenium complex **III** (80.4 mg, 0.106 mmol), carboxylic acid **IId** (69.9 mg, 0.117 mmol), HCTU (57.5 mg, 0.139 mmol) and *N*,*N*-diisopropylethylamine (137 mg, 1.06 mmol) gave, after purification by silica-gel flash column chromatography (cyclohexane/EtOAc/$CHCl_3$/MeOH = 20/20/55/5), the desired coumarin–Ru complex **Ru6** (34.4 mg, 26.3%) as a green solid.

^{1}H-NMR (400 MHz, $CDCl_3$, δ) 1.21–1.30 (m, 12H), 2.37–2.45 (br m, 18H), 3.45 (q, 4H, J = 7.3 Hz), 3.56–3.68 (m, 31H), 3.99 (dd, 1H, J_1 = J_2 = 10.5 Hz), 4.25 (dd, 1H, J_1 = J_2 = 10.5 Hz), 4.53–4.62 (br m, 1H), 4.91 (sept, 1H, J = 6.1 Hz), 6.49 (d, 1H, J = 2.3 Hz), 6.64 (dd, 1H, J_1 = 2.3 Hz, J_2 = 8.8 Hz), 6.80 (d, 1H, J = 7.6 Hz), 6.86 (dd, 1H, J = 7.6 Hz), 6.90 (dd, 1H, J_1 = 1.9 Hz, J_2 = 7.6 Hz), 7.03–7.07 (br m, 4H), 7.42 (d, 1H, J = 8.8 Hz), 7.48 (ddd, 1H, J_1 = 1.9 Hz, J_2 = J_3 = 7.6 Hz), 8.68 (s, 1H), 9.00 (s, 1H), 16.47 (s. 1H);

HRMS (ESI) *m*/*z* 1234.4603 (1234.4593 calcd for $C_{61}H_{84}Cl_2N_5O_{11}Ru$, $[M+H]^+$).

Preparation of **1a**

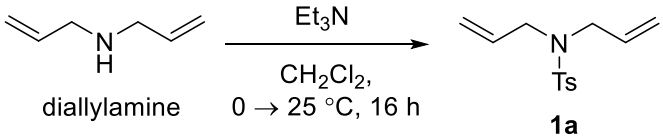

To a solution of diallylamine (1.18 g, 12.1 mmol, 1.2 equiv) and triethylamine (1.23 g, 12.2 mmol, 1.2 equiv) in dry CH_2Cl_2 (40 mL) was added *p*-toluenesulfonyl chloride (1.91 g, 10.0 mmol, 1.0 equiv) at 0 °C. The mixture was then stirred at room temperature for 16 h. After addition of H_2O, the product was extracted with CH_2Cl_2. The combined organic layers were then washed with brine, dried over Na_2SO_4, and concentrated *in vacuo*. The crude product was purified by silica gel column chromatography (hexane/EtOAc = 8/2) to give **1a** as a colorless oil (2.41 g, 95.9%). Characterization matched a previous report of this known compound.[9]

^{1}H-NMR (400 MHz, $CDCl_3$, δ) 2.43 (s, 3H), 3.80 (d, 4H, J = 6.4 Hz), 5.11–7.17 (m, 4H), 5.61 (ddt, 2H, J_1 = 6.4 Hz, J_2 = 9.8 Hz, J_3 = 17.4 Hz), 7.30 (d, 2H, J = 8.1 Hz), 7.71 (d, 2H, J = 8.1 Hz);

HRMS (ESI) *m*/*z* 252.1053 (252.1053 calcd for $C_{13}H_{18}NO_2S$, $[M+H]^+$).

Preparation of **VI**

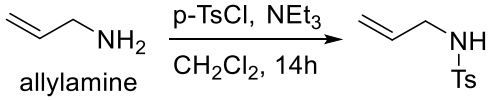

VI

To a solution of allylamine (1.0 g, 17.5 mmol, 1.0 equiv) in dry CH_2Cl_2 (20 mL) was added triethylamine (4.9 mL, 35.0 mmol, 2.0 equiv) and *p*-toluenesulfonyl chloride (3.5 g, 18.4 mmol, 1.1 equiv) at room temperature. The mixture was then stirred for 14 h. After addition of sat. aq. NH_4Cl, the product was extracted with EtOAc. The combined organic layers were then washed with H_2O, dried over Na_2SO_4, and concentrated *in vacuo*. The crude product was purified by silica gel column chromatography (hexane/EtOAc = 5/1) to give the **VI** as a colorless oil (3.5 g, 95%). Characterization matched a previous report of this known compound.[9]

^{1}H-NMR (400 MHz, $CDCl_3$, δ) 2,42 (s, 3H), 3,57 (tt, 2H, *J* = 6,3 Hz, *J* = 1,5 Hz), 5,04 (br, t, *J* = 6.1 Hz), 5.07 (dd, 1H, *J* = 10.2 Hz, *J* = 1,3 Hz), 5.16 (dd, 1H, *J* = 17.2 Hz, *J* = 1,4 Hz), 7.30 (d, 2H, *J* = 8.2 Hz), 7.77 (d, 2H, *J* = 8.3 Hz).

Preparation of **1b**

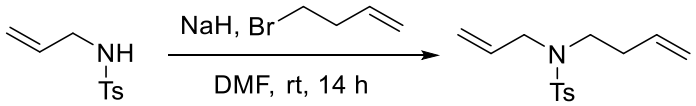

VI **1b**

To a solution of **VI** (523 mg, 2.48 mmol, 1.0 equiv) in dry DMF (10 mL) was added sodium hydride (238 mg, 9.92 mmol, 4.0 equiv) and 4-bromobut-1-ene (501 mg, 3.71 mmol, 1.5 equiv) at room temperature. The mixture was then stirred for 14 h. After addition of sat. aq. NH_4Cl, the product was extracted with EtOAc. The combined organic layers were then washed with H_2O, dried over Na_2SO_4, and concentrated *in vacuo*. The crude product was purified by silica gel column chromatography (hexane/EtOAc = 5/1) to give **1b** as a colorless oil (460 mg, 70%). Characterization matched a previous report of this known compound.[10]

^{1}H-NMR (400 MHz, $CDCl_3$, δ) 2.27 (dd, 2H, *J* = 15.0 Hz, *J* = 7.1 Hz), 2.42 (s, 3H), 3.18 (t, 2H, *J* = 7.5 Hz), 3.81 (d, 2H, *J* = 6.4 Hz), 5.01 (br. d, 1H, *J* = 10.1 Hz), 5.04 (dd, 1H, *J* = 17.1 Hz, *J* = 1.7 Hz), 5.14 (dd, 1H, *J* = 10.1 Hz, *J* = 1.2 Hz), 5.18 (dd, 1H, *J* = 17.1 Hz, *J* = 1.4 Hz), 5.58–5.76 (m, 2H), 7.30 (d, 2H, *J* = 8.1 Hz), 7.70 (d, 2H, *J* = 8.3 Hz);

HRMS (ESI) *m*/*z* 266.1217 (266.1209 calcd for $C_{14}H_{19}NO_2S$, $[M+H]^+$).

Preparation of **1c**

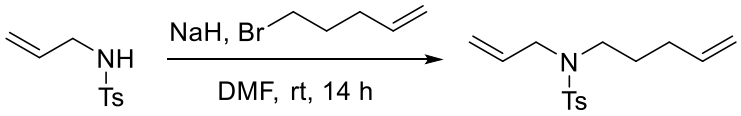

VI **1c**

To a solution of **VI** (597 mg, 2.83 mmol, 1.0 equiv) in dry DMF (10 mL) was added sodium hydride (271 mg, 11.3 mmol, 4.0 equiv) and 4-bromopent-1-ene (631.5 mg, 4.24 mmol, 1.5 equiv) at room temperature. The mixture was then stirred for 14 h. After addition of sat. aq. NH_4Cl, the product was extracted with EtOAc. The combined organic layers were then washed with H_2O, dried over Na_2SO_4, and concentrated *in vacuo*. The crude product was purified by silica gel column chromatography (hexane/EtOAc = 5/1) to give **1c** as a colorless oil (593 mg, 75%). Characterization matched a previous report of this known compound.[10]

^{1}H-NMR (400 MHz, $CDCl_3$, δ) 1.58–1.67 (m, 2H), 2.03 (dd, 2H, *J* = 14.3 Hz, *J* = 7.2 Hz), 2.42 (s, 3H), 3.11 (t, 2H, *J* = 7.5 Hz), 3.79 (d, 2H, *J* = 6.4 Hz), 4.93–5.04 (m, 2H), 5.09–5.20 (m, 2H), 5.63 (ddt, 1H, *J* = 16.6 Hz, *J* = 10.1 Hz, *J* = 6.4 Hz), 5.76 (ddt, 1H, *J* = 16.9 Hz, *J* = 10.2 Hz, *J* = 6.6 Hz), 7.30 (d, 2H, *J* = 8.0 Hz), 7.69 (d, 2H, *J* = 8.3 Hz);

HRMS (ESI) *m*/*z* 280.1362 (280.1366 calcd for $C_{15}H_{21}NO_2S$, $[M+H]^+$).

Preparation of **VII**

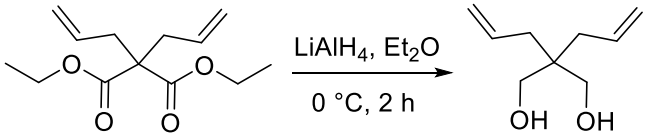

diethyl diallylmalonate **VII**

To a suspension of $LiAlH_4$ (119 mg, 3.12 mmol, 1.5 equiv) in Et_2O (10 mL) at 0 °C was slowly added an Et_2O solution of the diethyl diallylmalonate (500 mg, 2.08 mmol, 1.0 equiv). The reaction mixture was stirred at 0 °C for 2 h. Water was then added very slowly until no more gas evolution was observed. Additional H_2O was added and the solution was further stirred at room temperature until the reaction mixture became white. The mixture was then filtered through a pad of Celite® and concentrated *in vacuo* to give **VII** as a colorless oil, which was used without further purification. Characterization matched a previous report of this known compound.[11]

^{1}H-NMR (400 MHz, $CDCl_3$, δ) 2.08 (d, 4H, *J* = 7.5 Hz), 2.75 (br. s, 2H), 3.57 (s, 4H), 5.09 (s, 4H), 5.11–5.15 (m, 2H), 5.78–5.90 (m, 2H);

Preparation of **1d**

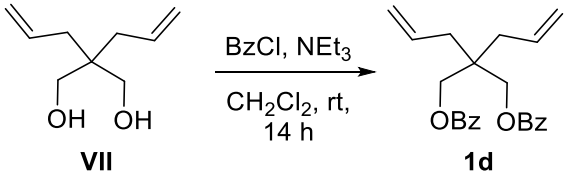

VII **1d**

To a solution of benzoyl chloride (337 mg, 2.4 mmol, 2.5 equiv) in CH_2Cl_2 (5 mL) at 0 °C was slowly added a CH_2Cl_2 solution of compound **VII** (150 mg, 0.96 mmol, 1.0 equiv) and triethylamine (535 μL, 3.84 mmol, 4.0 equiv). The reaction mixture was heated up to room temperature and stirred for 14 h. The reaction was quenched by addition of sat. aq. Na_2CO_3 and the product was extracted by EtOAc. The organic layer was then washed with brine, dried over Na_2SO_4, filtered, and then concentrated *in vacuo*. The crude product was purified by silica gel column chromatography (hexane/EtOAc = 5/1) to give **1d** as a colorless oil (331 mg, 98%).

^{1}H-NMR (400 MHz, $CDCl_3$, δ) 2.33 (d, 4H, *J* = 7.6 Hz), 4.33(s, 4H), 5.13 (d, 2H, *J* = 5.5 Hz), 5.17 (s, 2H), 5.80–5.97 (m, 2H), 7.38–7.45 (m, 4H), 7.49–7.58 (m, 2H), 8.05 (d, 4H, *J* = 7.1 Hz);

^{13}C-NMR (100 MHz, $CDCl_3$, δ) 36.6, 40.8, 66.6, 119.4, 128.5, 129.6, 130.1, 130.6, 132.5, 133.1, 166.3;

HRMS (ESI) *m*/*z* 387.1566 (387.1567 calcd for $C_{23}H_{24}O_4$, $[M+Na]^+$).

Preparation of **1e**

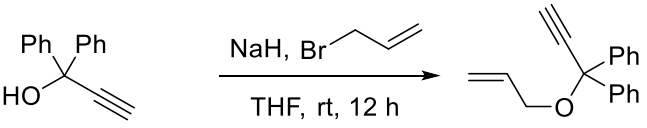

1,1-diphenylpropyn-1-ol **1e**

To a suspension of sodium hydride (63.4 mg, 2.64 mmol, 1.1 equiv) in dry DMF, 1,1-diphenylpropyn-1-ol (500 mg, 2.4 mmol, 1.0 equiv) in THF (3 mL) was added dropwise at 0 °C. After gas evolution (~15 min), allylbromide was added at 0 °C and the resulting mixture was stirred at room temperature for 12 h. To workup, the reaction was quenched by addition of water and the product was extracted by EtOAc. The organic layer was then washed with brine, dried over Na_2SO_4, filtered, and then concentrated *in vacuo*. The crude product was purified by silica gel column chromatography (hexane/EtOAc = 10/1) to give the **1e** as a colorless oil (408 mg, 68%). Characterization matched a previous report of this known compound.[12]

^{1}H-NMR (400 MHz, $CDCl_3$, δ) 2.87 (s, 1H), 4.04 (dt, 2H, *J* = 5.2 Hz, *J* = 1.5 Hz), 5.16 (dq, 1H, *J* = 10.5 Hz, *J* = 1.6 Hz), 5.36 (dq, 1H, *J* = 17.1 Hz, *J* = 1.8 Hz), 5.99 (ddt, 1H, *J* = 17.1 Hz, *J* = 10.5 Hz, *J* = 5.1 Hz), 7.19–7.34 (m, 6H), 7.55–7.57 (m, 2H), 7.58–7.62 (m, 2H);

Preparation of **2a**

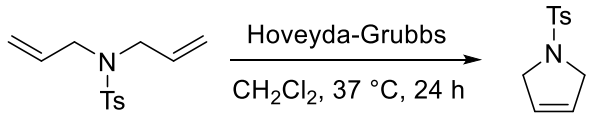

1a **2a**

Prepared according to General Procedure C. Characterization matched a previous report of this known compound.[9]

^{1}H-NMR (400 MHz, $CDCl_3$, δ) 2.43 (s, 3H), 4.12 (s, 4H), 5.65 (s, 2H), 7.32 (d, 2H, *J* = 8.1 Hz), 7.72 (d, 2H, *J* = 8.1 Hz);

HRMS (ESI) *m*/*z* 224.0745 (224.0740 calcd for $C_{11}H_{14}NO_2S$, $[M+H]^+$).

Preparation of **2b**

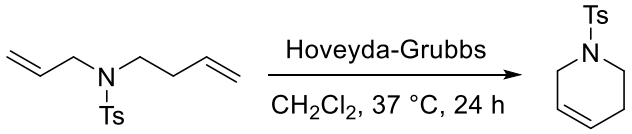

1b **2b**

Prepared according to General Procedure C. Characterization matched a previous report of this known compound.[10]

^{1}H-NMR (400 MHz, $CDCl_3$, δ) 2.21 (ddq, 2H, *J* = 8.5 Hz, *J* = 5.8 Hz, *J* = 2.8 Hz), 2.43 (s, 3H), 3.17 (t, 2H, *J* = 5.7 Hz), 3.53–3.61 (m, 2H), 5.58–5.64 (m, 1H), 5.72–5.79 (m, 1H), 7.32 (d, 2H, *J* = 8.0 Hz), 7.67 (d, 2H, *J* = 8.2 Hz);

HRMS (ESI) *m*/*z* 238.0900 (238.0896 calcd for $C_{12}H_{15}NO_2S$, $[M+H]^+$).

Preparation of **2c**

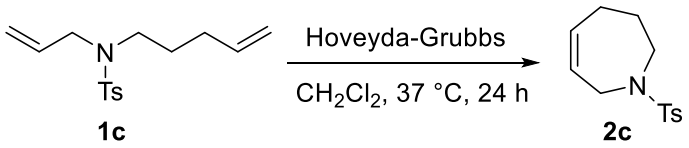

1c **2c**

Prepared according to General Procedure C. Characterization matched a previous report of this known compound.[10]

^{1}H-NMR (400 MHz, $CDCl_3$, δ) 1.80 (dt, 2H, *J* = 11.9 Hz, *J* = 6.0 Hz), 2.15–2.21 (m, 2H), 2.42 (s, 3H), 3.39 (t, 2H, *J* = 6.1 Hz), 3.83 (dd, 2H, *J* = 4.9 Hz, *J* = 1.2 Hz), 5.61–5.68 (m, 1H), 5.73–5.80 (m, 1H), 7.29 (d, 2H, *J* = 8.1 Hz), 7.68 (d, 2H, *J* = 8.3 Hz);

HRMS (ESI) *m*/*z* 252.1055 (252.1053 calcd. for $C_{13}H_{17}NO_2S$, $[M+H]^+$).

Preparation of **2d**

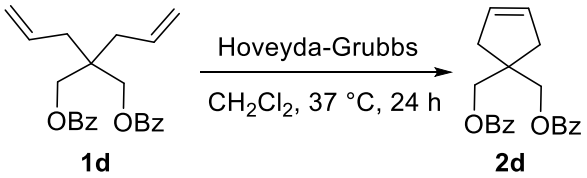

1d **2d**

Prepared according to General Procedure C. Characterization matched a previous report of this known compound.[13]

^{1}H-NMR (400 MHz, $CDCl_3$, δ) 2.47 (s, 4H), 4.41 (s, 4H), 5.70 (s, 2H), 7.43 (t, 4H, *J* = 7.7 Hz), 7.56 (t, 2H, *J* = 7.5 Hz), 8.02 (d, 4H, *J* = 8.2 Hz);

HRMS (ESI) *m*/*z* 359.1252 (359.1254 calcd. for $C_{21}H_{20}O_4$, $[M+Na]^+$).

Preparation of **2e**

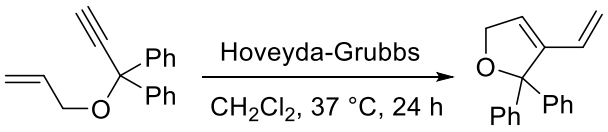

1e **2e**

Prepared according to General Procedure C. Characterization matched a previous report of this known compound.[14]

^{1}H-NMR (400 MHz, $CDCl_3$, δ) 4.79 (d, 2H, *J* = 1.6 Hz), 5.10 (d, 1H, *J* = 11.6 Hz), 5.32 (d, 1H, *J* = 18.1 Hz), 6.19 (br. s, 1H), 6.23 (ddd, 1H, *J* = 17.8 Hz, *J* = 11.0 Hz, *J* = 0.8 Hz), 7.27–7.37 (m, 10H);

HRMS (ESI) *m*/*z* 231.1213 (231.1216 calcd. for $C_{18}H_{16}O$, $[M+Na]^+$).

Preparation of **VIII**

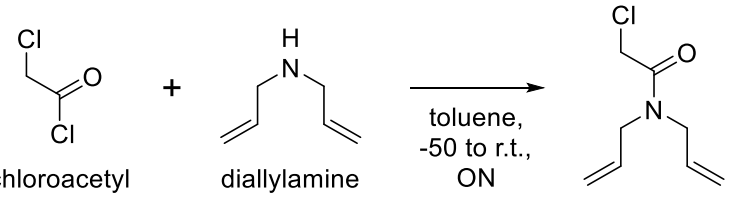

chloroacetyl chloride diallylamine **VIII**

To a solution of diallylamine (630 µL, 5.1 mmol, 1.0 equiv) in toluene (5 mL) at −50 °C was dropwise added a toluene solution of chloroacetyl chloride (210 µL, 2.6 mmol, 0.5 equiv). The reaction mixture was stirred at –50 °C within 10 min and then allowed to reach room temperature and stirred for 20 hours. After this time the mixture was filtered, solid washed with EtOAc and filtrate was concentrated *in vacuo*. The crude product was purified by silica gel column chromatography (hexane/EtOAc = 7/3). Compound **VIII** was obtained as a colorless oil (360 mg, 80%). Characterization matched a previous report of this known compound.[15]

^{1}H-NMR (400 MHz, $CDCl_3$, δ) 3.97 (d, 2H, *J* = 5.0 Hz), 4.01 (d, 2H, *J* = 5.9 Hz), 4.07 (s, 2H), 5.15–5.28 (m, 4H), 5.70–5.88 (m, 2H).

Preparation of **1f**

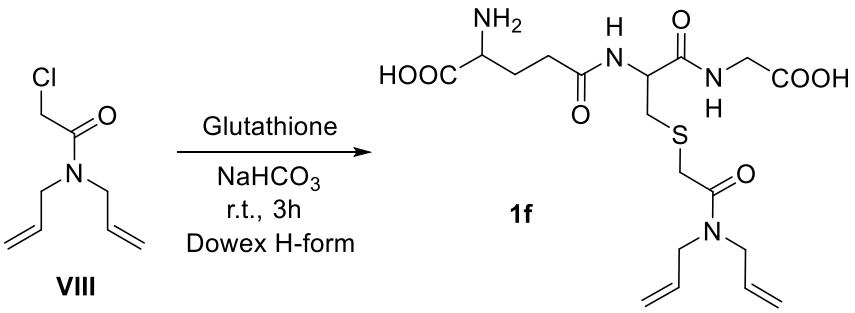

To a solution of glutathione (105 mg, 0.34 mmol, 1.0 equiv) in water (3 mL) was added compound **VIII** (89 mg, 0.51 mmol, 1.5 equiv) in ethanol (3 mL). A saturated aq. $NaHCO_3$ (1 mL) was added to the reaction mixture and stirred at room temperature for 3h. To workup, the reaction was concentrated *in vacuo*. The crude product was purified by silica gel column chromatography (CH_3CN/H_2O = 3/1) to give the sodium salt of **1f**, which was then redissolved in a mixture of H_2O–MeOH (6 mL, 1:1, v/v), treated with ion-exchange resin Dowex® 50WX8 hydrogen form (200–400 mesh) (50 mg), and stirred at room temperature for 2 h. The solution was then filtered and concentrated *in vacuo* to produce compound **1f** was as a white solid in acidic form (90 mg, 64%)

^{1}H-NMR (400 MHz, DMSO-d_6, δ) 1.95 (q, 2H, J = 7.1 Hz), 2.34 (t, 2H, J = 7.1 Hz), 2.70 (dd, 1H, J_1 = 9.6 Hz, J_2 = 13.7 Hz), 2.97 (dd, 1H, J_1 = 4.6 Hz, J_2 = 13.7 Hz), 3.43 (d, 1H, J = 14.2 Hz), 3.47 (d, 1H, J = 14.2 Hz), 3.58 (t, 1H, J = 7.1 Hz), 3.74 (d, 2H, J = 6.0 Hz), 3.86 (t, 2H, J = 6.0 Hz), 3.92 (d, 2H, J = 5.0 Hz), 4.49 (td, 1H, J_1 = 4.6 Hz, J_2 = 8.7 Hz), 5.09–5.21 (m, 4H), 5.72 (ddt, 1H, J_1 = 5.0 Hz, J_2 = 10.3 Hz, J_3 = 17.6 Hz), 5.85 (ddt, 1H, J_1 = 5.5 Hz, J_2 = 9.8 Hz, J_3 = 17.4 Hz), 8.36 (d, 1H, J = 8.7 Hz), 8.49 (t, 1H, J = 6.0 Hz);

^{13}C-NMR (100 MHz, DMSO-d_6, δ) 26.2, 30.8, 33.3, 34.0, 40.8, 47.2, 49.5, 51.9, 116.7, 116.8, 133.3, 133.9, 168.4, 170.5, 170.8, 170.9, 171.2;

HRMS (ESI) *m*/*z* 443.1605 (443.1600 calcd for $C_{18}H_{27}N_4O_7S_1$ [M–H]$^-$).

Preparation of **2f**

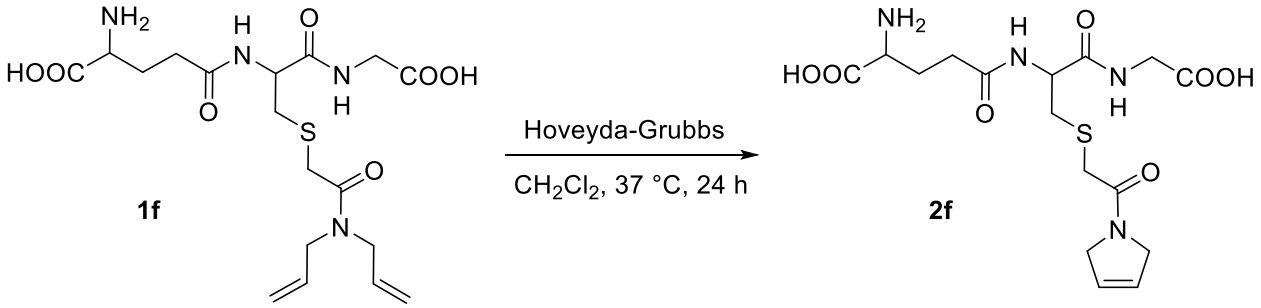

Prepared according to General Procedure C. Compound **2f** was obtained as a white solid (11 mg, 68%).

^{1}H-NMR (400 MHz, DMSO-d_6, δ) 1.93–2.10 (m, 2H), 2.27–2.44 (m, 2H), 2.70 (dd, 1H, J_1 = 9.2 Hz, J_2 = 13.7 Hz), 2.96 (dd, 1H, J_1 = 4.6 Hz, J_2 = 13.7 Hz), 3.42 (s, 2H), 3.77 (d, 1H, J = 6.0 Hz), 3.96 (br d, 1H, J = 5.5 Hz), 4.06–4.09 (m, 2H), 4.27–4.30 (m, 2H), 4.52 (td, 1H, J_1 = 4.6 Hz, J_2 = 8.9 Hz), 5.91 (s, 2H), 8.28 (br d, 2H, J = 3.2 Hz), 8.31–8.36 (m, 2H);

^{13}C-NMR (100 MHz, DMSO-d_6, δ) 26.0, 30.6, 34.0, 34.2, 40.7, 51.6, 51.9, 53.0, 125.7, 125.8, 166.8, 170.5, 170.8, 170.95, 171.02;
HRMS (ESI) *m*/*z* 415.1289 (415.1287 calcd for $C_{16}H_{23}N_4O_7S_1$ [M–H]$^-$).

Preparation of **X**

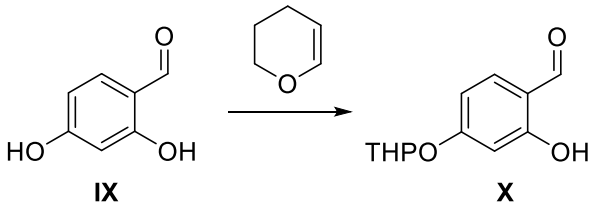

IX **X**

To a suspension of **IX** (2.76 g, 20 mmol, 1.0 equiv) and dihydropyran (4.01 mL, 44 mmol, 2.2 equiv) in CH_2Cl_2 (20 mL) was added pyridinium *p*-toluenesulfonate (216 mg, 0.860 mmol, 0.043 equiv). The reaction mixture was stirred at room temperature for 4 h. To workup, the reaction was quenched by the addition of sat. aq. $NaHCO_3$. The product was then extracted with CH_2Cl_2, dried over Na_2SO_4, and concentrated *in vacuo*. The crude product was purified by silica gel column chromatography (Hexane/EtOAc = 9/1) to give **X** as a colorless solid (3.99 g, 90%). Characterization matched a previous report of this known compound.[16]
^{1}H-NMR (300MHz, $CDCl_3$, δ) 1.52–1.78 (m, 4H), 1.82–1.91 (m, 2H), 3.61–3.65 (m, 1H), 3.79–3.87 (m, 1H), 5.50 (t, 1H, *J* = 3.0 Hz), 6.63 (d, 1H, *J* = 2.2 Hz), 6.66 (dd, 1H, *J* = 8.6 Hz, *J* = 2.2 Hz), 7.44 (d, 1H, *J* = 8.5 Hz), 9.73 (s, 1 H), 11.37 (s, 1H);

Preparation of **XI**

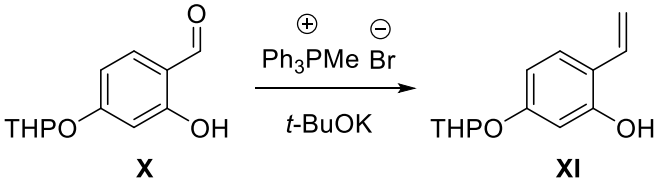

X **XI**

To a suspension of methyltriphenylphosphonium bromide (9.64 g, 27.0 mmol, 1.50 equiv) in dry THF (30 mL) was added potassium *tert*-butoxide (6.06 g, 54.0 mmol, 3.00 equiv). The mixture was stirred at room temperature for 1 h and then cooled to –78 °C, before dropwise addition of compound **X** (3.99 g, 18.0 mmol, 1.00 equiv) in dry THF (15 mL). The mixture was then allowed to warm up to room temperature and stirred for 30 min. To workup, the reaction was quenched by the addition of sat. aq. NH_4Cl. The product was then extracted with EtOAc, washed with brine, dried over Na_2SO_4, and concentrated *in vacuo*. The crude product was purified by silica gel column chromatography (hexane/EtOAc = 3:1) to give vinylphenol **XI** as a white solid (3.93 g, 98 %). Characterization matched a previous report of this known compound.[6]
^{1}H-NMR (400 MHz, CD_3OD, δ) 1.49–1.69 (m, 3H), 1.70–1.85 (m, 2H), 1.89–2.0 (m, 1H), 3.52–3.59 (m, 1H), 3.80–3.89 (m, 1H), 5.02 (dd, 1H, *J* = 11.2 Hz, *J* = 1,7 Hz), 5.31 (t, 1H, *J* = 3.4 Hz), 5.57 (dd, 1H, *J* = 17.8 Hz, *J* = 1,8 Hz), 6.45 (d, 1H, *J* = 2.4 Hz), 6.48 (dd, 1H, *J* = 5.1 Hz, *J* = 2,4 Hz), 6.88 (dd, 1H, *J* = 17.8 Hz, *J* = 11.3 Hz), 7.27 (d, 1H, *J* = 8.4 Hz).

Preparation of **XII**

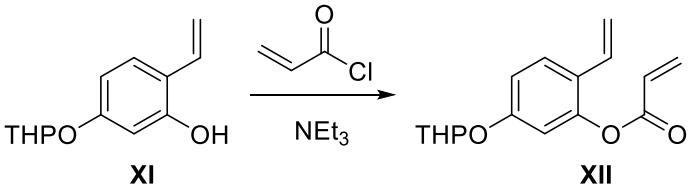

XI **XII**

A solution of **XI** (1.0 g, 4.54 mmol, 1.00 equiv) in CH_2Cl_2 (15 mL) was treated with triethylamine (1.27 mL, 9.1 mmol, 2.00 equiv), followed by the slow addition of acryloyl chloride (553 µL, 6.8 mmol, 1.50 equiv). The reaction mixture was stirred at room temperature for 20 min. To workup, the reaction was concentrated *in vacuo*. The crude product was purified by silica gel column chromatography (hexane/EtOAc = 9/1) to give acrylate **XII** as a colorless oil (1.07 g, 86 %). The compound was directly used in the next step due to low stability. Characterization matched a previous report of this known compound.[6]

^{1}H-NMR (400 MHz, $CDCl_3$, δ) 1.80–1.84 (m, 2H), 1.92–2.03 (m, 1H), 3.56–3.66 (m, 1H), 3.78–3.93 (m, 1H), 5.21 (dd, 1H, *J* = 11.1 Hz, *J* = 1.1 Hz), 5.43 (t, 1H, *J* = 3.0 Hz), 5.64 (dd, 1H, *J* = 17.6 Hz, *J* = 1.1 Hz), 6.03 (dd, 1H, *J* = 10.4 Hz, *J* = 1.3 Hz), 6.34 (dd, 1H, *J* = 17.3 Hz, *J* = 10.4 Hz), 6.59–6.73 (m, 2H), 6.83 (d, 1H, *J* = 2.5 Hz), 6.95 (dd, 1H, *J* = 8.6 Hz, *J* = 2.4 Hz), 7.50 (d, 1H, *J* = 8.7 Hz).

Preparation of **XIII**

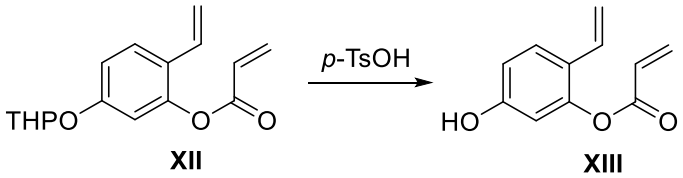

XII **XIII**

To a solution of **XII** (0.87 g, 3.2 mmol, 1.0 equiv) in a mixture of MeOH–THF (20 mL, 1:1, v/v) was added *p*-toluenesulfonic acid monohydrate (60.3 mg, 317 µmol, 10 mol%) and then the solution was stirred at room temperature for 1 h. To workup, the mixture was quenched with sat. aq. NH_4Cl and extracted with EtOAc. The combined organic layers were washed with water and brine, dried over Na_2SO_4, filtered, and concentrated *in vacuo*. The crude product was then purified by silica gel column chromatography (hexane/EtOAc = 7:3) to give compound **XIII** as a colorless oil (540 mg, 90 %). Characterization matched a previous report of this known compound.[6]

^{1}H-NMR (400 MHz, $CDCl_3$, δ) 5.17 (dd, 1H, *J* = 11.1 Hz, *J* = 1.1 Hz), 5.59 (dd, 1H, *J* = 17.6 Hz, 1.0 Hz), 6.05 (dd, 1H, *J* = 10.5Hz, *J* = 1.0 Hz), 6.34 (dd, 1H, *J* = 17.2 Hz, *J* = 10.4 Hz), 6.39 (br. s, 1H), 6.51 (d, 1H, *J* = 2.5 Hz), 6.57–6.67 (m, 3H), 7.40 (d, 1H, *J* = 8.6 Hz).

Preparation of **1g**

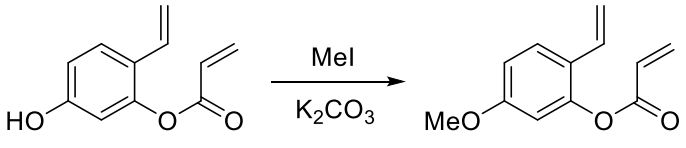

XIII **1g**

To a solution of **XIII** (350 mg, 1.84 mmol, 1.00 equiv) in dry acetone (15 mL), the reagents K_2CO_3 (381 mg, 2.76 mmol, 1.50 equiv), and MeI (520 mg, 3.68 mmol, 2.0 equiv) were consecutively added. The mixture was stirred at room temperature for 16 h. To workup, the mixture was filtered and concentrated *in vacuo*. The crude product was purified by silica gel column chromatography (hexane/EtOAc = 9/1) to give **1g** as a colorless oil (176 mg, 47 %). Characterization matched a previous report of this known compound.[17]

^{1}H-NMR (400 MHz, $CDCl_3$, δ) 3.80 (s, 3H), 5.20 (dd, 1H, J_1 = 1.4 Hz, J_2 = 10.5 Hz), 5.63 (dd, 1H, J_1 = 1.4 Hz, J_2 = 17.4 Hz), 6.05 (dd, 1H, J_1 = 1.4 Hz, J_2 = 10.5 Hz), 6.35 (dd, 1H, J_1 = 10.5 Hz, J_2 = 17.4 Hz), 6.61–6.69 (m, 3H), 6.81 (dd, 1H, J_1 = 2.7 Hz, J_2 = 8.7 Hz), 7.51 (d, 1H, J = 8.7 Hz).

Preparation of **2g**

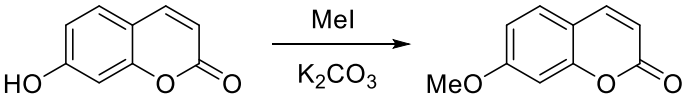

Umbelliferone **2g**

To a suspension of umbelliferone (407 mg, 2.51 mmol, 1.00 equiv) in dry acetone (25 mL), the reagents K_2CO_3 (414 mg, 3.01 mmol, 1.20 equiv), and MeI (712 mg, 5.02 mmol, 2.0 equiv) were consecutively added. The mixture was stirred at room temperature for 16 h. To workup, the mixture was filtered and concentrated *in vacuo*. The crude product was purified by silica gel column chromatography (hexane/EtOAc = 7/3) to give **2g** as a slightly yellow solid (365 mg, 83 %). Characterization matched a previous report of this known compound.[18]

^{1}H-NMR (400 MHz, $CDCl_3$, δ) 3.09 (s, 3H), 6.25 (d, 1H, J = 9.5 Hz), 6.81–6.87 (m, 2H), 7.38 (d, 1H, J = 8.4 Hz), 7.64 (d, 1H, 9.5 Hz).

Preparation of **XIV**

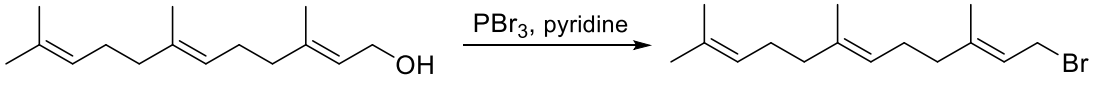

(E,E)-Farnesol **XIV**

To a solution of *trans,trans*-Farnesol (400 mg, 1.8 mmol, 1.00 equiv) and pyridine (122 µL, 1.5 mmol, 0.85 equiv) in Et_2O (15 mL) was added phosphorus tribromide (220 µL, 2.30 mmol, 1.3 equiv) in one portion at 0 °C. The reaction mixture was warmed to room temperature and stirred for 20 min. To workup, the reaction was quenched by the addition of water and extracted by Et_2O. The organic layers were washed with brine, dried over $MgSO_4$, filtered, and concentrated *in vacuo* to give the bromide **XIV** as a residual brown oil, which was used in the next step without purification.

Preparation of **1h**

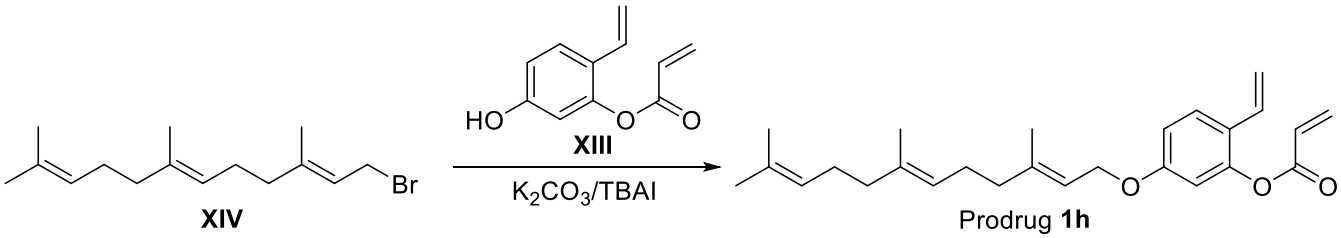

To a solution of **XIII** (175 mg, 0.92 mmol, 1.00 equiv) in dry acetone (15 mL), tetrabutylammonium iodide (17 mg, 0.046 mmol, 5 mol%), K_2CO_3 (170 mg, 1.23 mmol, 1.30 equiv), and **XIV** (524 mg, 1.84 mmol, 2.0 equiv) were consecutively added. The mixture was stirred at 50 °C for 16 h. To workup, the mixture was filtered and concentrated *in vacuo*. The crude product was purified by silica gel column chromatography (hexane/EtOAc = 9/1) to give the prodrug **1h** as a colorless oil (217 mg, 60 %).

^{1}H-NMR (400 MHz, $CDCl_3$, δ) 1.60 (s, 6H), 1.68 (s, 3H), 1.73 (s, 3H), 1.95–2.15 (m, 8H), 4.52 (d, 2H, J = 6.6 Hz), 5.07–5.13 (m, 2H), 5.19 (dd, 1H, J_1 = 0.9 Hz, J_2 = 11.0 Hz), 5.47 (td, 1H, J_1 = 0.9 Hz, J_2 = 6.6 Hz), 5.63 (dd, 1H, J_1 = 0.9 Hz, J_2 = 10.5 Hz), 6.04 (dd, 1H, J_1 = 0.9 Hz, J_2 = 10.5 Hz), 6.35 (dd, 1H, J_1 = 10.5 Hz, J_2 = 17.4 Hz), 6.61–6.69 (m, 3H), 6.81 (dd, 1H, J_1 = 2.7 Hz, J_2 = 8.7 Hz), 7.50 (d, 1H, J = 8.7 Hz);

^{13}C-NMR (100 MHz, $CDCl_3$, δ) 16.0, 16.7, 17.7, 25.7, 26.2, 26.7, 39.5, 39.7, 65.1, 108.4, 113.4, 114.0, 119.0, 122.7, 123.6, 124.3, 127.0, 127.6, 129.8, 131.3, 132.9, 135.5, 141.7, 148.5, 159.3, 164.2;

HRMS (ESI) *m*/*z* 395.2584 (395.2581 calcd for $C_{26}H_{34}O_3$, $[M+H]^+$).

Preparation of **2h** (Umbelliprenin)

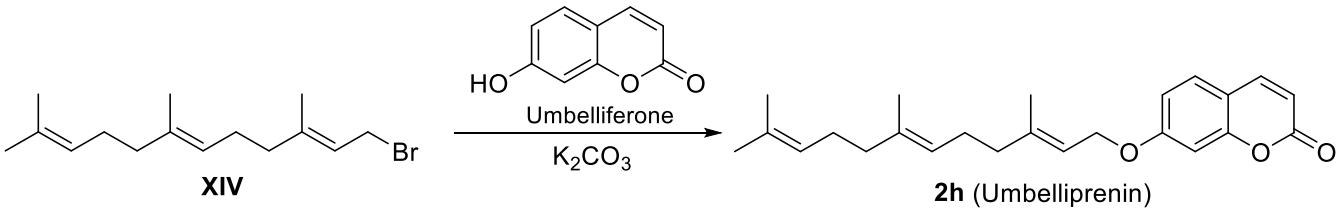

To a solution of umbelliferone (500 mg, 3.1 mmol, 1.00 equiv) in dry acetone (50 mL), tetrabutylammonium iodide (57 mg, 0.05 mmol, 5 mol%), K_2CO_3 (180 mg, 1.30 mmol, 1.30 equiv), and **XIV** (700 mg, 1.98 mmol, 2.0 equiv) were consecutively added. The mixture was stirred at reflux for 16 h. To workup, the mixture was filtered and concentrated *in vacuo*. The crude product was purified by silica gel column chromatography (hexane/EtOAc = 9/1) to yield umbelliprenin **2h** as a white solid (980 mg, 86 %).

^{1}H-NMR (400 MHz, $CDCl_3$, δ) 1.60 (s, 6H), 1.68 (s, 3H), 1.77 (s, 3H), 1.90–2.18 (m, 8H), 4.60 (d, 2H, J = 6.6 Hz), 5.08–5.10 (m, 2H), 5.47 (td, 1H, J = 6.6 Hz, J = 1.1 Hz), 6.24 (d, 1H, J = 9.5 Hz), 6.82 (d, 1H, J = 2.3 Hz), 6.85 (dd, 1H, J = 8.5 Hz, J = 2.4 Hz), 7.36 (d, 1H, J = 8.5 Hz), 7.63 (d, 1H, J = 9.5 Hz);

^{13}C-NMR (100 MHz, $CDCl_3$, δ) 16.1, 16.8, 17.8, 25.8, 26.2, 26.8, 39.6, 39.8, 65.6, 101.7, 112.6, 113.0, 113.4, 118.6, 123.7, 124.5, 128.8, 131.5, 135.8, 142.6, 143.6, 156.1, 161.5, 162.4;

HRMS (ESI) *m*/*z* 367.2266 (367.2268 calcd for $C_{24}H_{30}O_3$, $[M+H]^+$).

Supplementary Discussions

Discussion on Binding Affinity

In this study, two different methods to monitor binding was used. The first approach is based on the quenching of intrinsic protein fluorescence (due to aromatic amino acids like tryptophan) upon ligand binding. Shown in Supplementary Figure 5A are the excitation and emission wavelengths of HSA in conditions used for this study. Saturation curves were then collected at λ_{EX} = 280 nm/λ_{EM} = 320 nm to quantify the binding affinity of ligands **Ru1-3,6** to HSA (Supplementary Figure 12). In general, ligands **Ru1** and **Ru2** had similar K_D values (within error), but then decreased slightly for ligands **Ru3** and **Ru6**. A possible explanation for this lowered affinity may be due to their longer PEG linker, which may disrupt optimal binding inside of the hydrophobic pockets of albumin. It should be noted that one pitfall of obtaining K_D values by this approach (measuring the change in albumin fluorescence upon ligand binding) is that that non-specific binding on protein surfaces or shallow pockets will also likely be accounted for.

The second approach instead measures the fluorescent emission of ligand binding to HSA. This approach is only possible where ligands are non-fluorescent in aqueous solutions, but become highly fluorescent in nonpolar environments, such as the hydrophobic binding pockets of HSA. Shown in Supplementary Figure 5B-E are the excitation and emission spectra of 1:1 ligand-to-albumin complexes using compounds **Ru1-3,6**. Saturation curves were then collected at λ_{EX} = 425nm/λ_{EM} = 460nm to quantify the binding affinity of ligands **Ru1-3,6** to HSA (Supplementary Figure 13).The measured K_D values generally show lower values than the ones obtained in Supplementary Figure 12, which is likely due to the elimination of non-specific binding that does not involve binding in hydrophobic surroundings. Again, it was observed that **Ru1 and Ru2** have slightly higher affinity to albumin than **Ru3** and **Ru6**.

Discussion on Binding Site Identification

By utilizing known site marker ligands of serum albumin, the potential binding site for **Ru1-3,6** can be indirectly determined. In literature, there are two well-known binding regions of human serum albumin: Sudlow's site I (located in subdomain IIA) and Sudlow's site II (located in subdomain IIIA). Bulky, heterocyclic molecules (ex/ warfarin) are known to bind to site I while aromatic carboxylates (ex/ ibuprofen) have a preference for site II. Both warfarin and ibuprofen are known to bind albumin with low micromolar K_D.

Experimentally, a 20 μM solution of albumin was preincubated with 2 equivalents of either site marker ligand (warfarin, ibuprofen) for 1 hr at 37 °C. The albumin/site marker ligand mixture was then used to construct saturation binding curves for **Ru1-3,6**, which are shown in Supplementary Figure 15. From this data, it can be clearly seen that binding of catalysts **Ru1-3,6** remains unaffected in the presence of ibuprofen, but decreases significantly with warfarin. This data suggests that the main binding pocket of these compounds is binding site I.

Discussion on Displacement Potential of Umbelliprenin

One important aspect to note for umbelliprenin is that it also contains a coumarin structural motif, which is similar to the coumarin anchor moiety of compounds **Ru1-3,6**. To determine whether umbelliprenin can act to displace compounds **Ru1-3,6** from the site I hydrophobic binding pocket of albumin, a series of experiments were conducted. First, the binding parameters were determined for umbelliprenin **2h** and the umbelliprenin prodrug **1h**, which can be seen in Supplementary Figure 14A-B. In general, the K_D values of **2h** (45 μM) and **1h** (74 μM) are much higher than that of compounds **Ru1-3,6** (12-20 μM). As a side note, the binding of coumarin precursor **1g** was also tested (Supplementary Figure 14C), which reveals it to be a rather poor ligand to albumin (measured K_D was found to be in the range of 129 μM). As such, it is expected that **1g** will likely have poor RCM reactivity with the alb-Ru complexes.

As a further check, a displacement assay with ligands **Ru1-3,6** was performed. The basis behind this experiment was to test the ability of umbelliprenin (at varying concentrations) to displace **Ru1-3,6** (10 μM) preincubated with albumin (10 μM). The percentage of bound **Ru1-3,6** can be determined by monitoring the fluorescence at λ_{EX}=425nm/λ_{EM}=460nm. As a control to ensure that intrinsic fluorescence does not interfere with wavelengths used for binding assays, it was confirmed that umbelliprenin is not fluorescent under these conditions (Supplementary Figure 6B). Results of this experiment, shown in Supplementary Figure 16, reveal that the 1:1 complex of **Ru1-3,6** with albumin is fairly resistant to displacement from umbelliprenin. At a 16× concentration of umbelliprenin, experimental data generally shows that 60-65% of **Ru1-3,6** remains bound.

Discussion on Differences in Quantum Yields

As shown in Supplementary Figure 7E, the quantum yields of **Ru1-3,6** increase significantly from 10% dioxane to 60% dioxane, as expected. Another trend that was noted correlates longer linker lengths of the **Ru** catalysts with higher quantum yields. For example, **Ru6** has much higher quantum yields compared to **Ru1**. A possible explanation for this phenomenon is the likelihood that the Hoveyda-Grubbs catalyst quenches coumarin-based fluorescence.

Discussion on Turnover Calculation

The turnover number (TON) is roughly defined as "the total number of turnovers the catalyst can achieve until its total decay, regardless of time".[19] Mathematically, this can be calculated using Supplementary Equation 4.

$$\mathrm{TON} = \frac{N_{prod}}{N_{catal\ sites}} \tag{4}$$

where N_{prod} is the total number of moles for the formed desired product formed, and $N_{catal\ sites}$ is the total number of moles for the number of active catalytic centers. Calculated TON values in this study were determined using this formula.

Discussion on Glutathione Protection (Molecular Modeling)

Experimental data has shown that albumin complexed with **Ru1-3** (PEG linker lengths of 1-3) are much more resistant to glutathione quenching than **Ru6** (PEG linker length of 6). To rationalize this observation, the molecular configurations of compounds **Ru1-3,6** docked into human serum albumin (PDB 1H9Z) were analyzed further.

One parameter of interest was the measured surface area of the whole ligand buried inside of the protein. It is assumed that buried surface area would not be accessible to the solvent (ex/ water molecules with a radius of 1.4Å). To determine this parameter, the solvent-accessible surface area (SASA) of the unbound protein, unbound ligands, and complex (protein + ligand) were determined using Supplementary Equation 5. Calculated values of buried ligand **Ru1-3,6** are shown in Supplementary Table 3.

$$\%Buried\ Area_{(ligand)} = \frac{Area_{(protein)} + Area_{(ligand)} - Area_{(protein+ligand)}}{2} \qquad (5)$$

The primary observation extrapolated from this data was that longer PEG linkers generally give lower values of buried ligand percentages. This is best represented by Supplementary Figure 29, which shows a sliced view of the albumin binding pocket docked with both the (R)- and (S)-enantiomers of **Ru1-3,6**. It appears that the binding pocket can accommodate the PEG linker increase from 1 to 2, but is unable to fully accommodate PEG linker lengths of 3 and 6. As a result, the binding pocket reaches its limit and the ruthenium moiety of **Ru3** (slightly) and **Ru6** protrudes out of the binding pocket (Supplementary Figure 30).

Although the solvent exposure of the whole ligand is a valuable parameter to understand the buried surface area, the principal aim is to determine the varying degrees of glutathione protection afforded to the Hoveyda-Grubbs catalytic moiety of **Ru1-3,6**. In this case, the SASA values of the individual atoms is needed, which focused specifically on Ru (the ruthenium metal), C_1 of the *N*-heterocyclic carbene (H_2Imes), and C_2 and O of the *ortho*-isopropoxybenzylidene moiety. Calculated SASA values for these atoms are shown in Supplementary Table 4, which as a control, also lists values obtained for the nitrogen atoms of various surface lysines (previously identified to react with the RIKEN click probe[20]), and the sulfur atom of cysteine residue 34 (this free sulfhydryl group of albumin represents the largest serum thiol source).

Supplementary References

1. Wohlfarth, C. *Refractive Indices of Pure Liquids and Binary Liquid Mixtures (Supplement to III/38)* (Springer Berlin Heidelberg, 2008).
2. Lakowicz, J. R. *Principles of Fluorescence Spectroscopy* (Kluwer Academic, 1999).
3. Ghuman, J. et al. Structural basis of the drug-binding specificity of human serum albumin. *J. Mol. Biol.* **353**, 38-52 (2005).
4. Petitpas, I. et al. Crystal structure analysis of warfarin binding to human serum albumin: Anatomy of drug site I. *J. Biol. Chem.* **276**, 22804-22809 (2001).
5. Lo, C. et al. Artificial metalloenzymes for olefin metathesis based on the biotin-(strept)avidin technology. *ChemComm* **47**, 12065-12067 (2011).
6. Kajetanowicz, A., Chatterjee, A., Reuter, R. & Ward, T. R. Biotinylated metathesis catalysts: Synthesis and performance in ring closing metathesis. *Catal. Lett.* **144**, 373-379 (2014).
7. Zhao, J., Kajetanowicz, A. & Ward, T. R. Carbonic anhydrase II as host protein for the creation of a biocompatible artificial metathesase. *Org. Biomol. Chem.* **13**, 5652-5655 (2015).
8. Taichi, M. et al. In situ ligation of high- and low-affinity ligands to cell surface receptors enables highly selective recognition. *Adv. Sci.* **4**, 1700147 (2017).
9. Poornachandran, M. & Raghunathan, R. Synthesis of pyrrolo[3,4-b]pyrroles and perhydrothiazolo[3′,4′-2,3]pyrrolo[4,5-c]pyrroles. *Tetrahedron* **64**, 6461-6474 (2008).
10. Che, C. et al. Magnetic nanoparticle-supported Hoveyda–Grubbs catalysts for ring-closing metathesis reactions. *ChemComm* **40**, 5990-5992 (2009).
11. Adrio, L. A., Quek, L. S., Taylor, J. G. & Kuok Hii, K. Copper-catalysed intramolecular O–H addition to unactivated alkenes. *Tetrahedron* **65**, 10334-10338 (2009).
12. Cadierno, V., Díez, J., García-Garrido, S. E. & Gimeno, J. $[Ru(\eta^3\text{-}2\text{-}C_3H_4Me)(CO)(dppf)][SbF_6]$: A mononuclear $16e^-$ ruthenium(II) catalyst for propargylic substitution and isomerization of $HC{\equiv}CCPh_2(OH)$. *ChemComm* **0**, 2716-2717 (2004).
13. Nagasawa, S., Sasano, Y. & Iwabuchi, Y. Synthesis of 1,3-cycloalkadienes from cycloalkenes: Unprecedented reactivity of oxoammonium salts. *Angew. Chem. Int. Ed. Engl.* **55**, 13189-13194 (2016).
14. Michrowska, A. et al. A new concept for the noncovalent binding of a ruthenium-based olefin metathesis catalyst to polymeric phases: Preparation of a catalyst on Raschig rings. *J. Am. Chem. Soc.* **128**, 13261-13267 (2006).
15. Żukowska, K., Pączek, Ł. & Grela, K. Sulfoxide-chelated ruthenium benzylidene catalyst: A synthetic study on the utility of olefin metathesis. *ChemCatChem* **8**, 2817-2823 (2016).
16. Kapeller, D. C. & Bräse, S. Towards a library of chromene cannabinoids: A combinatorial approach on solid supports. *Synlett* **2011**, 161-164 (2011).
17. Polito, L., Cravini, M., Poletti, L. & Lay, L. Simple synthesis of versatile coumarin scaffolds. *Synth. Commun.* **36**, 2203-2209 (2006).
18. Trost, B. M., Toste, F. D. & Greenman, K. Atom economy. Palladium-catalyzed formation of coumarins by addition of phenols and alkynoates via a net C−H insertion. *J. Am. Chem. Soc.* **125**, 4518-4526 (2003).
19. Kozuch, S. & Martin, J. M. L. "Turning Over" Definitions in Catalytic Cycles. *ACS Catal.* **2**, 2787-2794 (2012).
20. Ogura, A. et al. A viable strategy for screening the effects of glycan heterogeneity on target organ adhesion and biodistribution in live mice. *ChemComm* **54**, 8693-8696 (2018).